

TRANSIENT FLOW FIELD ANALYSIS OF A PLANE
BLAST WAVE INTERCEPTING A STATIONARY
CONE AT ZERO ANGLE OF ATTACK

By

WILLIAM N. JACKOMIS

Bachelor of Science
University of Notre Dame
Notre Dame, Indiana
1954

Master of Science
Oklahoma State University
Stillwater, Oklahoma
1962

Submitted to the Faculty of the Graduate School of
the Oklahoma State University
in partial fulfillment of the requirements
for the degree of
DOCTOR OF PHILOSOPHY
May, 1965

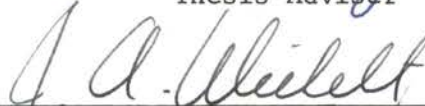
SEP 20 1965

TRANSIENT FLOW FIELD ANALYSIS OF A PLANE
BLAST WAVE INTERCEPTING A STATIONARY
CONE AT ZERO ANGLE OF ATTACK

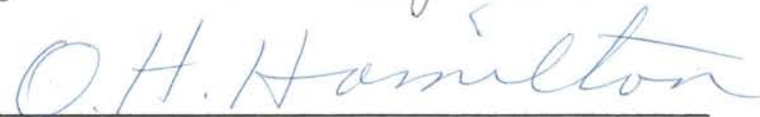
Thesis Approved:

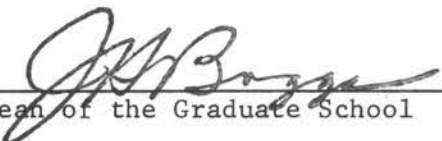


Thesis Adviser









Dean of the Graduate School

PREFACE

This analysis, undertaken as part of an active research contract titled "The Interaction of a Blast Wave and the Base Pressure Region of a Missile Re-Entering the Atmosphere," was completed under the sponsorship of the Sandia Corporation, Albuquerque, New Mexico. The area of analysis described in this dissertation concerns the transient flow field which results when a plane blast wave intercepts a stationary cone at zero angle of attack. A companion dissertation, also part of this current investigation, is being conducted by Mr. Lynn Tyler and is concerned with the transient flow field properties resulting from a plane shock wave emerging into both still and supersonic streams. Shock tube experiments are being conducted to verify this analysis.

Future investigations relating to this work are being conducted by Mr. William Walker and Mr. Roger Eaton, both Ph.D. candidates at Oklahoma State University. Mr. Walker's concern will be the study of blast waves interacting with turbulent jet mixing regions. Mr. Eaton will perform studies to determine the various influencing parameters affecting a missile as it emerges from a blast. Both of these investigations should provide considerable knowledge of the mechanisms of blast-missile interactions.

The author wishes to take this opportunity to express his sincere appreciation to his academic advisor, Dr. Glen W. Zumwalt, Associate

Professor of Aerospace Engineering at Oklahoma State University, for his genuine interest and suggestions. His guidance and instruction have proven invaluable in the accomplishment of this work.

Appreciation is also extended to Professor L. J. Fila, Dr. J. A. Wiebelt, and Dr. O. H. Hamilton, Ph.D. committee members, whose cooperation and support during all phases of this research were of extreme value.

Acknowledgment is also extended to the Air Force Institute of Technology, United States Air Force, whose educational programs have made this advanced study possible. In addition, gratitude is expressed to the Air Force Weapons Laboratory (AFWL), Kirtland AFB, Albuquerque, New Mexico, whose computing facilities were made available for this work.

In accord with this opportunity, the author would be remiss if he failed to mention the sacrifices made during the preparation of this dissertation by his wife, Bobbie, and his two daughters, Patti and Terri, to whom this paper is dedicated.

TABLE OF CONTENTS

Chapter	Page
I. INTRODUCTION	1
II. BLAST-FOREBODY INTERACTION: WHITHAM'S THEORY AND TESTS	6
Method Analysis: Phase I	8
Computer Solution for Forebody Blast Passage . . .	17
Shock Tube Pressure Tests	24
Test Facility	24
Test Model	27
Test Analysis and Results	31
III. BLAST-BASE INTERACTION: RUSANOV'S METHOD	44
Method Analysis: Phase II	46
Boundary Conditions	53
Initial Shock Wave Representation	58
Dimensionalization Technique	61
Computer Solution for Blast-Base Interaction . . .	68
Analysis and Results of Computer Solution	69
Forebody Exploratory Problem	102
IV. BASE PRESSURE ANALYSIS	103
Method Analysis: Phase III	105
V. CONCLUSIONS AND RECOMMENDATIONS	116
Conclusions	116
Specific Recommendations	118
SELECTED BIBLIOGRAPHY	120

TABLE OF CONTENTS
(Continued)

APPENDICES	Page
A. Whitham's Ray Tube Analogy	124
B. Whitham's A-M Relation	128
C. Whitham's Shock-Shock Relations	131
D. Computer Program for Axi-Symmetric Cone Solution. .	136
E. Moving Blast Wave Transformation	138
F. Calculations Using the Analysis of Zumwalt and Tang	141
G. Calculations for Shock Wave Initial Conditions -- Phase II	145
H. Computer Solution for Blast-Base Interaction -- Phase II	150
I. Stagnation Point Calculations	163
J. Computer Program for Forebody Exploratory Problem	165

LIST OF TABLES

Table	Page
I. Computer Calculations for Cone of 28.8 Degree Semi-Apex Angle	19
II. Computer Calculations for Cone of 13.347 Degree Semi-Apex Angle	21
III. Test Information for Pressure Tests	25
IV. Calculated Mach Shock Properties for Cone of 13.347 Degree Semi-Apex Angle	35
V. Selected Time Planes With Corresponding Time Calculations from Computer Solution	66

LIST OF FIGURES

Figure	Page
1. Schematic of Experimental Test Facility and Instrumentation System for Pressure Tests	26
2. Conical Model Configuration for Pressure Tests.	28
3. Typical Test Photograph of Plane Shock Wave Passing Stationary Conical Model.	29
4. Base Pressure-Time History Plots Obtained From Tests. . .	30
5. Calculated Position of a Shock Wave Diffracted by a Cone ($R = 1.2$, $\theta_c = 28.8^\circ$).	37
6. Calculated Position of a Shock Wave Diffracted by a Cone ($R = 1.03728$, $\theta_c = 13.347^\circ$).	38
7. Calculated Position of a Shock Wave Diffracted by a Cone for Various Mach Number Ratios	39
8. Plot of Mach Number Ratio, R , versus Shock-Shock Angle, χ , Semi-Cone Angle, θ_c , and Ray Angle, θ	40
9. Adaptation of Whitham's Solution for Shock Wave Representation in Phase II	43
10. Time Plane Versus Dimensionless Time From Computer Solution	67
11. Shock Position--Time Plane 0	73
12. Velocity Vector Plot in Base Region--Time Plane 66.	74
13. Constant Pressure Lines (Isobars) for Base Region--Time Plane 66	75
14. Constant Velocity Lines for Base Region--Time Plane 66. . .	76
15. Velocity Vector Plot in Base Region--Time Plane 126 . . .	77

LIST OF FIGURES (Continued)

Figure	Page
16. Constant Pressure Lines (Isobars) for Base Region-- Time Plane 126	78
17. Constant Velocity Lines for Base Region--Time Plane 126 .	79
18. Velocity Vector Plot in Base Region--Time Plane 166 . . .	80
19. Constant Pressure Lines (Isobars) for Base Region-- Time Plane 166.	81
20. Constant Velocity Lines for Base Region--Time Plane 166 .	82
21. Velocity Vector Plot in Base Region--Time Plane 196 . . .	83
22. Constant Pressure Lines (Isobars) for Base Region-- Time Plane 196.	84
23. Constant Velocity Lines for Base Region--Time Plane 196 .	85
24. Velocity Vector Plot in Base Region--Time Plane 260 . . .	86
25. Constant Pressure Lines (Isobars) for Base Region-- Time Plane 260.	87
26. Constant Velocity Lines for Base Region--Time Plane 260 .	88
27. Velocity Vector Plot in Base Region--Time Plane 320 . . .	89
28. Constant Pressure Lines (Isobars) for Base Region-- Time Plane 320.	90
29. Constant Velocity Lines for Base Region--Time Plane 320 .	91
30. Velocity Vector Plot in Base Region--Time Plane 380 . . .	92
31. Constant Pressure Lines (Isobars) for Base Region-- Time Plane 380.	93
32. Constant Velocity Lines for Base Region--Time Plane 380 .	94
33. Velocity Vector Plot in Base Region--Time Plane 440 . . .	95

LIST OF FIGURES (Continued)

Figure	Page
34. Constant Pressure Lines (Isobars) for Base Region-- Time Plane 440.	96
35. Constant Velocity Modulus Lines for Base Region-- Time Plane 440.	97
36. Pressure Pattern Curves Past Base Positions Over Range of Time Planes.	98
37. Blast Wave Simulation on a Water Table.	99
38. Comparison of Pressure History on the Base by Experiment and by Computation	102
39. Steady, Non-Bleed, Base Pressure Solution Using Zumwalt's Conical Wake Analysis	106
40. Flow Model for Zumwalt's Steady-State Conical Wake Analysis	108
41. Boundary Layer Development Over Cone for Various Blast Wave Positions	113

LIST OF SYMBOLS

A	area of ray tube
A_b	area of base
c	speed of sound
e	total energy; sum of kinetic energy and internal energy per unit volume
F^x	vector function defined on page <u>47</u>
F^y	vector function defined on page <u>47</u>
f	vector function defined on page <u>47</u>
g	conversion constant; $32.16 \frac{\text{lb}_m}{\text{lb}_f \text{ sec}^2}$ in English units
h_1	incremental spacing in x-direction; $h_1 = \Delta x$
h_2	incremental spacing in y-direction; $h_2 = \Delta y$
K(M)	function defined in Appendix B, Page <u>128</u>
k	term defined on page <u>48</u> ; $k = \frac{\sqrt{h_1^2 + h_2^2}}{h_1 h_2} \tau$
k_1	term defined on page <u>48</u> ; $k_1 = k \sin \chi$
k_2	term defined on page <u>48</u> ; $k_2 = k \cos \chi$
M	Mach number
\dot{m}	mass bleeding rate into or from the base region; lb_m/sec
max	maximum value
n	constant equal to 5.0743 in Chapter II; unit vector normal to shock-shock surface in Appendix C
P	pressure gauge locations (Figure 2, page <u>28</u>)

p	pressure
p_o	stagnation pressure of flow; psia
R	Mach number ratio; $R = M/M_s$
R_b	radius of base
\mathcal{R}	gas constant; $53.35 \frac{\text{lb}_f - \text{ft}}{\text{lb}_m - \text{of}}$ for air
r	horizontal mass flux component
s	vertical mass flux component
T	temperature
T_o	stagnation temperature of flow; $^{\circ}\text{R}$
t	time
t_v	time viscous mass entrainment begins
u	horizontal velocity component
v	vertical velocity component
w	modulus of velocity vector; $w = \sqrt{u^2 + v^2}$
x,r	coordinate distance along axis of symmetry and radial direction, respectively
x,y	coordinates of reference coordinate system

Greek

α	coordinate representing shock position in Whitham's Theory; "weighting factor" in x-direction in Rusanov's Theory
β	coordinate representing orthogonal trajectory, or ray of shock position in Whitham's Theory; "weighting factor" in y-direction in Rusanov's Theory
γ	ratio of specific heats; $\gamma = 1.4$ for air
ΔL	elemental length on a circular cylinder
\mathcal{K}	non-dimensional base bleed number; $\mathcal{K} \equiv \frac{\dot{m} \sqrt{T_o}}{A_b p_o} \sqrt{\frac{\mathcal{R}}{g\gamma}}$

η	angle variable; $\eta = \tan^{-1} r/x$
θ	angle made by the tangent of a ray at a point and the axis
θ_c	cone semi-apex angle
θ_w	conical shock wave angle
μ	function defined in Appendix B, page <u>128</u>
ν	viscosity term; $\nu = 1$ for axial symmetry
ρ	density
σ	Courant number; $\sigma_{m,\ell}^n = k(w+c)_{m,\ell}^n$
σ_o	constant defined on page <u>50</u>
τ	incremental time; $\tau = \Delta t$
Φ	vector function defined on page <u>48</u>
χ	shock-shock angle in Whitham's Theory; tangent relationship of grid system ($\chi = \tan^{-1} h_2/h_1$) in Rusanov's Theory
Ψ	function defined on page <u>47</u>
ω	constant defined on page <u>49</u>
∇	gradient

Subscripts

l	conditions relating to shock-shock position as used in Chapter II; condition before sudden expansion in base region as used in Chapter IV
b	condition at base of sudden expansion
c	conditions relating to cone surface
i	indicates successive positions
m, ℓ	coordinate distances in x and y direction, respectively
o	stagnation condition
s	conditions relating to shock wave

st steady-state condition
t condition at time t
t+ Δt condition at time t+ Δt
x conditions in undisturbed region ahead of shock
y conditions behind the shock
 ∞ free stream condition

Superscripts

n indicates nth time plane
n+1 indicates n+1th time plane

CHAPTER I

INTRODUCTION

The problem concerning the transient flow field caused by a plane blast wave intercepting a stationary blunt-based missile is one on which a great deal of attention has recently been focused. Concern has increased for the vulnerability of these missiles to structural failure upon flying through blast waves resulting from nuclear blasts. Such blasts might occur from an anti-missile device.

In testing for structural or radiation effects, however, it is often expedient to test the missile while it is stationary. This is currently being performed both in shock-tube tests at various laboratories and by high-explosive blasts past stationary models. These techniques provide excellent opportunities to evaluate the analytical methods suggested in the literature, and to provide a strong foundation for extensions to more complex blast interaction problems.

The recent work of G. W. Zumwalt and H. H. Tang (38)¹ was concerned with the analysis of a blast wave after it had passed beyond the immediate region of the body. They considered only missiles at supersonic speeds, having a highly evacuated base region and adjacent flow field already formed. Thus, the blast became a disturbance on the flow field. In Zumwalt and Tang's analysis, the very short time-pressure transients

1 () Refers to Selected Bibliography

in the base region due to wave reflections as the blast passes were neglected. For the aerodynamicist, this is admissible since the effect on drag is small. The structural analyst, however, must know how the forces are applied no matter how short their time duration. Hence, the purpose of this study is to seek detailed knowledge of the flow properties and wave patterns of a stationary blunt-based conical vehicle during the transient blast passage leading to the quasi-steady flow condition.

In conducting this study, the following limitations are specified:

- (a) The blast wave is planar; that is, its radius of curvature is extremely large in comparison to the conical body length.
- (b) The blast wave approaches the conical body from the head-on axial direction; that is, interception is at zero angle of attack.
- (c) The velocity of propagation of the blast wave is assumed constant throughout; that is, decay of the wave strength is negligible during passage around the body.
- (d) The flow behind the blast front is steady; that is, the decay of the pressure field occurs very slowly compared to the rate of blast wave passage.
- (e) Body configurations are limited to axi-symmetric conical shapes. Specifically, data is sought for a 13.347 degree semi-apex angle conical body.
- (f) The conical body is considered stationary for all times.
- (g) Turbulent flow exists in the separated boundary layer.
- (h) Ionization and other real gas effects are not included in

the analysis.

Within the spectrum of these assumptions, the main objectives include the establishment of techniques or methods of computing the various physical parameters associated with the flow. Since the flow is highly transient it is unsteady and contains both subsonic and supersonic regions.

In order to determine the various physical and thermodynamic parameters affecting the blast condition from the time the blast wave intercepts the conical body nose until the quasi-steady base flow condition is established, it is feasible to consider the analysis in three major phases:

Phase I: Blast wave diffraction over the stationary conical forebody.

Phase II: Interaction of the blast wave with the base region of the conical body.

Phase III: Transition to a steady separated flow condition at the base.

The Phase I problem will not, in this paper, be extended to include the transient conditions near the cone forebody which follow the passage of the shock wave. However, a short exploratory work is included to show the way to the solution of this phase of the phenomenon. The main effort will be concentrated on the more troublesome base region; i.e., Phases II and III.

Although no exact system for solving this highly transient flow problem can be found in the literature, several methods and techniques have been developed. Among the many existing theories or computation methods are those of Whitham (35), Lighthill (18), Chisnell (4),

Bryson and Gross (1), Von Neumann and Richtmyer (31), Lax (12), Payne (24), Ludloff and Friedman (19), Godunov (9), and Rusanov (27). Each has a different approach so that the theories differ in their applicable cases.

These and numerous other authors (see Selected Bibliography) have made significant contributions toward the understanding of shock propagation problems and attendant phenomena. The methods they have proposed, as well as other similar proposed methods, all share one limitation; the difficulty in solving the non-linear equations of motion reliably to describe the physical phenomena associated with a highly transient flow field. Even with many simplifications, an accurate determination of the time history of the expected flow properties requires heavy reliance on numerical procedures. The methods proposed in this analysis, however, attempt to utilize the most favorable combinations of these methods for the accomplishment of transient solutions for all phases of the problem.

In reviewing the literature, the methods proposed by Whitham (35) and Rusanov (27) appeared to possess the potential qualities necessary to successfully apply to the existing flow problem. For the Phase I condition, that is, diffraction of a plane shock wave by the stationary conical forebody, Whitham's (35) axi-symmetric similarity solution was adopted. Associated with this solution is the ability to predict the locus of the shock triple point as well as the shape and curvature of the Mach shock. For the Phase II solution, involving the interaction of the blast wave with the base region of the conical body, Rusanov's (27) finite difference technique was adapted. For Phase III, a mating

of the Phase II results with the steady-state base flow studies of Zumwalt and Tang was required.

Details of Whitham's method and its specific application to the cone of semi-apex angle of 13.347° are presented in Chapter II. In addition, Chapter II presents the experimental information from shock tube tests provided by Sandia Corporation and compares this data with results obtained from Whitham's technique. Chapter III outlines Rusanov's numerical scheme and includes the extension of his method to the analysis of flow conditions which occur at the base of the cone using Whitham's shock solution for the initial condition.

Various detailed computing procedures, computer programs, and supporting information are included in appendices, figures, and tables. The figures include shock propagations resulting from Whitham's solution, as well as numerous plots of the transient flow conditions obtained as a result of the adaptation of Rusanov's technique to the conical body. Among these are plots showing lines of constant pressure, constant velocity, and flow directions obtained for selected time planes leading to the final quasi-steady flow conditions. From these conditions, as discussed in Chapter III, the final base pressure analysis of Chapter IV is obtained. Finally, in Chapter V, a summary of conclusions and suggestions for continuing investigations is given.

CHAPTER II

BLAST-FOREBODY INTERACTION: WHITHAM'S THEORY AND TESTS

In this chapter, Whitham's technique (35) for the approximate calculation of the diffraction of shock waves past stationary bodies is adopted for the Phase I solution of the conical forebody. Associated with this solution is the ability to predict the locus of the shock triple point as well as the shape and location of the Mach shock at any time. Since this locus represents a Mach shock moving along the incident shock, Whitham calls it a "shock-shock." As part of the description of a shock-shock for a conical diffraction, it may be described as a discontinuity in Mach number and shock slope. Specifically, a shock-shock locus may be regarded as a straight line emanating from the cone apex and inclined by an angle χ (shock-shock angle) with respect to the conical axis of symmetry. Details of Whitham's shock-shock relations are discussed in Appendix C.

Essentially based on kinematic considerations, the theory predicts only the shock wave pattern. It does not yield the pressure distribution over the diffracted body, or the flow field following the shock, nor does it predict the shape or curvature of reflected shocks. Given the shock pattern, one must develop other techniques for the determination of pressure distribution; for example, a numerical field-computation method such as Rusanov's (27).

Initially, Whitham (34) investigated two-dimensional problems on the interaction of a blast wave with various stationary bodies. In these investigations, disturbances to the flow are considered as wave propagations on the shocks. These wave propagations cause variations in the Mach number and slope of the shock. In one particular investigation, Whitham (34) compared his approximate calculation of a blast wave diffracted past a stationary wedge with that calculated by Lighthill (17,18). In Lighthill's analysis, the disturbed flow is regarded as a small perturbation with respect to the uniform flows, separated by the blast wave. Lighthill's conical flow techniques were later extended by Smyrl (28) to a wedge traveling at supersonic speeds. Smyrl's closed form solution for the pressure field behind an arbitrary plane shock was also applied to thin, supersonic airfoils.

After his two-dimensional investigations, Whitham (35) extended his approximate theory of shock dynamics to include general three-dimensional problems. The extension is merely a mathematical manipulation of equations; the basic assumptions remain the same. Generally, Whitham applied his theories to cones of arbitrary semi-cone angles. Specifically, he obtained results for a cone of 28.8° semi-apex angle.

Bryson and Gross (1) obtained experimental confirmation of Whitham's axi-symmetric calculations for a cone. They also extended his technique for blunt bodies and obtained experimental confirmation for cylinders and spheres.

In the present study, Whitham's axi-symmetric analytical results are reproduced using the IBM 1410 electronic computer. A detailed discussion of the techniques used, along with specific application to the cone of

semi-apex angle of 13.347° , is presented in the following analysis.

Method Analysis: Phase I

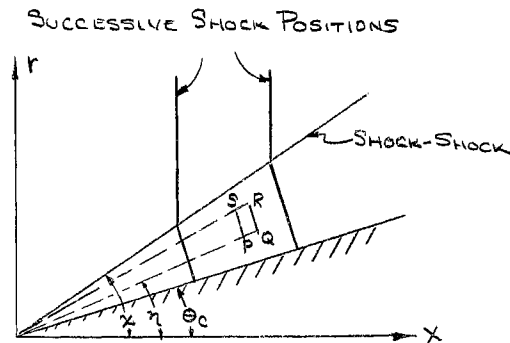
For axi-symmetrical problems such as the diffraction of a plane shock wave past a cone, the flow may be described in terms of independent variables based on purely kinematic relationships. To establish these relationships, Whitham considered the set of curves formed by the successive positions of a curved shock as it moves through a uniform medium. The orthogonal "trajectories" or lines of progress of this set of curves, termed rays, are introduced so as to form a general network of shock positions and rays. This typical network can be considered as the basis for orthogonal coordinates in the plane. Accordingly, the coordinates (α, β) are introduced such that the shock positions are the curves $\alpha = \text{constant}$ and the orthogonal trajectories are the curves $\beta = \text{constant}$.

In his analysis, Whitham considered a portion of the shock wave moving along a narrow tube of neighboring rays. This was suggested by the similarity of the propagation in a ray tube to the propagation of a shock in a tube with solid walls. In Appendix A, this analogy is discussed with a view toward developing the appropriate mathematical relationships. Whitham's basic theoretical assumption is that the Mach number, M , of the shock wave and the area, A , of the ray tube are functionally related; that is, A is a function of M only.

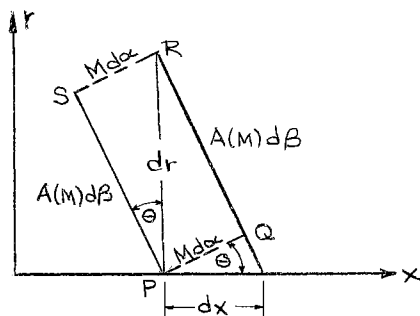
$$A = A(M) \quad . \quad (1)$$

This relationship was taken directly from results obtained from Chisnell (4), and is further discussed in Appendix B.

To develop the relationships used in the analysis, consider the cross section of a cone in the (x, r) plane.



In curvilinear coordinates, isolating the elemental region $PQRS$ results in the following.



Note that the solid lines are the constant α lines and represent successive shock positions. The dotted lines are constant β lines and represent the orthogonal trajectories, or rays, of the shock positions. Further, the angle $\theta(\alpha, \beta)$ is the angle of the tangent of the ray at a fixed point from the axial direction. M , of course, is the shock Mach number and is a function of α and β .

In this coordinate system, the choice of independent variables based

on the shock positions and rays is formulated by describing the motion of the shock as

$$c_x t = \alpha(x, r) \quad . \quad (2)$$

In this expression, t is the time at which the shock occupies a specific position and c_x is the speed of sound in the undisturbed gas ahead of the shock.

Geometrically, the above sketch yields the following relationships in terms of M and θ . That is,

$$\cos \theta = \frac{M(\alpha, \beta) d\alpha}{dx} \quad \text{and} \quad \sin \theta = \frac{M(\alpha, \beta) d\alpha}{dr} \quad . \quad (3)$$

Since $\alpha = \alpha(x, r)$, it is possible to write these expressions as

$$\alpha_x \equiv \frac{\partial \alpha}{\partial x} = \frac{\cos \theta}{M} \quad \text{and} \quad \alpha_r \equiv \frac{\partial \alpha}{\partial r} = \frac{\sin \theta}{M} \quad . \quad (4)$$

Taking the partial derivative of α_x with respect to r and the partial derivative of α_r with respect to x , these expressions become

$$\alpha_{xr} = \frac{\partial^2 \alpha}{\partial x \partial r} = \frac{\partial}{\partial r} \left[\frac{\cos \theta}{M} \right] \quad \text{and} \quad \alpha_{rx} = \frac{\partial^2 \alpha}{\partial r \partial x} = \frac{\partial}{\partial x} \left[\frac{\sin \theta}{M} \right] \quad .$$

However, for continuous functions,

$$\frac{\partial^2 \alpha}{\partial x \partial r} = \frac{\partial^2 \alpha}{\partial r \partial x} \quad .$$

Therefore, the expression above simply reduces to

$$\frac{\partial}{\partial x} \left[\frac{\sin \theta}{M} \right] - \frac{\partial}{\partial r} \left[\frac{\cos \theta}{M} \right] = 0 \quad . \quad (5)$$

From his ray tube analogy (See Appendix A), Whitham obtained the kinematic relations

$$\nabla \cdot \left[\frac{M}{A} \nabla \alpha \right] = 0 \quad \text{and} \quad M = \frac{1}{|\nabla \alpha|} \quad . \quad (6)$$

In cylindrical coordinates, the first expression may be expanded as

$$\nabla \cdot \left[\frac{M}{A} \nabla \alpha \right] = \frac{1}{r} \frac{\partial}{\partial r} \left[r \frac{M}{A} (\nabla \alpha)_r \right] + \frac{\partial}{\partial x} \left[\frac{M}{A} (\nabla \alpha)_x \right] = 0 \quad .$$

However, from the definition of gradient and from equation (4), the relations

$$(\nabla \alpha)_x \equiv \frac{\partial \alpha}{\partial x} = \frac{\cos \theta}{M} \quad \text{and} \quad (\nabla \alpha)_r \equiv \frac{\partial \alpha}{\partial r} = \frac{\sin \theta}{M} \quad ,$$

are obtained. Substituting these values into the equation above, the expression reduces to

$$\nabla \cdot \left[\frac{M}{A} \nabla \alpha \right] = \frac{\partial}{\partial r} \left[\frac{r \sin \theta}{A} \right] + r \frac{\partial}{\partial x} \left[\frac{\cos \theta}{A} \right] = 0 \quad .$$

Since r is an independent variable, the resulting geometrical relationship may be expressed as

$$\frac{\partial}{\partial x} \left[\frac{r \cos \theta}{A} \right] + \frac{\partial}{\partial r} \left[\frac{r \sin \theta}{A} \right] = 0 \quad . \quad (7)$$

In Whitham's cone solution, the only parameters prescribed are the initial shock Mach number, M_s , and the cone semi-apex angle, θ_c ; there is no length. Therefore, in the solution M and θ must be functions of the single variable η , where

$$\eta = \tan^{-1} r/x \quad (8)$$

Of course, since A is functionally related to M , an expression involving A and θ as functions of η must also be obtained. Hence, it is desired to write equations (5) and (7) in terms of the given variable. This may be accomplished by differentiating equation (5) and simplifying to give:

$$\left[\cos \theta \frac{\partial \eta}{\partial r} - \sin \theta \frac{\partial \eta}{\partial x} \right] \frac{1}{M} \frac{\partial M}{\partial \eta} = - \left[\cos \theta \frac{\partial \eta}{\partial x} + \sin \theta \frac{\partial \eta}{\partial r} \right] \frac{\partial \theta}{\partial \eta} .$$

Differentiation of equation (8), gives

$$\frac{\partial \eta}{\partial x} = \frac{-r}{x^2+r^2} \quad \text{and} \quad \frac{\partial \eta}{\partial r} = \frac{x}{x^2+r^2} .$$

Substituting these two expressions and rearranging terms:

$$\frac{1}{M} \frac{\partial M}{\partial \eta} = \left[\frac{\tan \eta - \tan \theta}{1 + \tan \eta \tan \theta} \right] \frac{\partial \theta}{\partial \eta} = \tan(\eta - \theta) \frac{\partial \theta}{\partial \eta} .$$

Since the dependent variables are functions of a single independent variable, this expression is written in its final form as

$$\frac{1}{M} \frac{dM}{d\eta} = \tan(\eta - \theta) \frac{d\theta}{d\eta} . \quad (9)$$

Hence, equation (5) is shown to be written in terms of η , where M and θ are functions of η only.

Similarly, to obtain equation (7) in terms of η , it is differentiated and simplified to

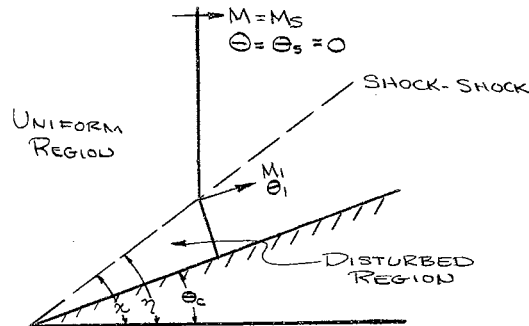
$$- \frac{1}{A} \frac{\partial A}{\partial \eta} = \left[\frac{\partial \theta}{\partial \eta} + \frac{\tan \theta}{\sin \eta \cos \eta (1 + \tan \eta \tan \theta)} \right] \cot(\eta - \theta) .$$

Since A and θ are functions of η only, the expression above, as reduced from equation (7), is written in its final form as

$$-\frac{1}{A} \frac{dA}{d\eta} = \left[-\frac{M}{A} \frac{dA}{dM} \right] \frac{1}{M} \frac{dM}{d\eta} = \left[\frac{d\theta}{d\eta} + \frac{\tan \theta}{\sin \eta \cos \eta (1 + \tan \eta \tan \theta)} \right] \cot(\eta - \theta) \quad (10)$$

Thus, Whitham was able to express the changes in Mach number and shock wave area in the η -direction, for an element of the shock wave, in terms of its η -direction and its direction of movement. Note that for the undiffracted shock far from the body, $\theta = 0$, and thus both $dM/d\eta$ and $dA/d\eta$ equal zero.

As can be seen from the following sketch, a shock-shock separates the uniform region from the disturbed region.



For the variable angle, η , equal to the shock-shock angle, χ , the equations

$$\tan(\theta_1 - \theta_s) = \frac{(M_1^2 - M_s^2)^{1/2} (A_s^2 - A_1^2)^{1/2}}{A_1 M_1 + A_s M_s}$$

and

$$\tan(\chi - \theta_s) = \frac{A_s}{M_s} \left[\frac{M_1^2 - M_s^2}{A_s^2 - A_1^2} \right]^{1/2}$$

(11)

must be satisfied (See Appendix C for details). Hence, a solution to equations (9) and (10) is required such that at $\eta = \chi$,

$$\left. \begin{aligned} \theta &= \theta_1, \quad M = M_1, \\ \tan \theta_1 &= \frac{(M_1^2 - M_s^2)^{1/2} (A_s^2 - A_1^2)^{1/2}}{A_1 M_1 + A_s M_s}, \\ \tan \eta &= \frac{A_s}{M_s} \left[\frac{M_1^2 - M_s^2}{A_s^2 - A_1^2} \right]^{1/2}, \end{aligned} \right\} \quad (12)$$

Similarly, at the cone, $\theta = \theta_c$ and $\eta = \theta_c$. These relations are essentially the boundary conditions.

For strong shock waves, the A-M relation, developed in Appendix B as

$$\frac{A}{A_s} \sim \left[\frac{M_s}{M} \right]^n, \quad \text{where } n = 5.0743, \quad (13)$$

is introduced into the calculations. The introduction of this relationship allows a solution for a given cone for all M_s . To obtain such a solution, the following procedure is utilized.

Designating $M/M_s = R$, then $A/A_s = R^{-n}$. Since AM^n is constant across the shock-shock for any given shock, then differentiating $AM^n = \text{constant}$ yields

$$AnM^{n-1} + M^n \frac{dA}{dM} = 0.$$

Then

$$\frac{dA}{dM} = - \frac{AnM^{n-1}}{M^n} = - \frac{An}{M},$$

such that

$$n = - \frac{M}{A} \frac{dA}{dM}. \quad (14)$$

With this expression, it is now possible to obtain a single equation for $\theta(n)$ from equations (9) and (10). Substituting equations (9) and (14) into equation (10), then rearranging terms, the equation

$$\frac{d\theta}{dn} = \frac{\tan \theta}{\sin n \cos n (1 + \tan n \tan \theta) (n \tan^2(n-\theta) - 1)} \quad (15)$$

is obtained.

In order to obtain a single expression for $R(n)$, simply substitute $M = M_s R$, where M_s is a known constant, into the left side of equation (9). Then, by differentiating the left side, it can be seen that

$$\frac{1}{M} \frac{dM}{dn} = \frac{1}{R} \frac{dR}{dn}$$

Therefore, equation (9) may be written in terms of $R(n)$ and $\theta(n)$ as

$$\frac{1}{R} \frac{dR}{dn} = \tan(n-\theta) \frac{d\theta}{dn} \quad (16)$$

To complete the development of the desired equations for a solution for a given cone, equation (12), at $n = \chi$, becomes

$$\tan \theta_1 = \frac{(M_s^2 R_1^2 - M_s^2)^{1/2} (A_s^2 - A_s^2 R_1^{-2n})^{1/2}}{(A_s R_1^{-n})(M_s R_1) + (A_s M_s)}$$

and

$$\tan \chi = \frac{A_s}{M_s} \left[\frac{M_s R_1^2 - M_s^2}{A_s^2 - A_s^2 R_1^{-2n}} \right]^{1/2}$$

These shock-shock relations reduce to final form in terms of R as

$$\tan \theta_1 = \frac{(R_1^2 - 1)^{1/2} (1 - R_1^{-2n})^{1/2}}{1 + R_1^{1-n}} \quad (17)$$

and

$$\tan \chi = \left[\frac{R_1^2 - 1}{1 - R_1^{-2n}} \right]^{1/2} \quad (18)$$

From the solutions for $\theta(\eta)$ and $R(\eta)$, as illustrated by equations (15) and (16), and the shock-shock relations of equation (17), the position of the shock wave at any time can be obtained. From similarity relationships, Whitham considers α to have the form $xf(\eta)/M_s$. Then

$$\alpha_x = \frac{1}{M_s} \left[f(\eta) - \sin^2 \eta f'(\eta) \right] = \frac{\cos \theta}{R}$$

and

$$\alpha_r = \frac{1}{M_s} \sin \eta \cos \eta f'(\eta) = \frac{\sin \theta}{R}$$

Combining these two expressions to solve for $f(\eta)$ yields

$$f(\eta) = \frac{\cos \theta + \sin \theta \tan \eta}{R}$$

Hence, at time t after the shock strikes the vertex of the cone,

$$\alpha = c_x t = \frac{xf(\eta)}{M_s} = \frac{c_x xf(\eta)}{u_s}$$

Therefore,

$$\frac{x}{u_s t} = \frac{1}{f(\eta)} = \frac{R}{\cos \theta + \sin \theta \tan \eta} \quad (19)$$

Also, since $x = r/\tan \eta$,

$$\frac{r}{u_s t} = \frac{1}{f(\eta)} \tan \eta = \frac{x}{u_s t} \tan \eta \quad (20)$$

Thus, Whitham has established, through equations (19) and (20), the position of the shock wave in terms of the parameter η .

Note that Whitham, from the preceding analysis, has shown that $x/u_s t$, $r/u_s t$, χ , and the distributions of θ and R with η are all independent of M_s . Hence, as specified for a given cone, all shock

waves go through exactly the same sequence of positions; the differences in u_s affect only the time scale. This theory fails to predict the conditions under which Mach reflection will not occur. For cone angles greater than 50° , or for very weak shocks ($M_s < 1.5$), regular reflection may occur and the Whitham results would be invalid.

Computer Solution for Forebody Blast Passage

To validate the computer program of Whitham's method, conditions were established to verify his results for a 28.8° semi-apex angle cone. Then the calculations were extended to include results for a 13.347° semi-apex angle cone. The equations for these solutions were programmed in FORTRAN IV on the IBM 1410 computer at Oklahoma State University. The detailed program is listed as Appendix D. Typical computer output for the two cones mentioned is illustrated in Tables I and II. The numerical integration of Whitham's first-order ordinary differential equations was accomplished by using Euler's Forward Integration Method.

To solve the problem, a value of Mach number ratio, R_1 , at the shock-shock, was selected. Then the shock-shock relations of equations (17) and (18) were solved to obtain the initial ray angle, θ_1 , and the shock-shock angle, χ . These angles were taken at a point where χ equals the angle variable, η ; that is, at $\eta_1 = \chi$. Using the initial values of θ_1 and η_1 at $\eta_1 = \chi$, the linear expression of equation (15) was integrated numerically to obtain new values of ray angle, θ , at successive positions. Simultaneously, equation (16) was integrated for corresponding values of R at the successive positions. The iteration procedure was continued until $\theta = \eta$, at which time the common value was the cone

semi-apex angle, θ_c . The position of the shock wave at any time was then found directly from equations (19) and (20). Whitham especially notes that the coordinate positions, as well as the other variables taken with respect to η , are all independent of the shock Mach number, M_s .

For the integration of equations (15) and (16), Euler's method was selected for two reasons. First, the procedure is a self-starting one; that is, it depends only on the initial conditions in order to compute the dependent variable approximation at the next increment of the independent variable. Secondly, since no rapid changes in the slope of the shock pattern was expected, the method, despite its limited accuracy, was deemed satisfactory.

Euler's method is based on the approximation that the gradient of the function at a specific point is the same as the gradient at the next succeeding point. Each succeeding step depends only on the values at the beginning of the step. Obviously, the increments must be taken very small in order to achieve good overall accuracy. In the computer solution, an increment of .003 radians seemed to work well. Computer round-off error, however, can limit the minimum usable value of this increment.

Referring to the computer printout results shown in Tables I and II, the values enclosed in the printed box denote values which have been linearly averaged to obtain the cone-surface solution. For example, the enclosed values at the bottom of the ETXD and THXD columns denote the values which have been averaged to obtain the cone semi-apex angle, θ_c . The symbols ETXD and THXD, as well as all other symbols used in the computer program given in Appendix D, are defined in the computer nomenclature tabulation following the tables.

TABLE I
 COMPUTER CALCULATIONS FOR CONE OF 28.8 DEGREE SEMI-APEX ANGLE*

ETD = 35.84954
 THD = 22.42310
 R = 1.20000

ETXD	THXD	RX	DIST1	DIST2
35.84954	22.42310	1.20000	1.00000	.72253
35.67765	22.58502	1.20080	1.00000	.72254
35.50577	22.74519	1.20158	1.00146	.71903
35.33388	22.90379	1.20234	1.00293	.71553
35.16199	23.06099	1.20306	1.00441	.71205
34.99010	23.21694	1.20376	1.00589	.70858
34.81822	23.37177	1.20444	1.00738	.70511
34.64633	23.52563	1.20509	1.00887	.70166
34.47444	23.67862	1.20572	1.01037	.69821
34.30255	23.83086	1.20633	1.01188	.69478
34.13067	23.98245	1.20692	1.01339	.69136
33.95878	24.13351	1.20748	1.01491	.68794
33.78689	24.28412	1.20803	1.01644	.68453
33.61501	24.43436	1.20855	1.01797	.68114
33.44312	24.58434	1.20906	1.01951	.67775
33.27123	24.73413	1.20955	1.02106	.67437
33.09934	24.88381	1.21002	1.02262	.67100
32.92746	25.03345	1.21047	1.02418	.66763
32.75557	25.18314	1.21091	1.02574	.66428
32.58368	25.33294	1.21133	1.02732	.66093
32.41179	25.48293	1.21173	1.02890	.65759
32.23991	25.63318	1.21211	1.03049	.65426
32.06802	25.78375	1.21247	1.03208	.65094
31.89613	25.93472	1.21282	1.03368	.64762
31.72424	26.08614	1.21315	1.03529	.64431
31.55236	26.23809	1.21347	1.03691	.64101
31.38047	26.39064	1.21376	1.03853	.63772

*For Nomenclature See Page 23

TABLE I (Continued)

31.20858	26.54385	1.21404	1.04017	.63443
31.03670	26.69779	1.21431	1.04181	.63115
30.86481	26.85252	1.21455	1.04345	.62788
30.69292	27.00812	1.21478	1.04511	.62461
30.52103	27.16465	1.21499	1.04677	.62135
30.34915	27.32219	1.21519	1.04845	.61810
30.17726	27.48080	1.21536	1.05013	.61485
30.00537	27.64057	1.21552	1.05181	.61161
29.83348	27.80155	1.21566	1.05351	.60837
29.66160	27.96384	1.21578	1.05522	.60515
29.48971	28.12751	1.21588	1.05693	.60192
29.31782	28.29265	1.21596	1.05866	.59871
29.14593	28.45933	1.21602	1.06039	.59550
28.97405	28.62764	1.21607	1.06213	.59229
28.80216	28.79768	1.21609	1.06389	.58909
28.63027	28.96955	1.21609	1.06565	.58590
Average = 28.7999 ^o			Average= 1.06477	Average= .587495

TABLE II

COMPUTER CALCULATIONS FOR CONE OF 13.347 DEGREE SEMI-APEX ANGLE

ETD = 26.32423
 THD = 4.71434
 R = 1.03728

ETXD	THXD	RX	DIST1	DIST2
26.32423	4.71434	1.03728	1.00000	.49475
26.15234	4.88251	1.03848	1.00000	.49475
25.98046	5.03666	1.03957	1.00031	.49118
25.80857	5.18037	1.04056	1.00062	.48761
25.63668	5.31595	1.04149	1.00094	.48406
25.46479	5.44501	1.04235	1.00127	.48052
25.29291	5.56873	1.04317	1.00161	.47698
25.12102	5.68800	1.04394	1.00195	.47347
24.94913	5.80350	1.04468	1.00230	.46996
24.77724	5.91580	1.04539	1.00265	.46646
24.60536	6.02535	1.04606	1.00301	.46297
24.43347	6.13251	1.04672	1.00337	.45949
24.26158	6.23759	1.04734	1.00374	.45602
24.08970	6.34088	1.04795	1.00411	.45256
23.91781	6.44259	1.04854	1.00449	.44911
23.74592	6.54292	1.04911	1.00488	.44567
23.57403	6.64206	1.04967	1.00526	.44224
23.40215	6.74016	1.05021	1.00566	.43882
23.23026	6.83736	1.05074	1.00606	.43540
23.05837	6.93378	1.05125	1.00646	.43200
22.88648	7.02955	1.05175	1.00687	.42860
22.71460	7.12476	1.05224	1.00728	.42521
22.54271	7.21950	1.05272	1.00770	.42183
22.37082	7.31388	1.05319	1.00812	.41845
22.19893	7.40797	1.05365	1.00854	.41509
22.02705	7.50185	1.05409	1.00898	.41173
21.85516	7.59559	1.05453	1.00941	.40838
21.68327	7.68926	1.05497	1.00985	.40504
21.51139	7.78294	1.05539	1.01030	.40170
21.33950	7.87667	1.05580	1.01074	.39837
21.16761	7.97052	1.05621	1.01120	.39505
20.99572	8.06456	1.05661	1.01166	.39173
20.82384	8.15883	1.05700	1.01212	.38843
20.65195	8.25339	1.05738	1.01259	.38512

TABLE II (Continued)

20.48006	8.34829	1.05776	1.01306	.38183
20.30817	8.44360	1.05813	1.01353	.37854
20.13629	8.53935	1.05850	1.01402	.37526
19.96440	8.63561	1.05885	1.01450	.37198
19.79251	8.73241	1.05921	1.01499	.36871
19.62062	8.82982	1.05955	1.01549	.36545
19.44874	8.92789	1.05989	1.01599	.36219
19.27685	9.02666	1.06022	1.01649	.35893
19.10496	9.12619	1.06055	1.01700	.35569
18.93307	9.22653	1.06087	1.01752	.35244
18.76119	9.32772	1.06118	1.01804	.34921
18.58930	9.42984	1.06149	1.01857	.34597
18.41741	9.53292	1.06179	1.01910	.34275
18.24553	9.63703	1.06208	1.01963	.33953
18.07364	9.74221	1.06237	1.02017	.33631
17.90175	9.84854	1.06265	1.02072	.33310
17.72986	9.95606	1.06293	1.02127	.32989
17.55798	10.06483	1.06320	1.02183	.32669
17.38609	10.17493	1.06346	1.02239	.32349
17.21420	10.28642	1.06371	1.02296	.32030
17.04231	10.39936	1.06396	1.02353	.31711
16.87043	10.51382	1.06420	1.02411	.31393
16.69854	10.62987	1.06444	1.02470	.31075
16.52665	10.74759	1.06466	1.02529	.30757
16.35476	10.86706	1.06488	1.02589	.30440
16.18288	10.98835	1.06509	1.02650	.30123
16.01099	11.11156	1.06530	1.02711	.29807
15.83910	11.23677	1.06549	1.02772	.29491
15.66722	11.36407	1.06568	1.02835	.29175
15.49533	11.49357	1.06585	1.02898	.28859
15.32344	11.62535	1.06602	1.02962	.28544
15.15155	11.75954	1.06618	1.03027	.28230
14.97967	11.89624	1.06632	1.03092	.27916
14.80778	12.03557	1.06646	1.03158	.27601
14.63589	12.17767	1.06658	1.03225	.27288
14.46400	12.32265	1.06670	1.03292	.26974
14.29212	12.47067	1.06680	1.03361	.26661
14.12023	12.62188	1.06688	1.03430	.26349
13.94834	12.77643	1.06696	1.03500	.26036
13.77645	12.93449	1.06701	1.03571	.25724
13.60457	13.09626	1.06706	1.03643	.25412
13.43268	13.26191	1.06708	1.03716	.25100
13.26079	13.43166	1.06709	1.03790	.24788

Average = 13.34676

Average=
1.03753Average=
.24944

COMPUTER NOMENCLATURE

Symbols Used in Computer Program	Corresponding Definitions
R	$R_1 = M_1/M_s$ (initial value)
P	$n = 5.0743$
A	$R_1^2 - 1$
B	$1 - R_1^{-2n}$
C	$1 + R_1^{1-n}$
TH	$\theta_1 = \tan^{-1} \frac{(R_1^2 - 1)^{1/2} (1 - R_1^{-2n})^{1/2}}{1 + R_1^{-2n}}$
ET	$\eta = \tan^{-1} \left[\frac{R_1^2 - 1}{1 - R_1^{-2n}} \right]^{1/2}$
THX	variable θ (radians)
ETX	variable η (radians)
RX	variable R along Mach shock
TANET	$\tan \eta = \sin \eta / \cos \eta$
TANTH	$\tan \theta = \sin \theta / \cos \theta$
E	$\sin \eta \cdot \cos \eta$
F	$1 + \tan \eta \cdot \tan \theta$
TANDE	$\tan(\eta - \theta) = \sin(\eta - \theta) / \cos(\eta - \theta)$
G	$n \tan^2(\eta - \theta) - 1$
DTH	$d\theta/d\eta = \frac{\tan \theta / \sin \eta \cos \eta (1 + \tan \eta \tan \theta)}{(n \tan^2(\eta - \theta) - 1)}$
DR	$dR/d\eta = R \tan(\eta - \theta) d\theta/d\eta$
ETD	η (degrees)
THD	θ (degrees)
ETXD	variable η (degrees)
THXD	variable θ (degrees)
DIST1	$x/u_s t = R / \cos \theta + \sin \theta \cdot \tan \eta$ (Shock Position-X direction)
DIST2	$r/u_s t = (x/u_s t) \tan \eta$ (Shock Position-Y direction)

Shock Tube Pressure Tests

An experimental check of the preceding analysis was provided under the sponsorship of Sandia Corporation, Albuquerque, New Mexico. For this experimental program, a series of tests to measure conical model pressures were run at the six-foot shock tube facility of the Air Force Weapons Laboratory (AFWL) at Kirtland Air Force Base. The results were published in Sandia Corporation Field Testing Data Reduction Reports, Series 172, and are as shown in Table III. The experimental data which resulted from these tests included pressure-time histories of blast wave passage as well as blast wave photographs.

Randall (25) has provided an approximate analysis for the forebody pressure responses by using steady flow, second-order, supersonic cone theory. His quasi-steady approach to the transient flow resulted in excellent predictions for the forebody pressure distributions for comparison with the experimental data.

Test Facility

The AFWL shock tube test facility and installation arrangement for these tests are shown schematically as part of Figure 1. As seen in this figure, gauges P1 and P2 were installed to record a stagnation and a static pressure measurement, respectively, near the tube exit. These gauges enabled the flow conditions for the tests to be defined. In order to record the shock wave displacement-time history in the shock tube, three additional static pressure gauges, synchronized in time, were mounted in the combustion chamber and at two shock tube stations.

TABLE III
TEST INFORMATION FOR PRESSURE TESTS

Run No.	Angle of Attack	Ambient Pressure	Ambient Temperature
172-1	0	*24.380 inches Hg	61 ^o F
172-2	5	24.288	58
172-3	10	24.262	68
172-4	20	24.390	62
172-5	30	24.378	74
172-6	40	24.540	62
172-7	50	24.436	74
172-8	0	24.490	56
172-9	10	24.387	76
172-10	40	24.370	60

* Ambient Pressure was not available for this Run. A pressure of 24.380 "Hg was estimated from standard atmosphere tables for the test altitude at Albuquerque.

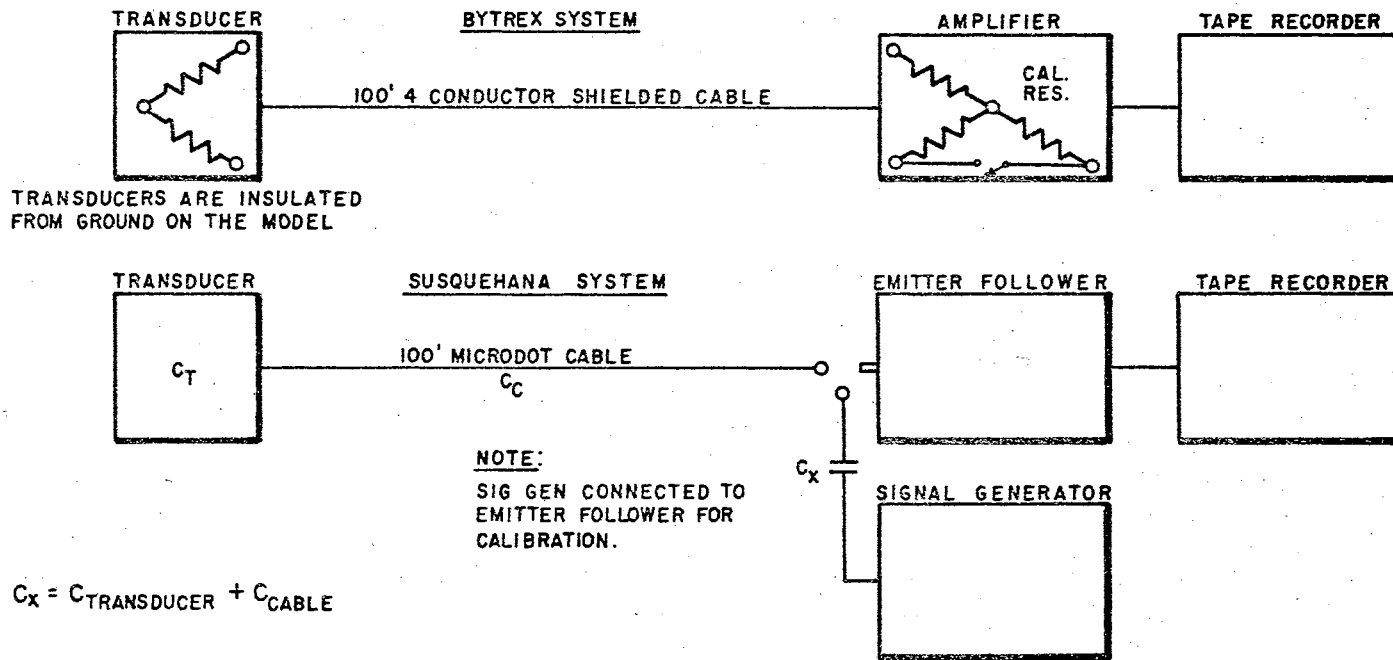
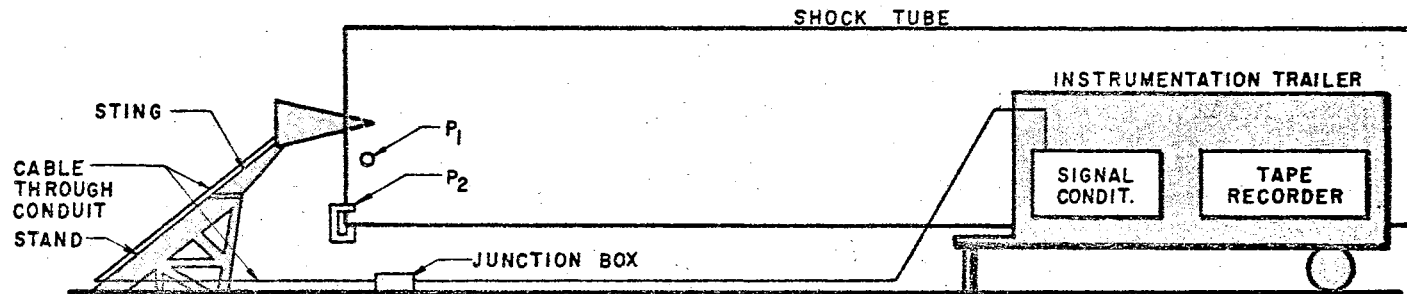


Fig. 1 SCHEMATIC OF EXPERIMENTAL TEST FACILITY AND INSTRUMENTATION SYSTEM FOR PRESSURE TESTS.

The facility consists of short flanged sections of six-foot diameter pipe bolted together to form a tube approximately 246 feet long. The tube is open to the atmosphere at the downstream end. A shock wave is generated by the detonation of primacord at the upstream end of the tube. During this series of tests, the maximum charge of 728 feet of 400 grain/foot primacord (approximately 41 pounds) was loaded over the first 20 feet of the tube. This produced peak shock overpressures of approximately 65 psi and a shock velocity of about 2800 feet per second at the open end of the tube. Holt and Crist(10) describe this facility in greater detail.

Test Model

The model tested consisted of a 13.347° half-angle cone with a spherical base formed by two tangent arcs. Six forebody pressures and three base pressures were recorded during the blast passage. The model configuration with dimensions and pressure locations is shown schematically in Figure 2. For the tests, the model was rigidly attached to a sting and support structure which was bolted to rails installed in the concrete pad at the tube exit. Model orientation was determined by a series of angle blocks installed between the model and sting, which resulted in discrete model pitch angles of 0, 5, 10, 20, 30, 40, and 50 degrees. Only the zero degree pitch angle is analyzed in this study; however, Randall considered all pitch angles. Figure 3 shows photographs of the shock passing the cone. The pressure-time history for the three transducers at the base of the cone is presented in Figure 4.

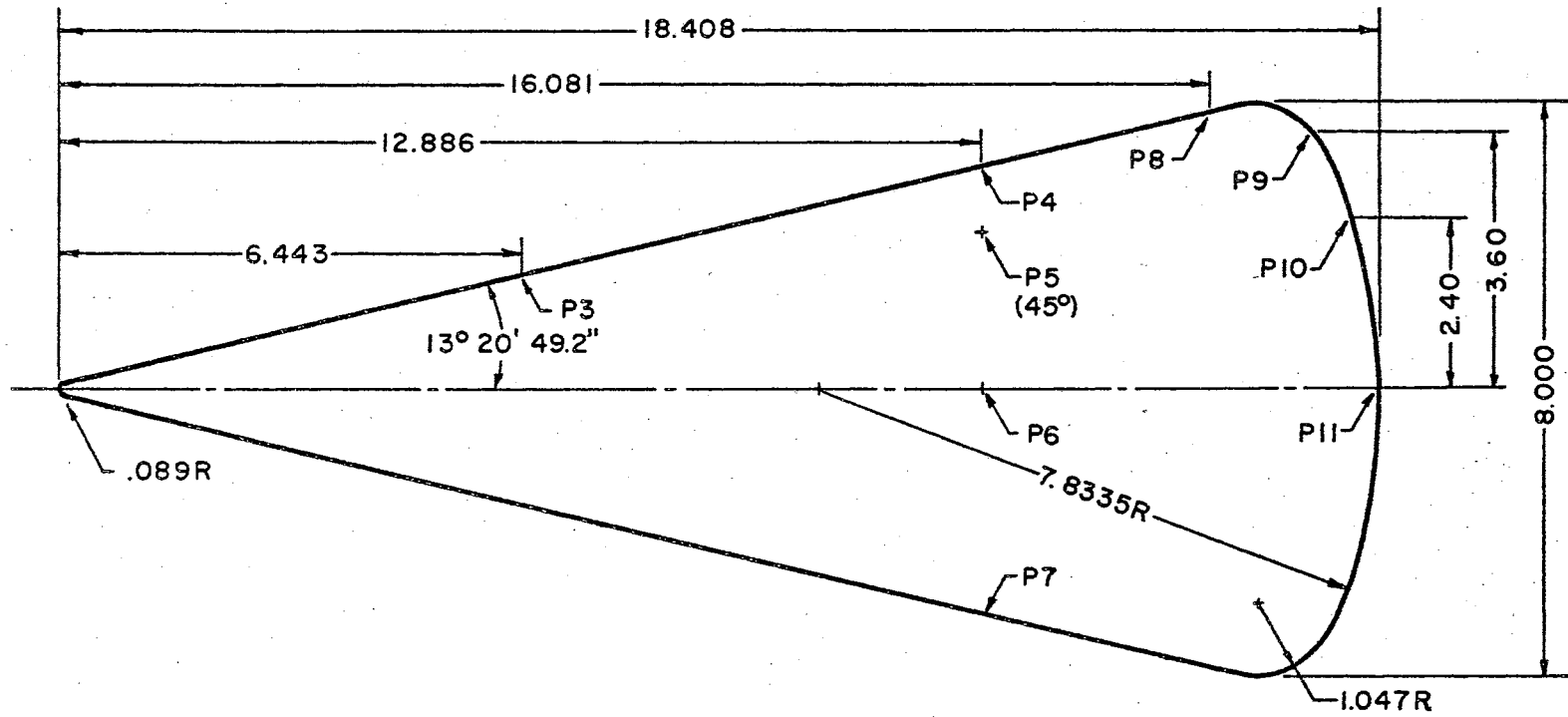


Fig. 2 CONICAL MODEL CONFIGURATION FOR PRESSURE TESTS

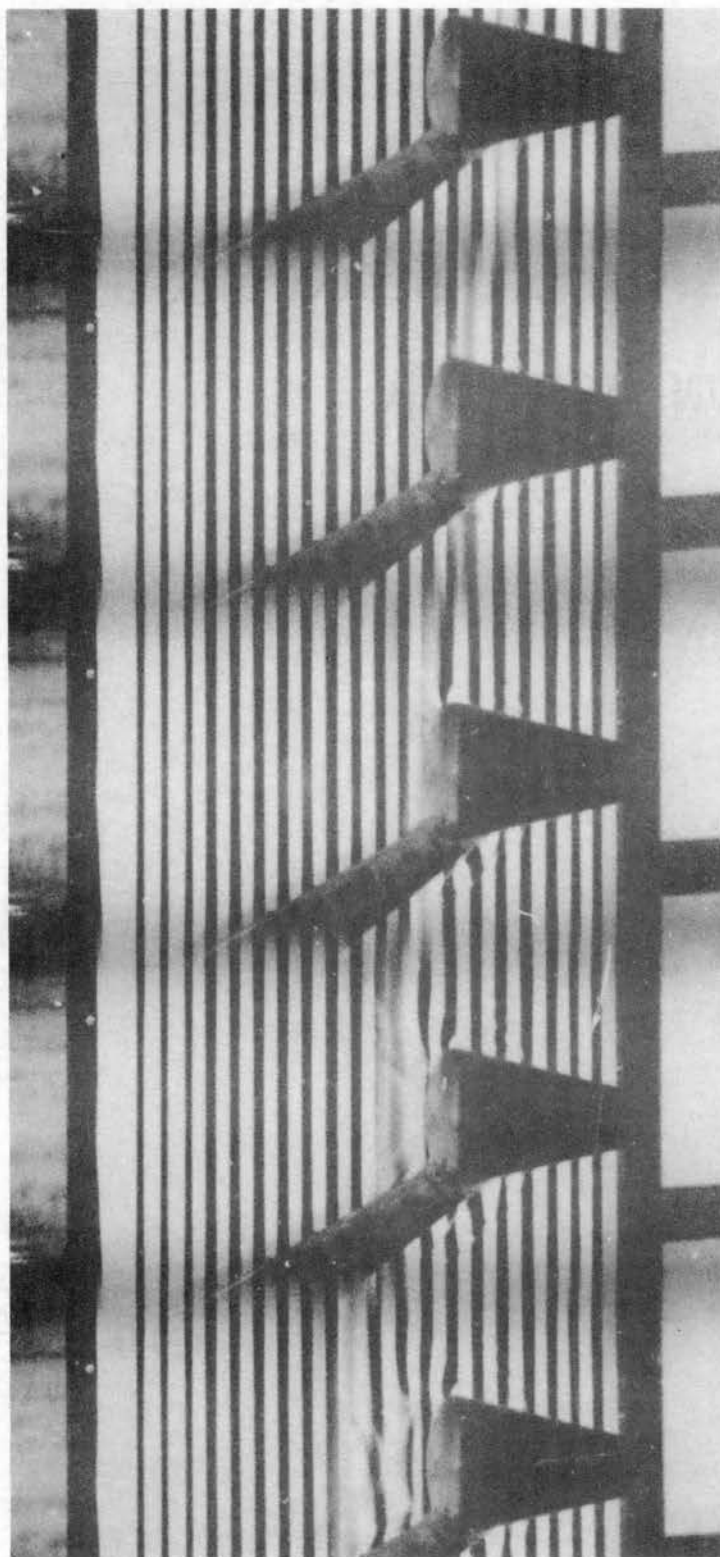


Fig. 3 Typical Test Photograph of Plane Shock Wave
Passing Stationary Conical Model

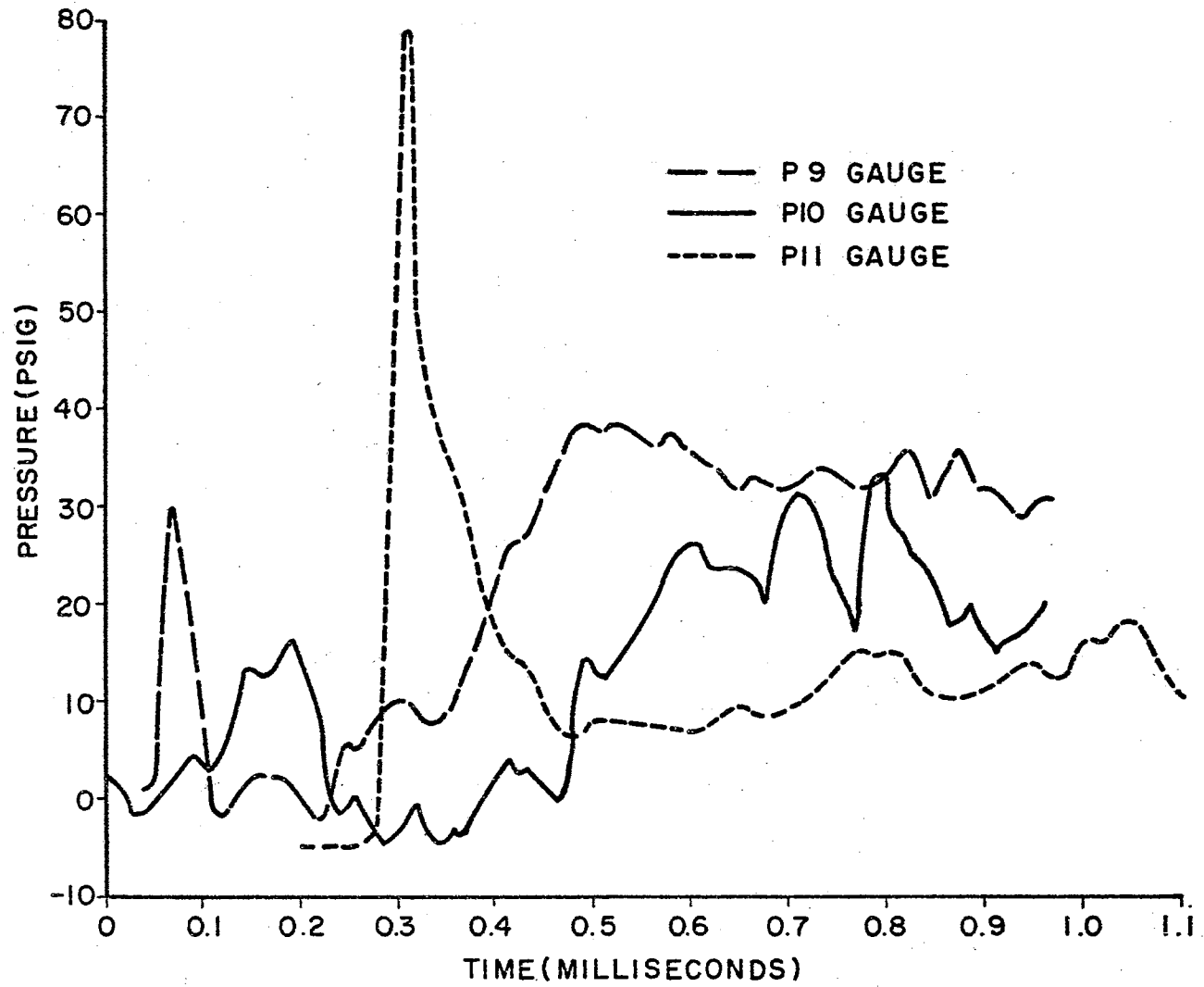


Fig. 4 BASE PRESSURE-TIME HISTORY PLOTS OBTAINED FROM TESTS.

Test Analysis and Results

In a preceding section, Whitham's theory was analyzed with a view toward establishing the appropriate solution for the Phase I shock diffraction problem. In this section, however, the experimental results of the shock tube tests are compared with Whitham's approximate technique. Although information is specifically sought for the 13.347° semi-apex angle cone, application may be made to cones of various semi-cone angles.

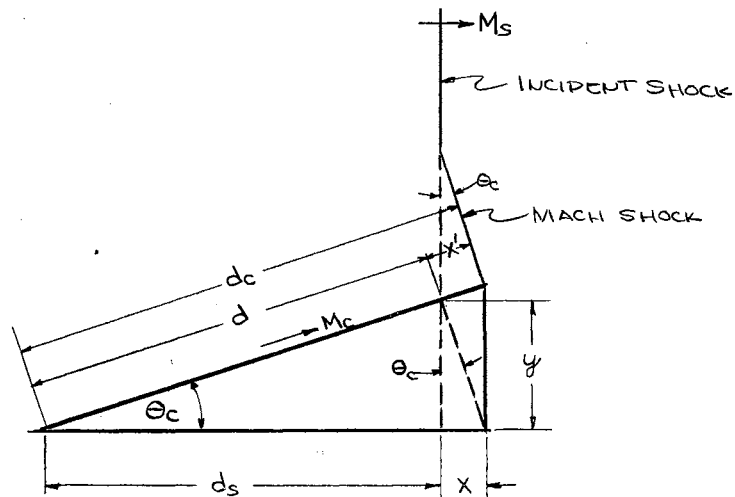
The analysis presented herein is based on a self-similar solution; that is, the size of the shock interaction configuration changes with time but not its shape. Since the period of time taken for a blast wave to pass over the forebody is relatively small, quasi-steady state conditions are assumed. This forms the basis for all calculations. The initial starting time, that is, time equals zero, occurs at the moment the blast wave intercepts the cone apex. The interaction begins with the head-on collision of the blast wave at the cone apex.

From the experimental data, the distance along the cone surface from pressure gauge P3 to pressure gauge P4 was 6.622 inches. The recorded true time for the shock to travel the distance from gauges P2 to P3 was determined to be 166 microseconds, and from gauges P2 to P4 was similarly recorded to be 337 microseconds. Hence, the true time for the shock wave to traverse the distance along the conical surface from gauges P3 to P4 was 171 microseconds. Therefore, a shock velocity, u_c , of approximately 3227 feet per second was produced over the conical model surface.

Although the ambient pressure was not available for this run (See Table III), the ambient temperature was recorded as 61° Fahrenheit. At this temperature, the velocity of sound was calculated to be 1118.9 feet per second. Since the shock Mach number is a function of the shock velocity and the speed of sound in the medium, the shock Mach number, M_c , at the conical surface was calculated to be 2.884. This value is assumed constant along the surface of the cone for all shock positions during the forebody blast passage.

Due to the manner in which the various pressure gauges and recording instruments were located and mounted for the experimental shock tube tests, minor difficulties were encountered in determining the actual shock velocity and strength before it intercepted the conical model. For example, the distance measurement between gauges used for the determination of the incident shock speed was not available in the data. Further, the quality of the test photographs (See Figure 3) did not permit exact locations of the shock wave to be determined for all times. Therefore, in order to use the test program data, it became necessary to rely upon an assumption of similarity of the wave pattern for determination of the incident shock properties and the attendant flow phenomenon.

To best illustrate this similarity relationship, consider the following sketch. In this representation the incident shock is assumed to be located a distance, d_s , from the cone apex measured along the axis of symmetry. For simplicity, this distance was specified as unity. The Mach shock, M_c , is assumed to be located a distance, d_c , from the cone apex measured along the surface of the cone. Hence,



the similarity relationship states that the ratio of the shock Mach number, M_c , along the surface of the cone, and the incident shock Mach number, M_s , is proportional to the ratio of their respective distances measured from the cone apex. That is,

$$\frac{M_c}{M_s} \sim \frac{d_c}{d_s}$$

Other physical dimensions relating to the sketch may be listed in the following manner:

$$d = d_s / \cos \theta_c = 1.02776$$

$$y = d_s \tan \theta_c = 0.23725$$

$$x = y \tan \theta_c = 0.05629$$

$$x' = x / \cos \theta_c = 0.05785$$

$$d_c = d + x' = 1.08561$$

Inserting the appropriate values into the similarity relationship, the incident shock Mach number, M_s , may be obtained as 2.657. This results in an experimental Mach number ratio, $R(\text{exp})$, of 1.0856.

Using this experimentally calculated value of M_s and the calculated value of the Mach number ratio, R , at the shock-shock (R is assumed constant along the Mach shock), the Mach number, M , at the shock-shock is obtained. From this value of M , using normal shock tables, the pressure, density, velocity, and other related properties across the shock may be determined.

In the report by Randall, the experimental incident shock wave velocity was estimated to be about 2800 feet per second. It was pointed out, however, that a consistently accurate measurement of the static pressure variation at the tube exit was extremely difficult, especially during passage of the shock front. The pressure response at this station apparently included a slight vibration of the experimental apparatus. As a result, it was necessary to use approximate values. Instrument response times undoubtedly contributed to these inaccuracies, at least to some degree. However, it is judged that Randall's value shows good correspondence with the experimental values obtained by the present analysis.

In comparing the results of these experimental calculations with that of Whitham, it is seen that remarkable agreement ensues, especially for the relationship of R at the surface of the cone. From the computer calculations of Whitham's theory as shown for point B at the cone surface in Table IV, the value of $R(\text{theory})$ is 1.067.

TABLE IV

CALCULATED MACH SHOCK PROPERTIES FOR CONE OF 13.347 DEGREE SEMI-APEX ANGLE

Point No.	RX	DIST1	DIST2	$M_X = M_s(RX)$	p_y/p_x	ρ_y/ρ_x	u_y	v_y
A	1.03728	1.00000	.49475	2.75569	8.69304	3.61769	2.29557	.54463
1	1.04672	1.00337	.45949	2.78077	8.85505	3.64377	2.32279	.55109
2	1.04734	1.00374	.45602	2.78242	8.86575	3.64542	2.32457	.55151
3	1.04795	1.00411	.45256	2.78404	8.87629	3.64704	2.32631	.55192
3a	1.04854	1.00449	.44911	2.78561	8.88648	3.64861	2.32800	.55232
4	1.05409	1.00898	.41173	2.80035	8.98232	3.66435	2.34412	.55615
5	1.05453	1.00941	.40838	2.80152	8.98991	3.66552	2.34538	.55645
6	1.05497	1.00985	.40504	2.80269	8.99751	3.66669	2.34664	.55675
6a	1.05539	1.01030	.40170	2.80381	9.00476	3.66781	2.34784	.55703
7	1.05989	1.01599	.36216	2.81576	9.08305	3.67976	2.36072	.56009
8	1.06022	1.01649	.35893	2.81664	9.08883	3.68064	2.36167	.56031
9	1.06055	1.01700	.35569	2.81751	9.09462	3.68151	2.36261	.56054
10	1.06087	1.01752	.35244	2.81836	9.10023	3.68236	2.36353	.56075
10a	1.06118	1.01804	.34921	2.81919	9.10567	3.68319	2.36441	.56096
11	1.06420	1.02411	.31393	2.82721	9.15862	3.69121	2.37306	.56302
12	1.06444	1.02470	.31075	2.82785	9.16283	3.69185	2.37375	.56318
13	1.06466	1.02529	.30757	2.82843	9.16668	3.69243	2.37438	.56333
14	1.06488	1.02589	.30440	2.82902	9.17054	3.69302	2.37501	.56348
15	1.06509	1.02650	.30123	2.82958	9.17422	3.69358	2.37561	.56362
16	1.06680	1.03361	.26661	2.83412	9.20421	3.69812	2.38051	.56478
17	1.06688	1.03430	.26349	2.83433	9.20561	3.69833	2.38074	.56484
18	1.06696	1.03500	.26036	2.83458	9.20723	3.69858	2.38101	.56490
19	1.06701	1.03571	.25724	2.83468	9.20789	3.69868	2.38111	.56493
20	1.06706	1.03643	.25412	2.83481	9.20877	3.69881	2.38126	.56496
B	1.06708	1.03753	.24944	2.83488	9.20920	3.69888	2.38133	.56498

It can be seen that the experimental value of R is slightly larger than the value predicted by theory. However, agreement exists within 1.7 percent between Whitham's theoretical calculations and the experimental results as deduced above.

According to Whitham, the Mach shock is almost a straight line, except for very small semi-apex angles. Actually, a slight curvature occurs which tends in the manner shown in Figures 5 and 6. These figures illustrate the calculated position and shape of the shock wave obtained from the computer output for two specific cones. In addition to the 13.347° semi-apex angle cone, several other semi-cone angles, along with their corresponding Mach number ratios, were considered. Several of the shock configurations obtained from these calculations were plotted and are presented in Figure 7. Note that in this figure an expended scale along the abscissa was used to facilitate a comparison of the variations in shock curvature for the various cones and Mach number ratios. In Figure 8, plots of various Mach number ratios, R , versus shock-shock angle, χ , semi-cone angle, θ_c , and ray angle, θ , are shown. These curves illustrate the relative relationships predicted by the theory for the variables indicated.

To determine the thermodynamic flow properties in the uniform flow behind the moving shock, a more complex procedure was employed. Since the blast is considered to be moving relative to a fixed coordinate system, the flow conditions are transient. In this physical plane, the total energy is not constant across the shock; therefore it becomes convenient to treat such a problem using a transformation of coordinates to a new transform plane having shock-fixed coordinates.

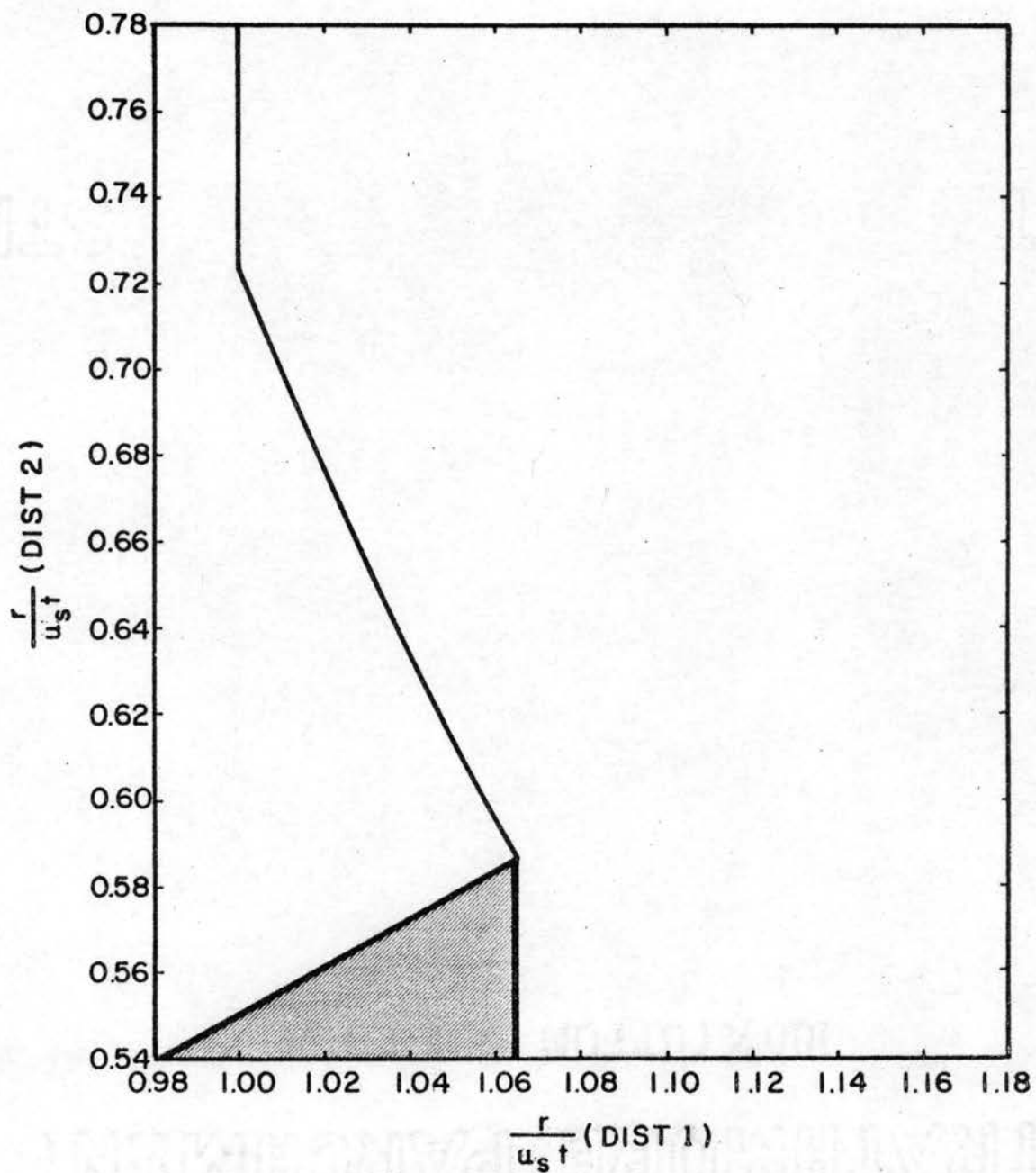


Fig. 5 CALCULATED POSITION OF A SHOCK WAVE DIF-FRACTED BY A CONE ($R=1.2$, $\theta_c = 28.8^\circ$)

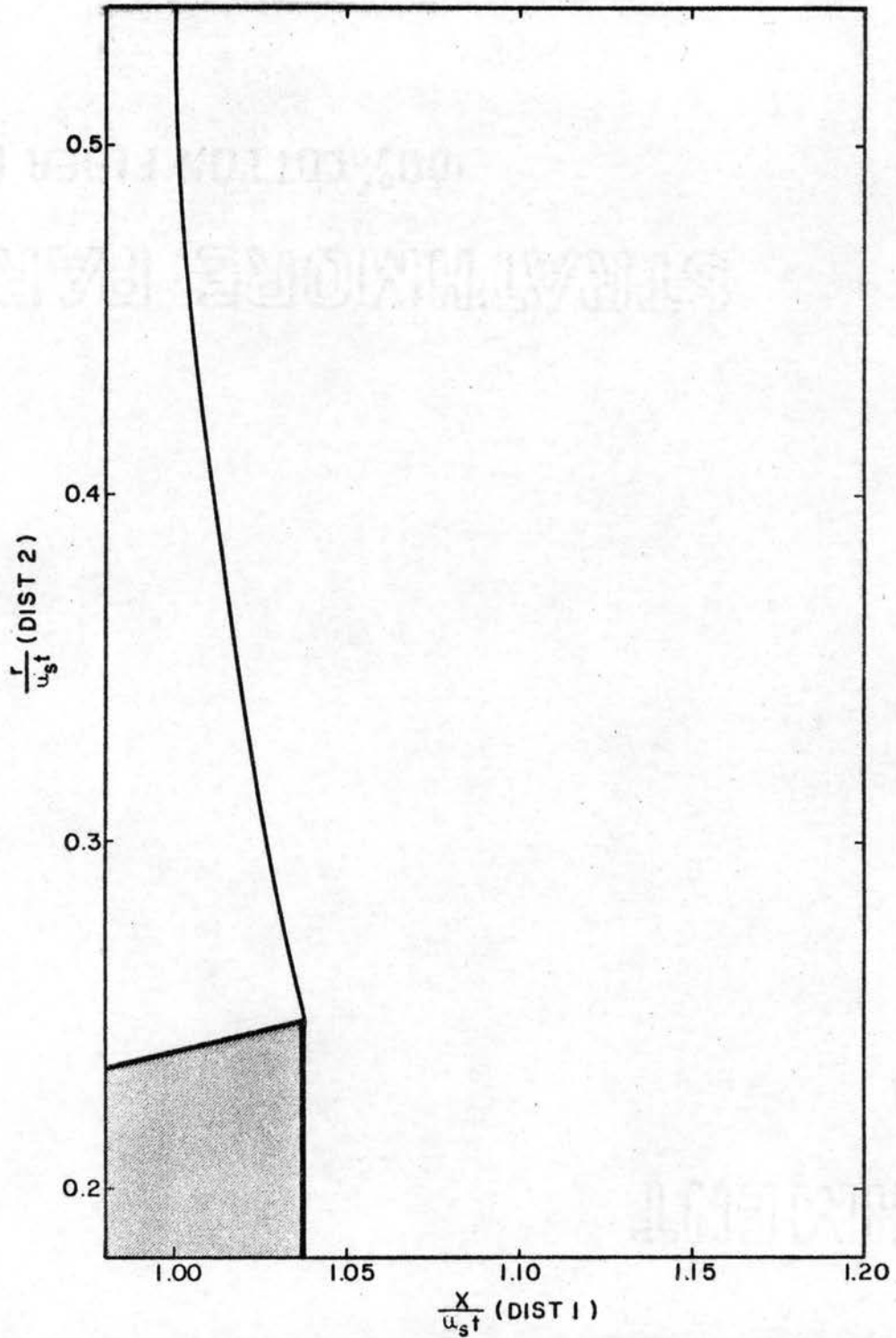


Fig. 6 CALCULATED POSITION OF A SHOCK WAVE DIFFRACTED BY A CONE ($R=1.03728$, $\theta_c = 13.347^\circ$)

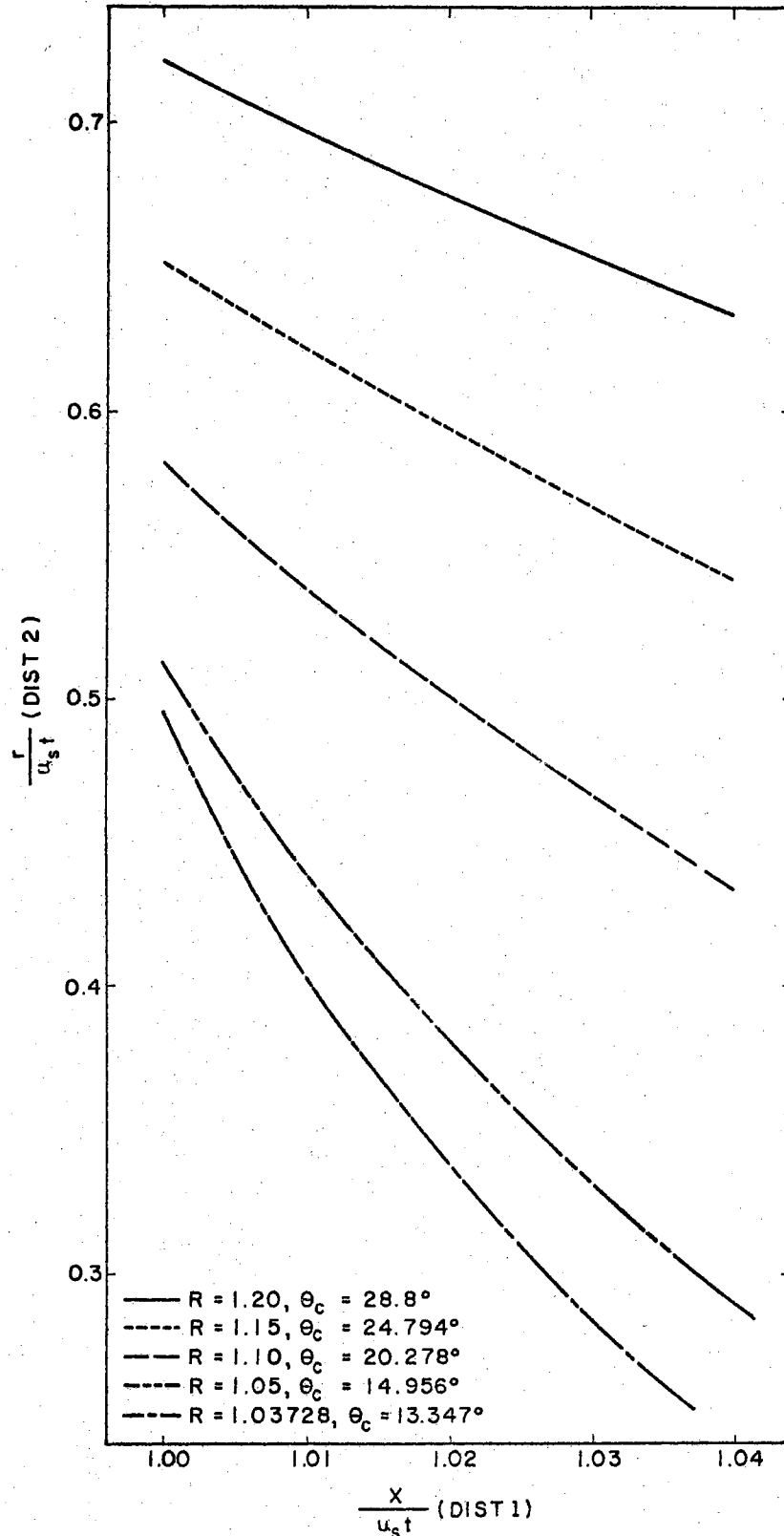


Fig. 7 CALCULATED POSITION OF A SHOCK WAVE DIFFRACTED BY A CONE FOR VARIOUS MACH NUMBER RATIOS.

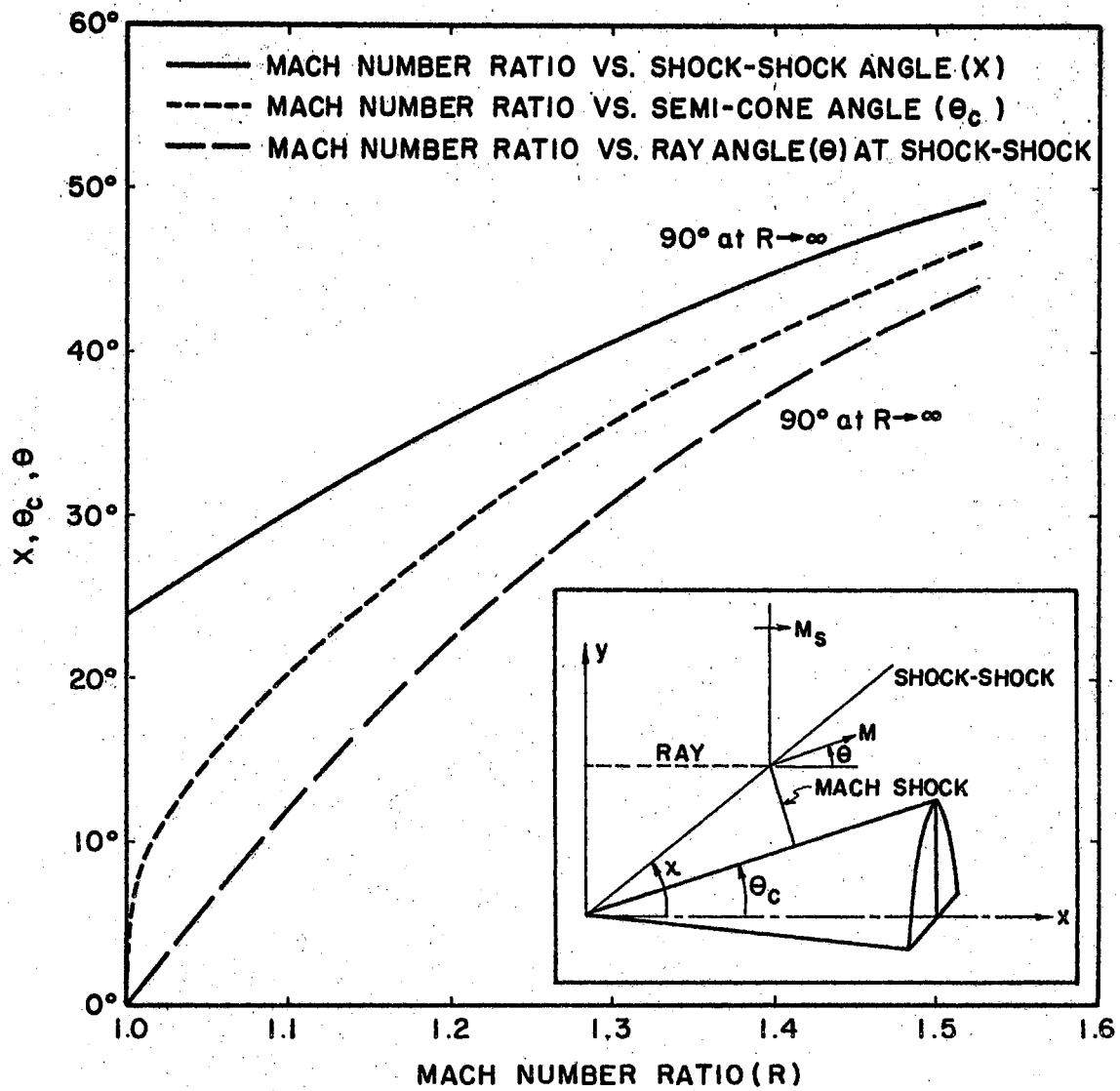


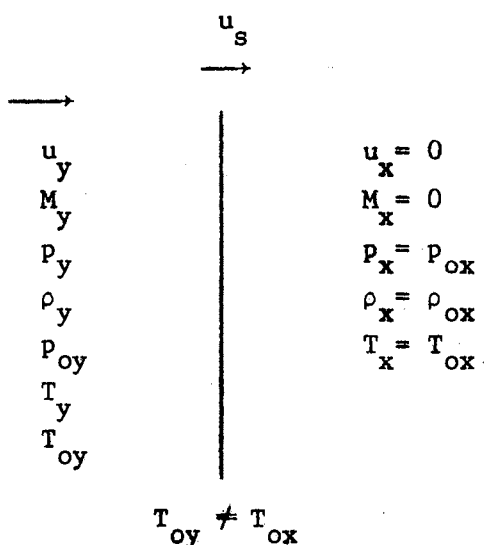
Fig. 8 PLOT OF MACH NUMBER RATIO R VERSUS X , θ_c , AND θ .

Then, after finding the desired flow properties, re-transform is made to the physical plane.

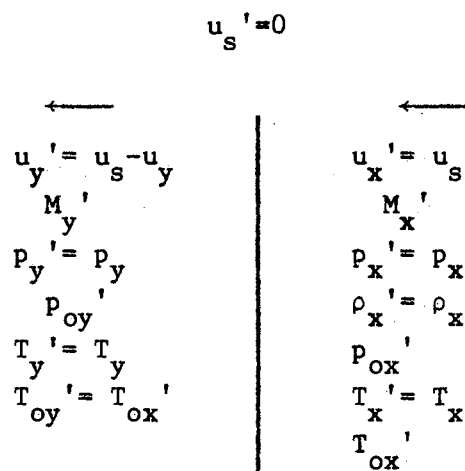
The calculations used to determine the Mach number of the incident shock implied a stationary shock in the transform plane. In this transform plane the blast wave is considered to be a normal shock wave. As such, the Rankine-Hugoniot relations were used to determine the unknown physical quantities in the flow field. For purposes of this analysis, the quantities in the transform plane are designated by a "prime" symbol, and quantities in the physical plane are designated without a "prime." Of specific note in this transformation, the stream properties remain invariant but stagnation properties change.

If the physical state of the quantities in front of the shock are denoted with an x subscript, the shock with an s subscript, and those behind the shock denoted with a y subscript, the following relationships are established.

Physical Plane (Moving Shock)



Transform Plane (Stationary Shock)



The arrows indicate flow direction relative to the respective coordinate systems. Note that the relationships in the transform plane are derived by superimposing an identical flow condition moving in a direction opposite to that in the physical plane. From the actual calculations, as shown in Appendix E, the flow Mach number behind the incident shock wave was 1.25.

For the 13.347° semi-apex angle cone, the property values, obtained by using this technique, are tabulated in Table IV for 25 selected Mach numbers at points along the Mach shock. In this table, point A identifies the point at the intersection of the incident shock and the Mach shock. Point B identifies the point where the Mach shock intersects the surface of the cone. The remaining 23 points correspond to selected intermediate shock Mach numbers along the Mach shock which were obtained from the iterative computer calculations. The relative locations of these points may be seen in Figure 9.

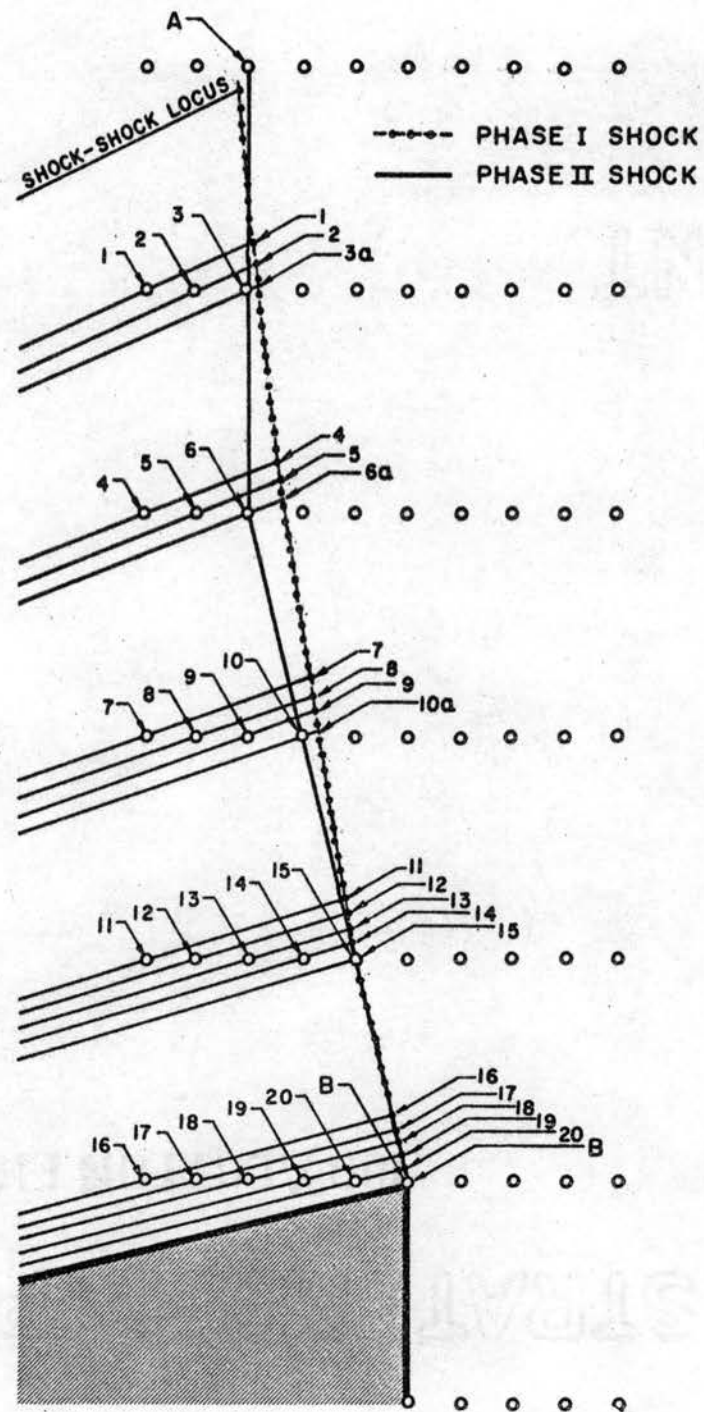


FIG. 9 - ADAPTATION OF WHITHAM'S SOLUTION FOR SHOCK-WAVE REPRESENTATION IN PHASE II.

CHAPTER III

BLAST-BASE REGION INTERACTION: RUSANOV'S METHOD

When solving an inviscid transient flow problem, such as encountered in this Phase II analysis, the solution leads to many mathematical complexities. The systems of partial differential equations which describe the complicated flow field are non-linear and cannot be integrated in closed form. Consequently, approximate methods of solution must be utilized. One of the most common and useful methods employed in the approximate integration of equations of this type, and which is of concern here, involves replacing the terms of the partial differential equations by their equivalent numerical relationships. Although many techniques have been devised to obtain such solutions, some of which are extremely ingenious from a practical point of view, the task of solving these equations still remains difficult.

Many authors have made significant contributions relating to approaches to the problem. Von Neumann and Richtmyer (31), for example, established an analysis for the stability of numerical calculations. In addition, they found that the inherent instabilities of these calculations are nearly eliminated if "artificial viscosity" terms are introduced. Successively, Lax (12), through modification of the time derivative in the finite difference technique, showed that these equations remain stable even without these pseudo-viscosity terms.

In contrast to Lax, Ludloff and Friedman (19) pointed out the advantages of leaving these equations in their original time-dependent form, that is, without modifying the time derivatives. To this end, they suggested solving these equations, whenever possible, not by reducing the number of independent variables through some transformation process, but by explicitly taking into account the non-steadiness of the problem. Later, Ludloff and Friedman formulated a two-dimensional solution to solve the problem of the reflection and diffraction of strong shocks around corners of arbitrary finite angles. They devised two methods, both of which involved finite difference schemes applicable to many non-linear problems.

Payne (24) used the finite difference technique of Lax to determine the flow behind converging cylindrical shocks over a large range of Mach numbers. In particular, his description of the increase in strength of converging shocks was shown to be in excellent agreement with the earlier studies of Chisnell (4). Payne's method introduced an artificial diffusion term which caused the pressure at the axis of symmetry to remain finite. However, a reflected diverging shock was obtained. Later, Chisnell obtained a higher order of approximation to this same problem to include re-reflected waves in his analysis.

Rusanov (27), in modifying the concepts of Lax's one-dimensional analysis, included solutions for both plane and axi-symmetric flows. His finite difference scheme, which is of special interest here, was applied successfully to the shock diffraction problem past the base of a cylinder. The scheme is constructed in such a way that discontinuities,

such as those caused by moving shock waves, can be included in the calculations. The discontinuities are actually considered as steep gradients in the physical parameters. Thus, the method permits calculations to be performed "through" discontinuities in the flow.

Rusanov's method utilizes the Eulerian system of coordinates which focuses attention on a fixed point in space. It specifies, at each instant of time, the physical parameters of the fluid particle which happens to occupy that point at that specific instant of time. Thus, the physical properties become functions of both time and location.

For the Phase II solution of this problem, that is, the interaction of the blast wave with the base region of a conical body, Rusanov's finite difference technique was utilized. An extension of his technique was accomplished to obtain the transient flow properties and the shock patterns from the time of blast-base interaction to the quasi-steady flow condition. Application of these concepts, as shown later in this chapter, yields excellent representations of the physical flow phenomena.

Method Analysis: Phase II

To describe the motion of the non-steady compressible flow as existing in this problem, an ideal gas with adiabatic index γ is assumed. The non-linear partial differential equations of motion are written in divergent form; that is, the coefficients of the derivatives are all equal to unity. This form of the equations ensures that the conservation laws are satisfied; hence, the unknown functions depend on the variables describing the state of the physical system.

The governing equations, in their divergent forms, are of the form

$$\frac{\partial f}{\partial t} + \frac{\partial F^x}{\partial x} + \frac{\partial F^y}{\partial y} + \psi = 0 \quad (21)$$

This expression represents the system of conservation equations which is to be satisfied numerically in order to solve for the various components of the vectors f , F^x , F^y , and ψ . The components of these four vectors are

$$f = \begin{Bmatrix} \rho \\ r \\ s \\ e \end{Bmatrix}, \quad F^x = \begin{Bmatrix} r \\ p+ru \\ rv \\ (e+p)u \end{Bmatrix}, \quad F^y = \begin{Bmatrix} s \\ su \\ p+sv \\ (e+p)v \end{Bmatrix}, \quad \psi = \frac{v}{y} \begin{Bmatrix} \rho \\ r \\ s \\ e+p \end{Bmatrix},$$

where $v=1$ when there is axial symmetry. In complete form, the conservation equations may be written as:

Conservation of mass:

$$\frac{\partial \rho}{\partial t} + \frac{\partial(\rho u)}{\partial x} + \frac{\partial(\rho v)}{\partial y} + \frac{v\rho}{y} = 0 \quad (22)$$

Conservation of two momentum components:

$$\frac{\partial r}{\partial t} + \frac{\partial(p+ru)}{\partial x} + \frac{\partial(su)}{\partial y} + \frac{vvr}{y} = 0 \quad (x\text{-direction}) \quad (23)$$

$$\frac{\partial s}{\partial t} + \frac{\partial(rv)}{\partial x} + \frac{\partial(p+sv)}{\partial y} + \frac{vvs}{y} = 0 \quad (y\text{-direction}) \quad (24)$$

Conservation of energy:

$$\frac{\partial e}{\partial t} + \frac{\partial\{(e+p)u\}}{\partial x} + \frac{\partial\{(e+p)v\}}{\partial y} + \frac{v(e+p)}{y} = 0 \quad (25)$$

where r , s , and e are defined as

$$r = \rho u, \quad s = \rho v, \quad \text{and} \quad e = \frac{\rho(u^2+v^2)}{2} + \frac{p}{\gamma-1} \quad (26)$$

If the vector ϕ is introduced such that

$$\phi = \begin{Bmatrix} u \\ v \\ p \\ \rho \end{Bmatrix}, \text{ with } w = \sqrt{u^2 + v^2} \text{ and } c = \sqrt{\frac{\gamma p}{\rho}}, \quad (27)$$

then the components of ϕ may be uniquely expressed in terms of the vector components of f as

$$u = \frac{r}{\rho}, \quad v = \frac{s}{\rho}, \quad \text{and } p = (\gamma - 1) \left[e - \frac{r^2 + s^2}{2\rho} \right]. \quad (28)$$

The dependence of the variables of ϕ on the various parameters of the problem is of special interest in this solution. Therefore, it is convenient to consider the equations in non-dimensional form. The dimensionalization technique used to satisfy this requirement is fully described in a later section of this chapter.

Essentially, the numerical solution for equations (22) to (25) consists of obtaining the numerical value of each unknown integral at pivotal points spaced in the (x, y, t) plane. A numerical network of pivotal points is established such that $\Delta x = h_1$, $\Delta y = h_2$, and $\Delta t = \tau$.

Designating

$$h = \sqrt{h_1^2 + h_2^2}, \text{ where } h_1 = h \cos \chi \text{ and} \\ h_2 = h \sin \chi,$$

and

$$k_i = \tau / h_i, \text{ where } k_1 = k \sin \chi \text{ and} \\ k_2 = k \cos \chi,$$

then it follows that

$$k = \sqrt{k_1^2 + k_2^2} = \frac{\sqrt{h_1^2 + h_2^2}}{h_1 h_2} \tau. \quad (29)$$

This expression is used to obtain the incremental time values for successive time planes of the entire flow region.

In the numerical analysis, the subscript (m, ℓ) is used to denote the pivotal point at which the derivative is to be evaluated. The subscripts $(m+1, \ell)$ and $(m-1, \ell)$ denote the pivotal points to the right and to the left of (m, ℓ) , respectively. Similarly, the subscripts $(m, \ell+1)$ and $(m, \ell-1)$ denote the pivotal points above and below (m, ℓ) , respectively. The superscript values denote the aggregate of pivotal points to be evaluated for a specific time plane. For example, the superscripts n and $n+1$ denote the n^{th} and the $(n+1)^{\text{th}}$ time planes, respectively.

The value of a quantity α at an interpolation point with coordinates $(mh_1, \ell h_2, n\tau)$ will be denoted by $\alpha_{m, \ell}^n$. Similarly, the value of a quantity β at an interpolation point with the same coordinates will be denoted by $\beta_{m, \ell}^n$. These quantities are defined as

$$\alpha_{m, \ell}^n = \omega k (w+c)_{m, \ell}^n \sin^2 \chi ,$$

and

$$\beta_{m, \ell}^n = \omega k (w+c)_{m, \ell}^n \cos^2 \chi .$$

The parameter ω is related to k and $(w+c)_{m, \ell}^n$ by the stability condition given in Reference 27 as

$$k^2 \left[(w+c)_{m, \ell}^n \right]^2 \leq \omega k (w+c)_{m, \ell}^n \leq 1 , \quad (30)$$

which must be satisfied for all (m, ℓ) . The quantity

$$\sigma_{m, \ell}^n = k (w+c)_{m, \ell}^n$$

is the Courant number at the point in question.

Designating

$$\sigma_0^n = \max_{m, \ell} \sigma_{m, \ell}^n, \quad ,$$

then stability condition, equation (30), is satisfied if for all n

$$\sigma_0^n \leq 1 \quad \text{and} \quad \sigma_0^n \leq \omega \leq \frac{1}{\sigma_0^n} \quad . \quad (31)$$

The value of σ_0 may be established for all time planes before the calculations are started. Then, once the calculations have started, the value of k for each time plane may be determined from the equation

$$k^n = \sigma_0^n / \max_{m, \ell} (w+c)_{m, \ell}^n \quad . \quad (32)$$

Then, the value of τ^n for each time plane can be calculated from equation (29). In computer computations, the value of k^n for each time plane may be automatically selected. This, Rusanov has indicated, is then sufficient for the constant parameters of the scheme, σ_0 and ω , to satisfy the stability criteria of equation (31).

To evaluate the space derivatives of equation (21), it is most convenient to choose the central difference scheme involving pivotal points symmetrically located with respect to the central (m, ℓ) point. These may be obtained by a Taylor's series expansion of the unknown function about the pivotal point. The Taylor's series expansion of $F^x(x+\Delta x)$ about x is given by

$$\begin{aligned} F^x(x+\Delta x) &= F^x(x) + (\Delta x) F_x^x(x) + \frac{(\Delta x)^2}{2!} F_{xx}^x(x) + \dots \\ &= \sum_{n=0}^{\infty} \frac{(\Delta x)^n}{n!} F_{(n)}^x(x) \quad , \end{aligned}$$

where $F_{(n)}^x(x)$ stands for $d^n F^x/dx^n$. Applying this equation to the expansions at $(x+\Delta x)$ and at $(x-\Delta x)$ for the existing grid:

$$F_{m+1,\ell}^x = F_{m,\ell}^x + (\Delta x) F_{x(m,\ell)}^x + \frac{(\Delta x)^2}{2!} F_{xx(m,\ell)}^x + \dots$$

$$F_{m-1,\ell}^x = F_{m,\ell}^x - (\Delta x) F_{x(m,\ell)}^x + \frac{(\Delta x)^2}{2!} F_{xx(m,\ell)}^x - \dots$$

Neglecting higher order terms, an approximate expression for $F_{x(m,\ell)}^x$ is immediately obtained by subtraction as

$$F_{m+1,\ell}^x - F_{m-1,\ell}^x = 2(\Delta x) F_{x(m,\ell)}^x$$

Therefore, the approximate expression for the first derivative of the term $\partial F^x/\partial x$ in equation (21) is

$$F_{x(m,\ell)}^x = \frac{1}{2(\Delta x)} \left[F_{m+1,\ell}^x - F_{m-1,\ell}^x \right] \quad (33)$$

A Taylor's series expansion of $F^y(y+\Delta y)$ about y will yield a similar expression for the term $\partial F^y/\partial y$ in equation (21). The resulting expression is easily shown to be

$$F_{y(m,\ell)}^y = \frac{1}{2(\Delta y)} \left[F_{m,\ell+1}^y - F_{m,\ell-1}^y \right] \quad (34)$$

Thus, equations (33) and (34) are obtained which satisfy the general space-derivative approximations for the numerical scheme.

For the general time-derivative approximation, Rusanov introduced an averaging technique similar to the one proposed by Lax. However, his technique is somewhat more complicated in that it "weighs" the pivotal values according to the respective distances of the neighboring

points. Hence, the technique combines both forward and central differences in addition to "dissipative" coefficients. The difference scheme for the time-derivative, which involves the general dependent variable f , may be written explicitly as

$$\frac{\partial f}{\partial t} = \frac{1}{\Delta t} \left\{ f_{m,\ell}^{n+1} - f_{m,\ell}^n - \frac{1}{2} \left[\phi_{m+\frac{1}{2},\ell}^x - \phi_{m-\frac{1}{2},\ell}^x + \phi_{m,\ell+\frac{1}{2}}^y - \phi_{m,\ell-\frac{1}{2}}^y \right] \right\}, \quad (35)$$

where the "dissipative" coefficients are defined as

$$\begin{aligned} \phi_{m+\frac{1}{2},\ell}^x &= \alpha_{m+\frac{1}{2},\ell}^n \left[f_{m+1,\ell} - f_{m,\ell} \right]^n \\ \phi_{m-\frac{1}{2},\ell}^x &= \alpha_{m-\frac{1}{2},\ell}^n \left[f_{m,\ell} - f_{m-1,\ell} \right]^n \\ \phi_{m,\ell+\frac{1}{2}}^y &= \beta_{m,\ell+\frac{1}{2}} \left[f_{m,\ell+1} - f_{m,\ell} \right]^n \\ \phi_{m,\ell-\frac{1}{2}}^y &= \beta_{m,\ell-\frac{1}{2}} \left[f_{m,\ell} - f_{m,\ell-1} \right]^n \end{aligned}$$

Furthermore, the following definitions apply:

$$\begin{aligned} \alpha_{m+\frac{1}{2},\ell}^n &= \frac{1}{2} \left[\alpha_{m+1,\ell} + \alpha_{m,\ell} \right]^n \\ \alpha_{m-\frac{1}{2},\ell}^n &= \frac{1}{2} \left[\alpha_{m,\ell} + \alpha_{m-1,\ell} \right]^n \\ \beta_{m,\ell+\frac{1}{2}}^n &= \frac{1}{2} \left[\beta_{m,\ell+1} + \beta_{m,\ell} \right]^n \\ \beta_{m,\ell-\frac{1}{2}}^n &= \frac{1}{2} \left[\beta_{m,\ell} + \beta_{m,\ell-1} \right]^n \end{aligned}$$

Combining the finite difference schemes of equations (33), (34), and (35), and substituting them for their corresponding differential terms in equation (21), the total equation becomes

$$\begin{aligned} \frac{1}{\Delta t} \left\{ f_{m,\ell}^{n+1} - f_{m,\ell}^n - \frac{1}{2} \left[\phi_{m+\frac{1}{2},\ell}^x - \phi_{m-\frac{1}{2},\ell}^x + \phi_{m,\ell+\frac{1}{2}}^y - \phi_{m,\ell-\frac{1}{2}}^y \right] \right\} \\ + \frac{1}{2(\Delta x)} \left[F_{m+1,\ell}^x - F_{m-1,\ell}^x \right]^n + \frac{1}{2(\Delta y)} \left[F_{m,\ell+1}^y - F_{m,\ell-1}^y \right]^n + \psi_{m,\ell}^n = 0 \end{aligned}$$

Multiplying through by Δt , and solving for $f_{m,l}^{n+1}$ yields

$$f_{m,l}^{n+1} = f_{m,l}^n - \Delta t \psi_{m,l}^n - \frac{\Delta t}{2(\Delta x)} \left[F_{m+1,l}^x - F_{m-1,l}^x \right]^n - \frac{\Delta t}{2(\Delta y)} \left[F_{m,l+1}^y - F_{m,l-1}^y \right]^n + \frac{1}{2} \left[\phi_{m+\frac{1}{2},l}^x - \phi_{m-\frac{1}{2},l}^x + \phi_{m,l+\frac{1}{2}}^y - \phi_{m,l-\frac{1}{2}}^y \right]$$

Since $\Delta t/\Delta x = \tau/h_1 = k_1$ and $\Delta t/\Delta y = \tau/h_2 = k_2$, this equation may be written in its final form as

$$f_{m,l}^{n+1} = f_{m,l}^n - \tau \psi_{m,l}^n - \frac{k_1}{2} \left[F_{m+1,l}^x - F_{m-1,l}^x \right]^n - \frac{k_2}{2} \left[F_{m,l+1}^y - F_{m,l-1}^y \right]^n + \frac{1}{2} \left[\phi_{m+\frac{1}{2},l}^x - \phi_{m-\frac{1}{2},l}^x + \phi_{m,l+\frac{1}{2}}^y - \phi_{m,l-\frac{1}{2}}^y \right] \quad (36)$$

Thus, a finite difference equation is established which is used as the general flow field equation for the problem. This expression is applied to the conservation equations, with ρ , r , s , and e as the unknown variables, in the numerical iteration.

Boundary Conditions

Many of the difficulties encountered in solving a transient flow field problem occur, not only in solving the conservation equations, but in satisfying the boundary conditions. The boundary conditions are established by the physical geometry of the problem and must satisfy all conservation requirements. Consequently, they must be handled discretely.

In Rusanov's analysis, the flow is considered to take place in either finite or infinite regions bounded by motionless rigid walls. Since flow discontinuities are not considered in the computations, the

boundaries are restricted to the axis of symmetry and the solid walls. The walls are all considered to be rectilinear and pass through the points of the net either parallel to the coordinate axes or along the diagonals of the matrix. Thus, the equations for calculating $f_{m,\ell}^n$ will differ, depending on whether the pivotal points are inside the flow region or on its boundary. Equation (36) has been established for all interior flow conditions; hence, modification of this equation is required to establish valid boundary conditions.

To apply boundary conditions to the finite difference scheme of equation (36), the row of pivotal points lying parallel to the x-axis was considered, where the region of flow is above the wall, that is, at a larger y value than the wall. The boundary equation, written explicitly, is

$$f_{m,\ell}^{n+1} = f_{m,\ell}^n - \tau \psi_{m,\ell}^n - \frac{k_1}{2} \left[F_{m+1,\ell}^x - F_{m-1,\ell}^x \right]^n - k_2 \left[F_{m,\ell+1}^y \right]^n + \frac{1}{2} \left[\phi_{m+\frac{1}{2},\ell}^x - \phi_{m-\frac{1}{2},\ell}^x \right] \quad (37)$$

Note that in this scheme, only the influence of neighboring points is considered. Although the lattice of points is assumed to be extended one row below the boundary wall, no variables are computed there. Thus, the effect of this row is

Following this same procedure, if the region of flow is below (at a smaller y than) the wall, the boundary equation then becomes

$$f_{m,\ell}^{n+1} = f_{m,\ell}^n - \tau \psi_{m,\ell}^n - \frac{k_1}{2} \left[F_{m+1,\ell}^x - F_{m-1,\ell}^x \right]^n + k_2 \left[F_{m,\ell-1}^y \right]^n + \frac{1}{2} \left[\phi_{m+\frac{1}{2},\ell}^x - \phi_{m-\frac{1}{2},\ell}^x \right] \quad (38)$$

From the physical boundary conditions, the value of the third component of the vector $f_{m,\ell}^{n+1}$, that is, $(\rho v)_{m,\ell}^{n+1}$, is equal to zero and does not need to be calculated. However, the remaining three components are required.

For pivotal points lying on a wall parallel to the y-axis, where the region of flow is to the right of the wall, the boundary equation is written explicitly as

$$f_{m,\ell}^{n+1} = f_{m,\ell}^n - \tau \psi_{m,\ell}^n - k_1 \left[F_{m+1,\ell}^x \right]^n - \frac{k_2}{2} \left[F_{m,\ell+1}^y - F_{m,\ell-1}^y \right]^n + \frac{1}{2} \left[\phi_{m,\ell+\frac{1}{2}}^y - \phi_{m,\ell-\frac{1}{2}}^y \right] \quad (39)$$

Similarly, for flow to the left of the wall the boundary equation becomes

$$f_{m,\ell}^{n+1} = f_{m,\ell}^n - \tau \psi_{m,\ell}^n + k_1 \left[F_{m-1,\ell}^x \right]^n - \frac{k_2}{2} \left[F_{m,\ell+1}^y - F_{m,\ell-1}^y \right]^n + \frac{1}{2} \left[\phi_{m,\ell+\frac{1}{2}}^y - \phi_{m,\ell-\frac{1}{2}}^y \right] \quad (40)$$

In equations (39) and (40), the value of the second component of the vector $f_{m,\ell}^{n+1}$, that is, $(\rho u)_{m,\ell}^{n+1}$, is equal to zero and does not need to be calculated.

The pivotal points which lie on the axis of symmetry, however, must be handled in a slightly different manner. As before, the lattice of points is extended one row below the axis of symmetry but no variables are computed there. Instead, the variables in this row are set equal to their calculated values one row above the axis except the signs of the vertical velocity terms are reversed. The purpose of this change

is to allow for the convergence of the moving shock wave at the axis. The finite difference equation may therefore be written explicitly in the form

$$f_{m,o}^{n+1} = f_{m,o}^n - \tau \hat{\psi}_{m,o}^n - \frac{k_1}{2} \left[F_{m+1,o}^x - F_{m-1,o}^x \right]^n - k_2 \left[F_{m,1}^y \right]^n + \frac{1}{2} \left[\phi_{m+1/2,o}^x - \phi_{m-1/2,o}^x + 2 \phi_{m,1/2}^y \right], \quad (41)$$

where the quantity v/y in $\hat{\psi}_{m,o}^n$ is taken at the point $(m,1)$. From physical considerations, note also that on the axis of symmetry

$$v = \frac{\partial p}{\partial y} = \frac{\partial \rho}{\partial y} = \frac{\partial u}{\partial y} = 0.$$

Thus, boundary equations for the solid walls and the axis of symmetry of the flow problem are established.

Since there is a series of pivotal points which lie on the surface of the cone and which pass along the diagonal of the points of the matrix, the equation for $f_{m,\ell}^{n+1}$ must be obtained by rotating the (x,y) coordinates through an angle χ . Equation (21) is transformed to coordinates orthogonal to the wall and then replaced by the difference equations. Explicitly, the intermediate vector $\tilde{f}_{m,\ell}^{n+1}$ is then written as

$$\begin{aligned} \tilde{f}_{m,\ell}^{n+1} = & \tilde{f}_{m,\ell}^n - \tau \tilde{\psi}_{m,\ell}^n - \frac{k_1 \cos \chi}{2} \left[\tilde{F}_{m+1,\ell+1}^x - \tilde{F}_{m-1,\ell-1}^x \right]^n \\ & - k \left[\tilde{F}_{m,\ell+1}^y \cos^2 \chi + \tilde{F}_{m-1,\ell}^y \sin^2 \chi \right]^n \\ & + \frac{\cos^2 \chi}{2} \left[\tilde{\phi}_{m+1/2,\ell+1/2}^x - \tilde{\phi}_{m-1/2,\ell-1/2}^x \right] \end{aligned} \quad (42)$$

The quantities on the right side of the equation, with the \sim sign, are computed in the same manner as the corresponding quantities without this sign. However, u and v are replaced everywhere by

$$\tilde{u} = u \cos \chi + v \sin \chi \quad \text{and} \quad \tilde{v} = v \cos \chi - u \sin \chi \quad .$$

The vector $f_{m,l}^{n+1}$ is obtained, after $\tilde{f}_{m,l}^{n+1}$ has been calculated, from the relations

$$\rho_{m,l}^{n+1} = \tilde{\rho}_{m,l}^{n+1} \quad , \quad r_{m,l}^{n+1} = \tilde{r}_{m,l}^{n+1} \cos \chi \quad ,$$

$$e_{m,l}^{n+1} = \tilde{e}_{m,l}^{n+1} \quad , \quad s_{m,l}^{n+1} = \tilde{s}_{m,l}^{n+1} \sin \chi \quad ,$$

where $\tilde{s}_{m,l}^{n+1} = 0$ is a boundary condition.

In order to use the numerical boundary equations thus far proposed, the flow matrix must include a large number of points. This is to preclude reflected boundary influences from propagating back into the flow field during the number of time increments used in the calculations. Physically, these propagations may be overcome by locating the boundaries at infinity. Numerically, however, this is hardly possible due to the limited memory capacities of present computers. Therefore, some means to allow the shock to "pass out through" the exterior boundaries must be devised. In the calculations for this analysis, several procedures were attempted, none of which were ideal. One of these methods, however, proved satisfactory and was used throughout. For the upper boundary, conditions were specified which assigned the pivotal points the same values which were calculated in the row of points just below the boundary during the previous time plane. This created an overlapping effect which tended to

prevent unwanted reflections from affecting the flow region of interest.

At the left upstream boundary of the flow matrix, all the variables were set equal to their initial values. At the right boundary, a scheme similar to that used for the upper boundary was devised. The right end downstream column of pivotal points, designated as (m, ℓ) points in the $(n+1)^{\text{th}}$ time plane, were replaced by the computed values of the $(m-1, \ell)$ column obtained from the n^{th} time plane. Thus, the shock wave was allowed to pass "through" the boundary. It must be acknowledged, however, that although this method produced results which were independent of the exterior boundaries, some room for improvement possibly exists. For the calculations in this problem, no better method could be devised.

Initial Shock Wave Representation

In Chapter II, Whitham's solution was shown to yield shock waves similar to those obtained from the experimental shock tube tests. Both of these analyses were performed to determine flow conditions which could be made compatible to the initial requirements of Rusanov's solution, the object being to ensure that similar flow conditions prevail during all phases of the problem.

As initial conditions for the Phase II cone solution, the shock wave configuration obtained from Whitham's solution was utilized. Figure (9) illustrates the technique used to adapt this shock to the network of points representing the Phase II flow matrix. In this figure, the dotted curve denotes the moving shock obtained from Whitham's solution, for which the variations in shock Mach number are known. Hence, the properties

behind the shock may be determined easily (See Appendix E). Property values for pre-selected points, labeled A through B in the figure, are tabulated in Table II.

To relate these known properties to the numerical network of Phase II, ray lines were drawn through the grid points from the cone apex to intersect the shock. The grid points were then assigned the same property values behind the shock as those computed for the pre-selected points. At points where a ray line did not exactly intersect a known point, the known values for points on both sides of the ray line were averaged linearly. This averaged value was then assigned to the corresponding grid point. Points which were averaged in this manner have the letter "a" following the number.

The Phase II shock wave was approximated through the network of points which most closely corresponded to the Phase I shock. This is shown as the dark solid line in the figure. Note that this shock is now assumed to possess the same property values as possessed by the original shock, but at slightly different locations. Thus Whitham's shock configuration is adapted for the initial conditions in the Phase II solution.

For later times, the flow field near the cone is transient, approaching the steady-state conical-shock field. To determine the extent of these transient changes behind the shock, the velocity profile obtained from Whitham's calculations was compared to one obtained from a steady-state solution having identical free stream flow properties. In Whitham's solution, the Mach number ratio, M_c/M_∞ , where $M_\infty = 1.25$, was calculated to be 1.067. This corresponds to a velocity ratio, u_c/u_∞ , of approximately

1.05. Hence, it can be seen that the velocity tends to increase as the cone surface is approached. In contrast to this, the steady-state solution yields a Mach number ratio, M_c/M_∞ , of 0.865, which corresponds to a velocity ratio, u_c/u_∞ , of 0.893. Thus, this velocity profile tends to show a decreasing velocity near the cone surface. Further, the steady-state shock angle would be 55.75° compared to the shock-shock angle of 26.32° . The time history of this transient is not known without a complete numerical computation of the forebody field. An exploratory work on this problem will be described later in this chapter.

This transient just described is the transition from a wave-induced flow to the steady-state condition for a continuing, steady, flow field following the shock. A second transient is superimposed upon this one. Flow following shocks cannot continue to be steady, but must eventually decay. Thus, the decay rate behind the shock influences the conditions of the flow past the base. Again, this can only be determined from a numerical solution to the forebody field.

For the present computation, these two transients were assumed to be changing very slowly, so that the flow properties at the left side of the computed field (points 1, 4, 7, 11, and 16 in Figure 9) were held constant. After a forebody solution becomes available, the values of the various fluid properties at these points can be inserted as boundary conditions at each time plane with no other change in the program. It is believed that the influence of such changes would be small for the problem which was treated in this study, but for high blast strengths or thin blast waves, i.e., rapidly decaying blasts, this could alter the results significantly.

To accommodate the moving shock as adapted for Rusanov's solution, it is represented, not as a finite discontinuity, but as a steep continuous function of the physical flow properties ahead of and behind the shock. Then, after the difference equations have been applied over the entire flow region, the shock wave is detected by rapid changes in the gradients of the physical parameters. This concept lends itself to a new approach wherein the shock wave is initially defined over two mesh thicknesses. Details of this approach, including the assumptions made, are discussed in Appendix G.

Dimensionalization Technique

Before discussing the method used to dimensionalize the quantities in the computer solution, two important considerations must be recalled. First, the gas properties were initially made dimensionless with respect to the gas properties in front of the shock wave. Second, the velocities were made dimensionless with respect to the sonic velocity in front of the shock. Thus, it can be logically reasoned that the procedure for dimensionalizing these quantities must be made with respect to the reference sonic velocity, that is, the sonic velocity in front of the shock.

In the following analysis, consider the "unprimed" conditions to be the initial dimensionless quantities. Similarly, consider the "primed" conditions to be the final quantities having the proper physical dimensions. In terms of x and y , the general system may be represented as in the following sketch.

$$u_s' = u_s \sqrt{\frac{p_x'}{\rho_x'}}$$

$p_y' = p_y (14.7) (144) \text{ lb}_f/\text{ft}^2$ $\rho_y' = \rho_y (.002378) \text{ slugs}/\text{ft}^3$ $T_y' = T_y (519) \text{ } ^\circ\text{R}$ $u_y' = u_y \frac{c_x'}{c_x} = u_y \sqrt{\frac{p_x'}{\rho_x'}}$ $v_y' = v_y \sqrt{\frac{p_x'}{\rho_x'}}$ $c_y' = \frac{c_y}{c_x} c_x' = c_y \sqrt{\frac{p_x'}{\rho_x'}}$		$p_x' = 1.0 (14.7) (144) \text{ lb}_f/\text{ft}^2$ $\rho_x' = 1.0 (.002378) \text{ slugs}/\text{ft}^3$ $T_x' = 1.0 (519) \text{ } ^\circ\text{R}$ $c_x' = \sqrt{\frac{\gamma p_x'}{\rho_x'}} = c_x \sqrt{\frac{p_x'}{\rho_x'}}$ $u_x' = 0$ $v_x' = 0$
---	--	---

Further, it should be noted that the magnitude of the velocity vector may be expressed by the relationship

$$w' = w \sqrt{\frac{p_x'}{\rho_x'}}$$

When actual calculations for the general system represented above are performed, the system in physical dimensions may be represented by the following sketch.

$$u_s' = 3080 \text{ ft}/\text{sec}$$

$p_y' = 18,390 \text{ lb}_f/\text{ft}^2$ $\rho_y' = 0.00859 \text{ slugs}/\text{ft}^3$ $T_y' = 1246 \text{ } ^\circ\text{R}$ $c_y' = 1730 \text{ ft}/\text{sec}$ $u_y' = 2165 \text{ ft}/\text{sec}$ $v_y' = 514 \text{ ft}/\text{sec}$		$p_x' = 2117 \text{ lb}_f/\text{ft}^2$ $\rho_x' = 0.002378 \text{ slugs}/\text{ft}^3$ $T_x' = 519 \text{ } ^\circ\text{R}$ $c_x' = 1116 \text{ ft}/\text{sec}$ $u_x' = 0$ $v_x' = 0$
---	--	--

The physical conditions shown in the above sketch actually represent the flow conditions determined for Point A indicated in Table IV and shown in Figure 9.

The problem involved in the dimensionalization of the time values used in the computer solution is somewhat more complex. However, the technique follows a very similar development to the one just developed except that a scaling parameter has been included. The scaling effect was introduced as a result of using rectangular mesh relationships consistent with the stability criteria required for Rusanov's time equation. The mesh relationship introduced into the computer solution required that the relationship between the h_1 increment along the axis of symmetry and the h_2 increment along the y direction be a function of the cone semi-apex angle θ_c . That is,

$$\tan \theta_c = \tan 13.347^\circ = 0.237254 = h_1/h_2 \quad . \quad (43)$$

Dividing the numerator and the denominator by 1/20, the ratio is preserved and h_1 equals 0.0119 and h_2 equals 0.05. These values of h_1 and h_2 were programmed into the computer solution. Since 6 mesh points (5 intervals) were considered along the cone base radius, h_2 may further be defined as

$$h_2 = R_b/5 \quad . \quad (44)$$

This relationship implies, by substitution of the h_2 value, that the cone base radius, R_b , is equal to a dimensionless value of 0.25. Therefore, to reference the base radius to a dimensionless value of unity, the value obtained above must be amplified by a factor of 4.

Since the time increment expression used in the computer solution is a function of mesh spacing and of the dimensionless value of k where $k = \sigma_0 / (w+c)_{\max}$, it may be expressed as

$$\tau = k \frac{h_1 h_2}{\sqrt{h_1^2 + h_2^2}} \quad (45)$$

The value of σ_0 has previously been defined as a constant resulting from stability considerations and is equal to 0.5. Note also that the overall time t , for any specific time plane printout, equals the summation of all time increments τ ; that is, $t = \sum \tau$.

Substituting expressions (43) and (44) into equation (45), the total dimensionless time for any time plane becomes

$$t = \sum k \frac{\left\{\frac{R_b}{5}\right\}^2 \tan \theta_c}{\left\{\frac{R_b}{5}\right\} \sqrt{\tan^2 \theta_c + 1}} = \sum \frac{k R_b \tan \theta_c}{5 \sqrt{\tan^2 \theta_c + 1}} \quad (46)$$

By inserting the value of $\tan \theta_c$ and the expression for k , this equation further reduces to

$$t = \sum \frac{0.0231 R_b}{(w+c)_{\max}} \quad (47)$$

The solution of this expression is actually the dimensionless time value obtained from the computer solution printout.

If the dimensional values of R_b , w , and c , that is, R_b' , w' , and c' , are substituted into equation (47), the dimensionless time may be expressed in terms of dimensional terms as

$$t = \sum \frac{0.0231 (R_b' / 4)}{(w' + c')_{\max}} \sqrt{\frac{\rho_x'}{\rho_x}} \quad (48)$$

To obtain a time reference factor necessary for conversion from dimensionless times to corresponding dimensional times, consider the following relationship.

$$\frac{t c_x}{R_b} = \frac{t' c_x'}{R_b'} \quad (49)$$

Solving this general relationship for the dimensional time factor yields

$$t' = \frac{R_b'}{R_b} \cdot \frac{c_x}{c_x'} \cdot t \quad (50)$$

Specifically applied to the cone with a base radius of 4 inches, the dimensional time factor becomes

$$t' = \frac{(0.333) \text{ ft}(1.1832)}{0.25(1116) \text{ ft/sec}} \cdot t = 0.001415 t \text{ seconds} \quad (51)$$

This expression yields a time conversion factor of 1415×10^{-6} which provides a simple relationship between the dimensionless times obtained from the computer solution and the corresponding real times in physical units. For convenience, and as an aid to rapid conversion, time calculations for selected time planes from the computer solution were performed. These are listed in Table V. In addition, a plot of time plane versus dimensionless time from the computer solution was accomplished. This plot, depicting the linear relationship between the two variables in the solution, is shown as Figure 10.

TABLE V

SELECTED TIME PLANES WITH CORRESPONDING
TIME CALCULATIONS FROM COMPUTER SOLUTION

TIME PLANE	TIME (Dimensionless)	TIME* (Microseconds)
1	.001341	1.898417
16	.021508	30.434840
36	.048094	68.053936
66**	.087029	123.146872
86	.112612	159.347295
106	.138041	195.328807
126**	.162121	229.401299
146	.187439	265.226637
166	.212809	301.125357
186	.238340	337.251807
196**	.251201	355.449797
240	.308301	436.245943
260**	.334114	472.772427
280	.359976	509.367285
320**	.412024	583.014681
340	.438227	620.091417
360	.464440	657.183746
380**	.490675	694.305719
400	.516945	731.478406
420	.543262	768.716621
440**	.569626	806.021214

* Note time reference factor equals 0.001415, that is,

$$t'(\text{seconds}) = 0.001415 \cdot t(\text{dimensionless})$$

** Time planes plotted for pressure distribution, velocity distribution, and flow direction.

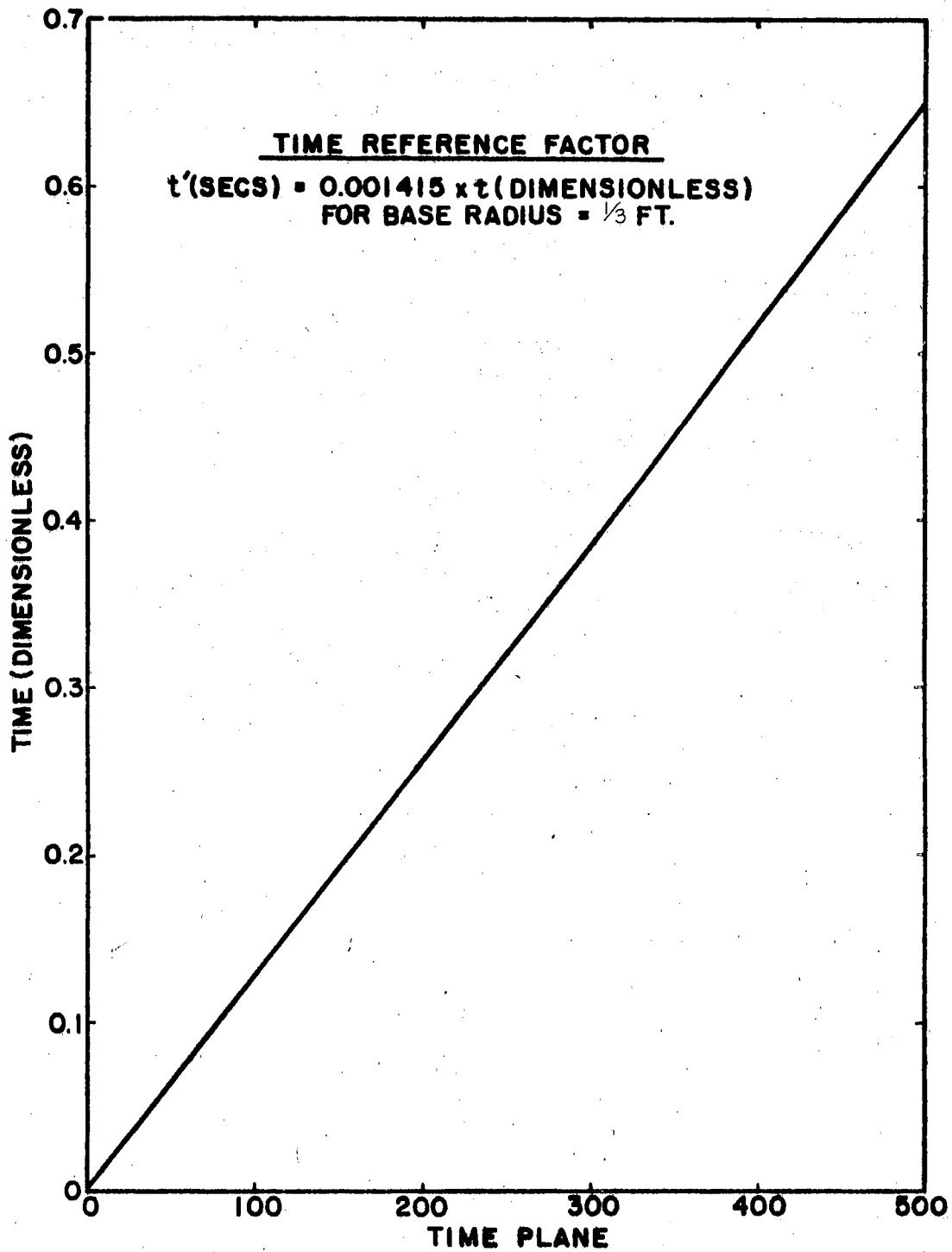


FIG. 10 TIME PLANE VERSUS DIMENSIONLESS TIME FROM COMPUTER SOLUTION.

Computer Solution for Blast-Base Interaction

In order to illustrate the feasibility of solving the blast-base interaction problem using the finite difference technique proposed by Rusanov, a program was written in FORTRAN IV, with format, for solution on the IBM 1410 computer. The results of this program were used to validate Rusanov's calculations for a moving shock past the base of a cylinder. Then, the finite difference equations were modified for adaptation to the blast-base interaction problem for the 13.347° semi-apex angle cone.

However, due to the limited memory capacity of this computer, the flow field matrix could not be made large enough to obtain satisfactory results. Consequently, arrangements were made to expand this flow matrix for use on a larger capacity computer. The Air Force Weapons Laboratory (AFWL), Kirtland AFB, Albuquerque, New Mexico, provided the use of their IBM 7044 computer which was able to accommodate this problem. The computer program was converted to the DIKEWOOD system to facilitate solution on this larger computer. This program is listed as Appendix H.

The flow field for each variable consisted of a matrix having 27 points radially and 105 points in the axial direction, or 2835 points. Approximately 35 hours of computing time were involved to obtain results for 440 time planes. This amount of computing time, however, should not be considered representative since it included numerous runs to convert to the new system.

To solve the problem, the program was written in six subroutine phases. The initial phase was used primarily to read into memory the

initial flow field matrices for ρ , p , u , and v . Using these known values and their explicit relationships previously defined, the matrices for r , s , and e were calculated and also read into memory. Thus, the entire flow field for the initial time plane, $n=0$ was established.

Since the solution to this problem is explicit in time, that is, from knowledge of all variables in the n^{th} time plane, the variables in the $n+1^{\text{th}}$ time plane can be computed, the next four phases were established to calculate the arrays for ρ , r , s , and e , respectively, for the $n+1^{\text{th}}$ time plane. Each of these arrays were successively stored on magnetic tape.

The final phase of this program was used to calculate the remaining variables, that is, u , v , and p for the $n+1^{\text{th}}$ time plane. Then, all of the arrays which were calculated for the $n+1^{\text{th}}$ time plane were printed out before replacing those in the n^{th} time plane. This method was continued until calculations were performed for each of the 440 time planes. To reduce computer time, only pre-selected time planes were printed out. Later, this program was modified to include printout arrays for the velocity modulus vector, w , and the direction, $\tan^{-1}v/u$, which were subsequently needed to plot the results.

Referring to the computer program of Appendix H, the nomenclature listed on the following page was used.

Analysis and Results of Computer Solution

In the preceding discussion of Rusanov's method, with regard to the Phase II solution, an attempt has been made to illustrate the various influences which govern the flow pattern at the base of a conical body.

NOMENCLATURE FOR THE BLAST-BASE INTERACTION PROGRAM

Symbol Used in Computer Program	Corresponding Symbol Used in Text
H1	h_1
H2	h_2
H1M	Maximum number of h_1 increments
H2M	Maximum number of h_2 increments
M,L	m, l subscripts
X	$\tan^{-1} h_2/h_1$
NU	ν
GAMMA	γ
OMEGA	ω
SIGMAO	σ_o
RHO	ρ
P	p
U	u
V	v
W	w
TEST	$\sqrt{u^2 + v^2} + \sqrt{\gamma p / \rho}$
MAX	Maximum $[\sqrt{u^2 + v^2} + \sqrt{\gamma p / \rho}]$
K	k
K1	k_1
K2	k_2
R	r
S	s
E	e
PSI	ψ
FX	F^x
FY	F^y
PHIX	ϕ^x
PHIY	ϕ^y

NOMENCLATURE
(Continued)

Symbol Used in Computer Program	Corresponding Symbol Used in Text
ALPHA	$\alpha_{m,l}$
ALPHA1	$\alpha_{m+1,l}$
ALPHA2	$\alpha_{m-1,l}$
BETA	$\beta_{m,l}$
BETA1	$\beta_{m,l+1}$
BETA2	$\beta_{m,l-1}$
RHO1	ρ^{n+1}
R1	r^{n+1}
S1	s^{n+1}
E1	e^{n+1}
CNT	Count (Number of Time Planes)
T	τ
YL	y
T1	$\Sigma\tau$

Specifically, the differential equations of motion, the finite difference equations, the associated boundary equations, the blast wave representation, and the dimensionalization technique all contribute to the overall solution of the problem. In addition, and perhaps of greater significance, these elements have all been formulated into a computer solution, for which results are presented in graphical form.

The results of this analysis are presented as Figures 11 through 36. Included are plots of lines of constant pressure, constant velocity and velocity vector distribution for time planes 0, 66, 126, 166, 196, 260, 320, 380, and 440. These time planes were pre-selected for plotting since they are considered to be representative of the overall solution. They will later be used in mating the blast passage with the formation of the separated flow region behind the body.

Figure 11 illustrates the initial shock position and configuration which has been superimposed upon the 27 by 105 point network, which represents the undisturbed flow matrix. The coordinate axes are measured with respect to the cone base radius. Note that although the pressure ratio for the unrefracted shock is 8.6930:1, this ratio increases to 9.2092:1 at the cone corner point. Thus, the initial shock wave is represented as a non-uniform discontinuity in the flow.

Figures 12, 13, and 14 illustrate the results obtained for time plane 66, after the shock has progressed beyond the corner and has traveled part of the way down the cone base. As the shock wave travels toward the axis of symmetry, its area decreases; hence the base pressure increases. Figure 12, the velocity vector plot, depicts the relative flow direction, the approximate centerline of the shock, the constant

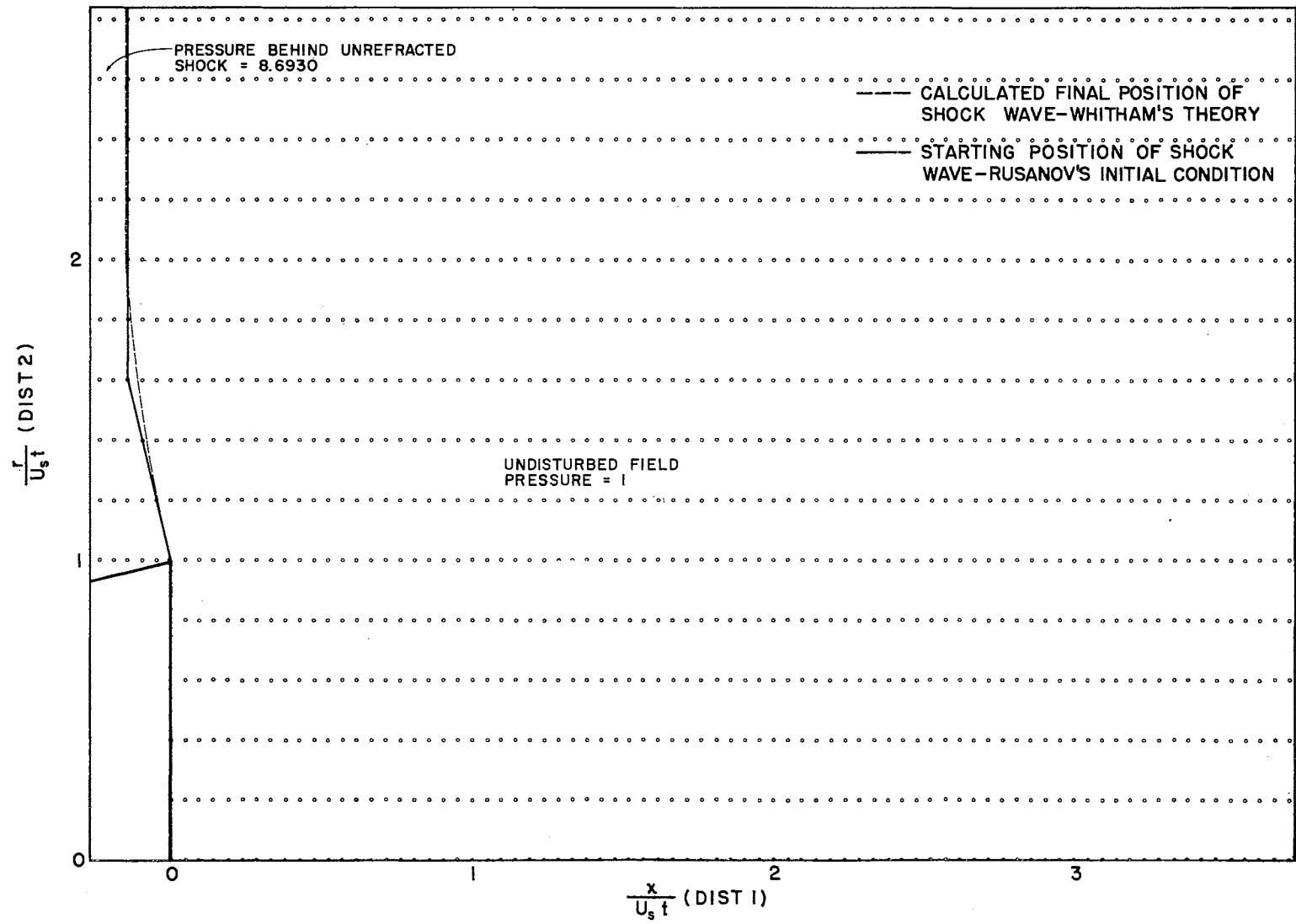


Fig. 11 Shock Position -- Time Plane 0

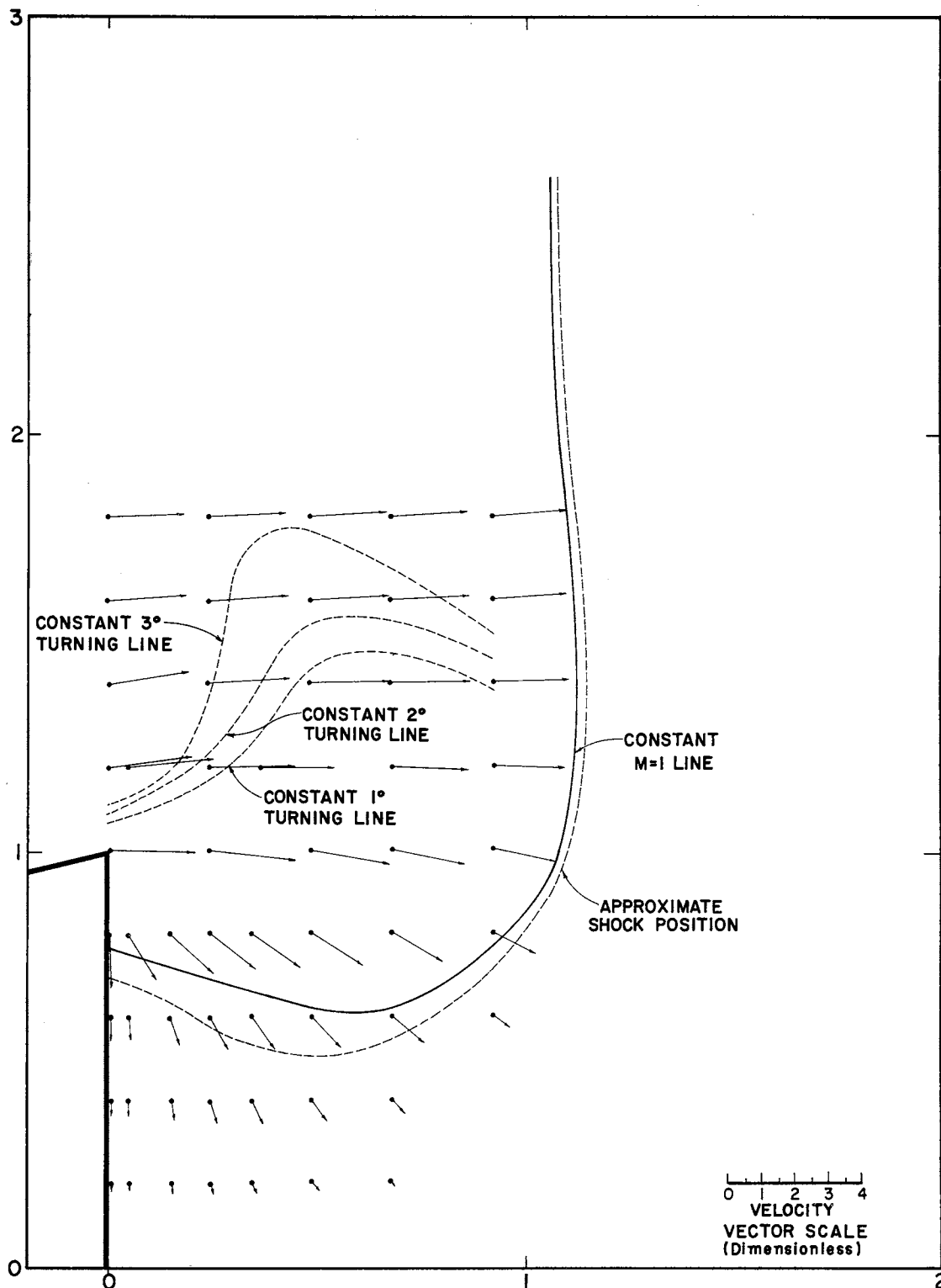


Fig. 12 Velocity Vector Plot in Base Region -- Time Plane 66

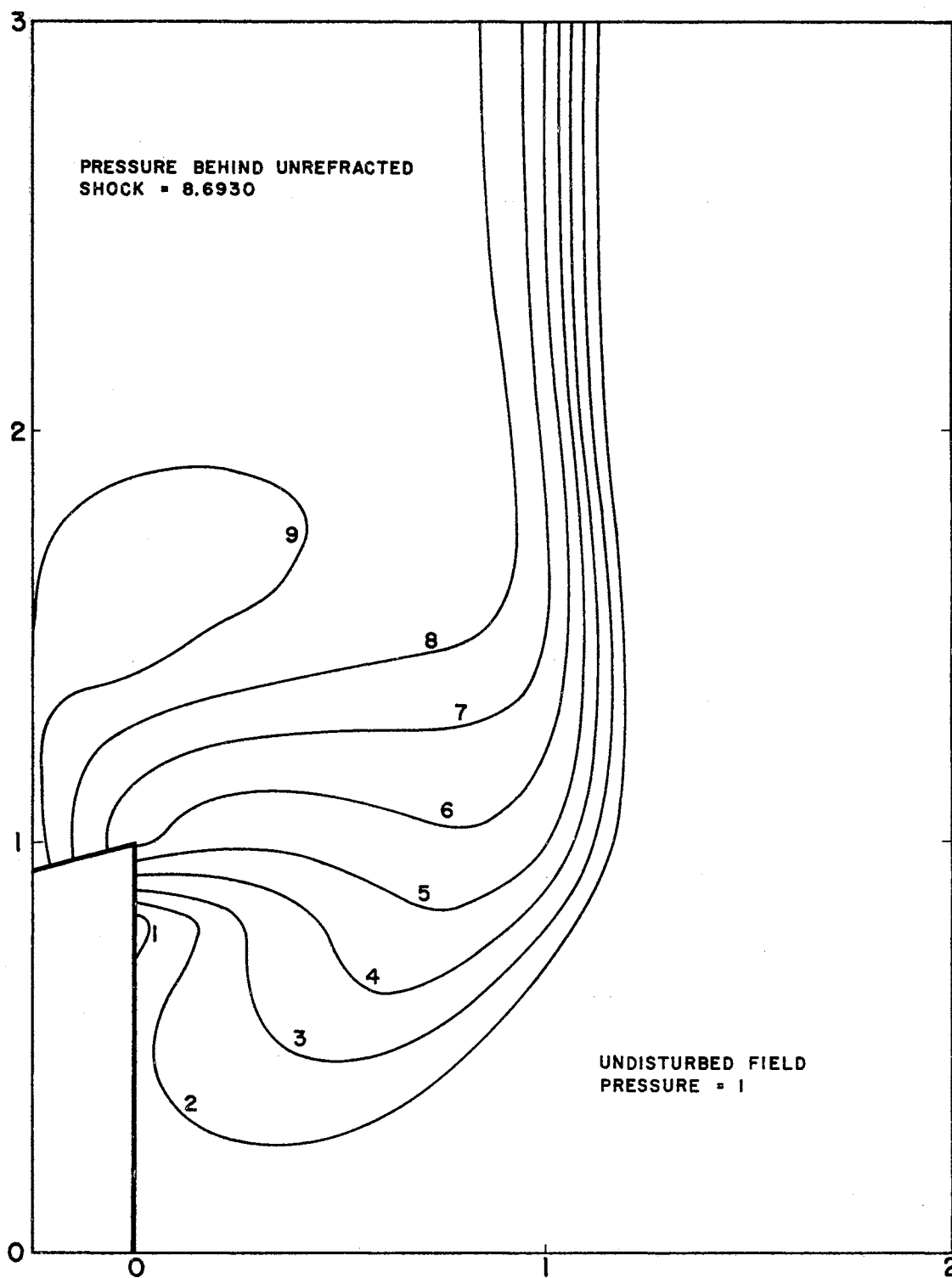


Fig. 13 Constant Pressure Lines (Isobars) for Base Region --
Time Plane 66

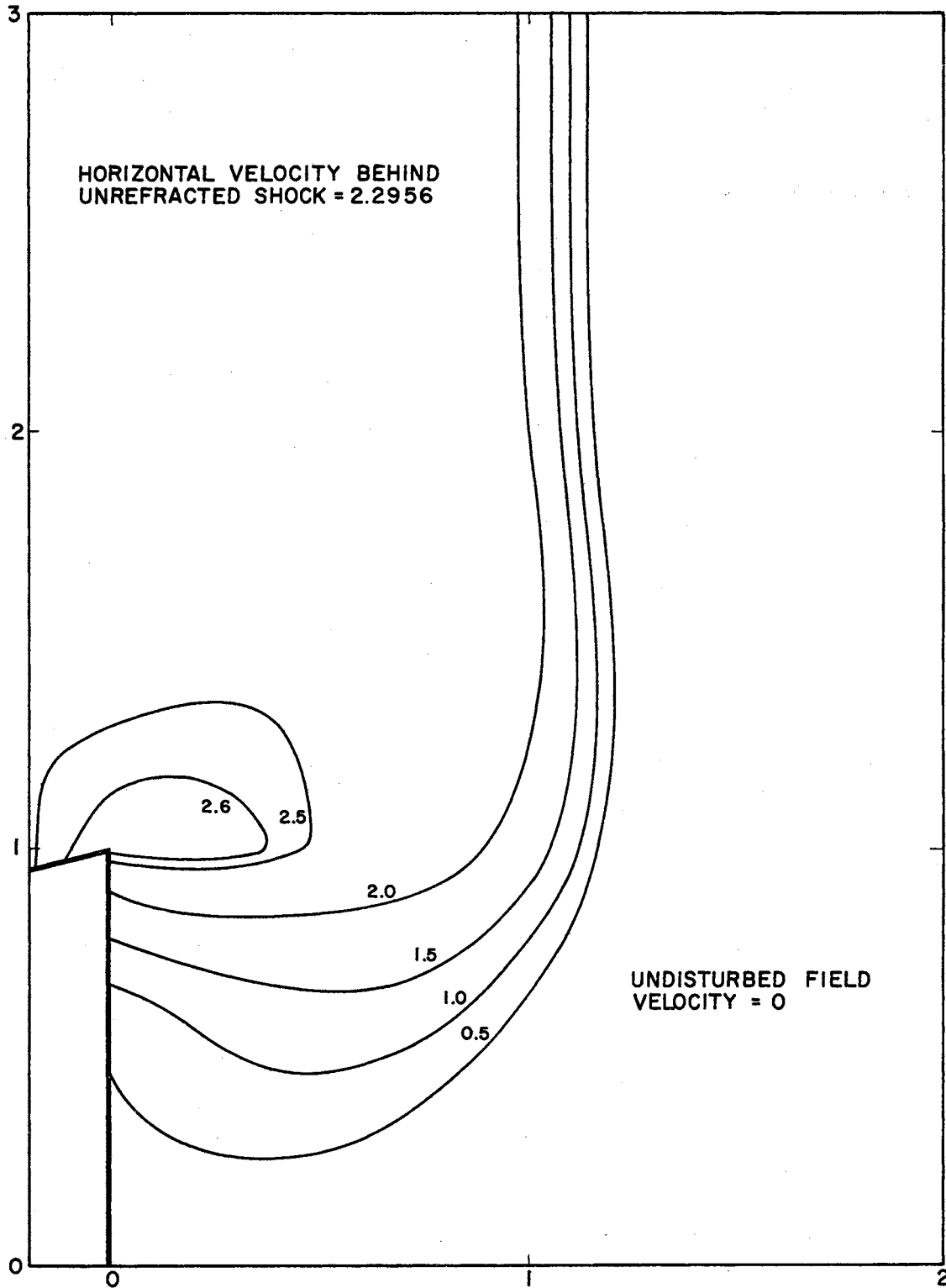


Fig. 14 Constant Velocity Lines for Base Region -- Time Plane 66

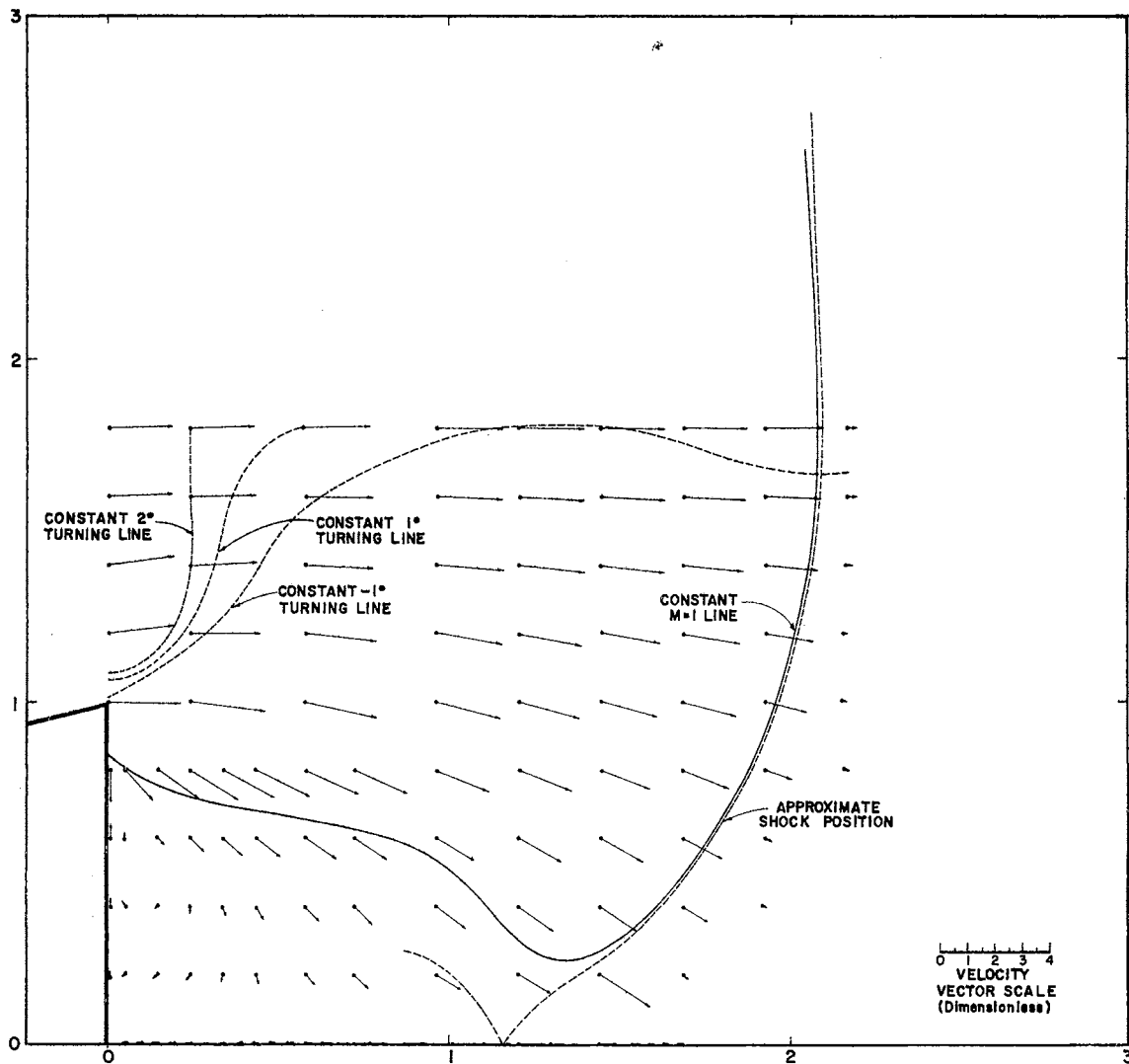


Fig. 15 Velocity Vector Plot in Base Region -- Time Plane 126

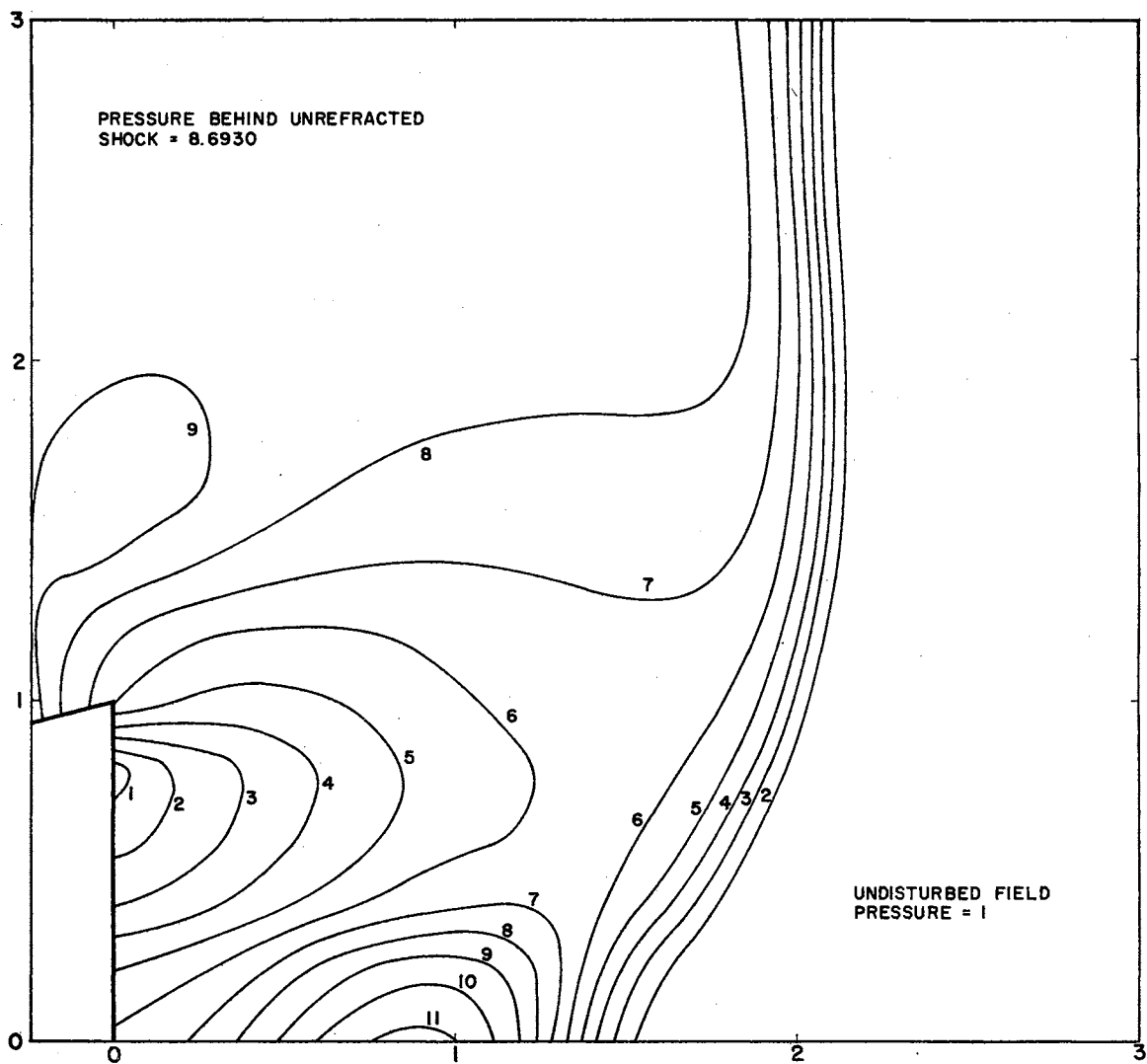


Fig. 16 Constant Pressure Lines (Isobars) for Base Region --
Time Plane 126

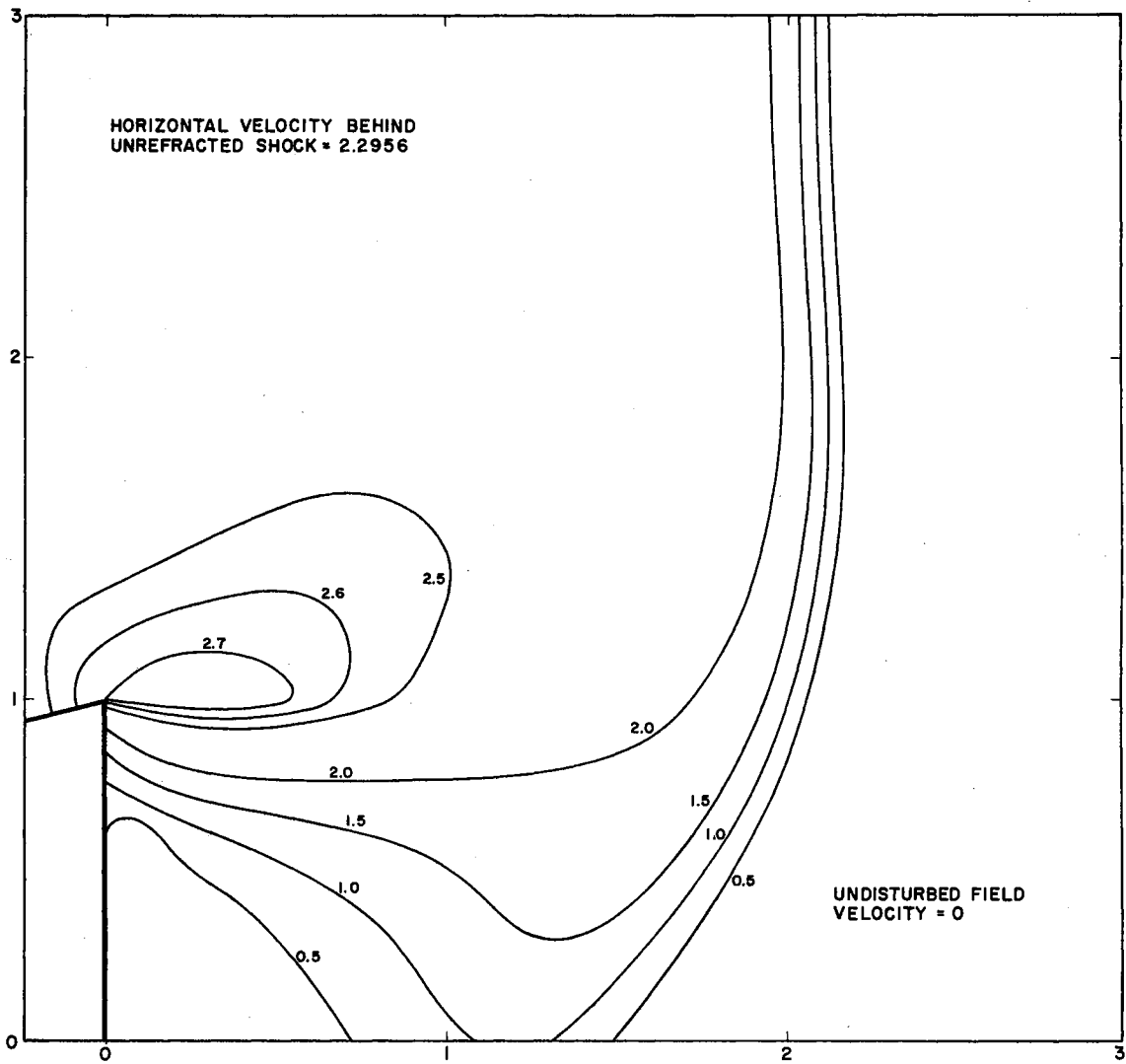


Fig. 17 Constant Velocity Lines for Base Region -- Time Plane 126

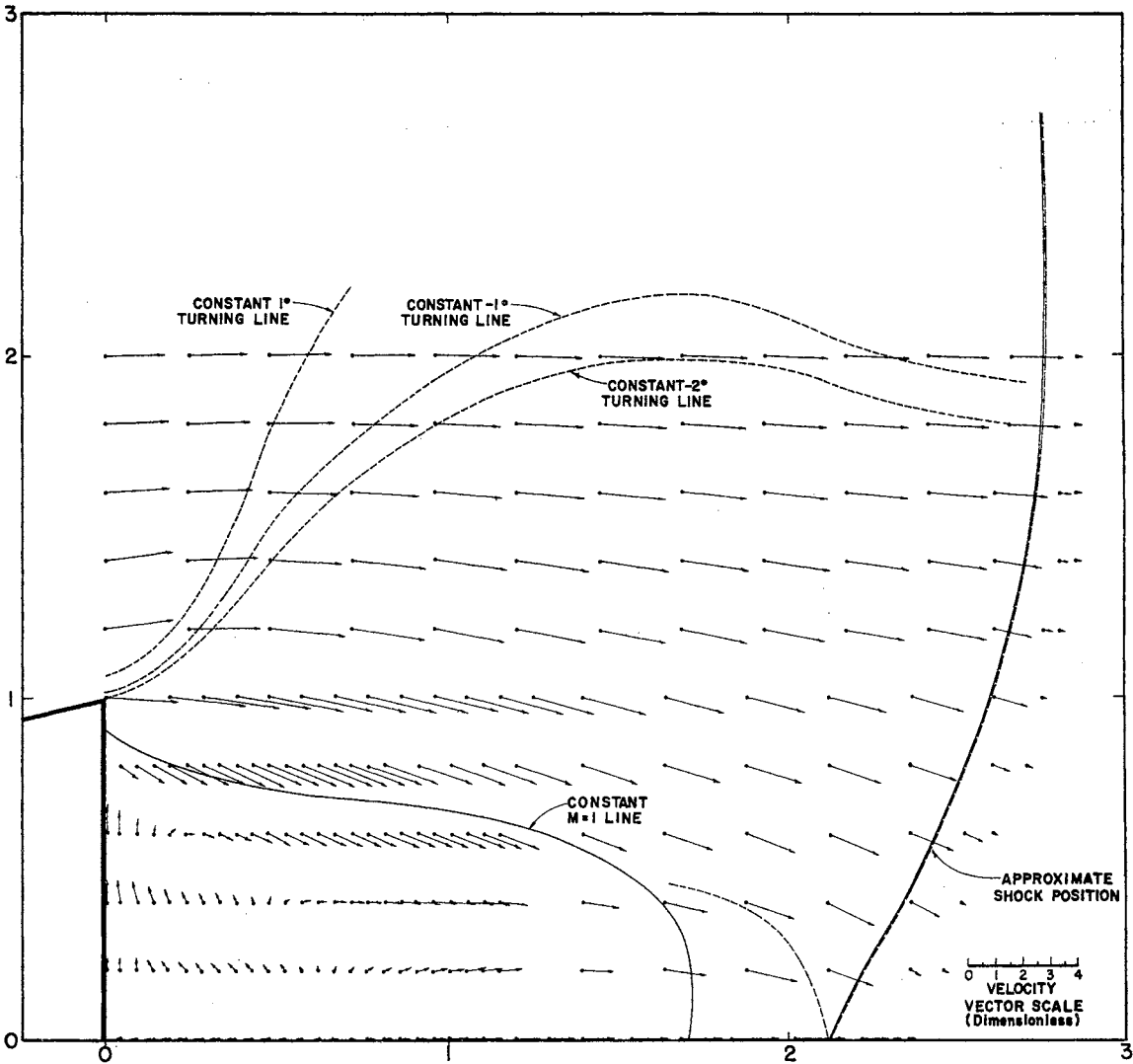


Fig. 18 Velocity Vector Plot in Base Region -- Time Plane 166

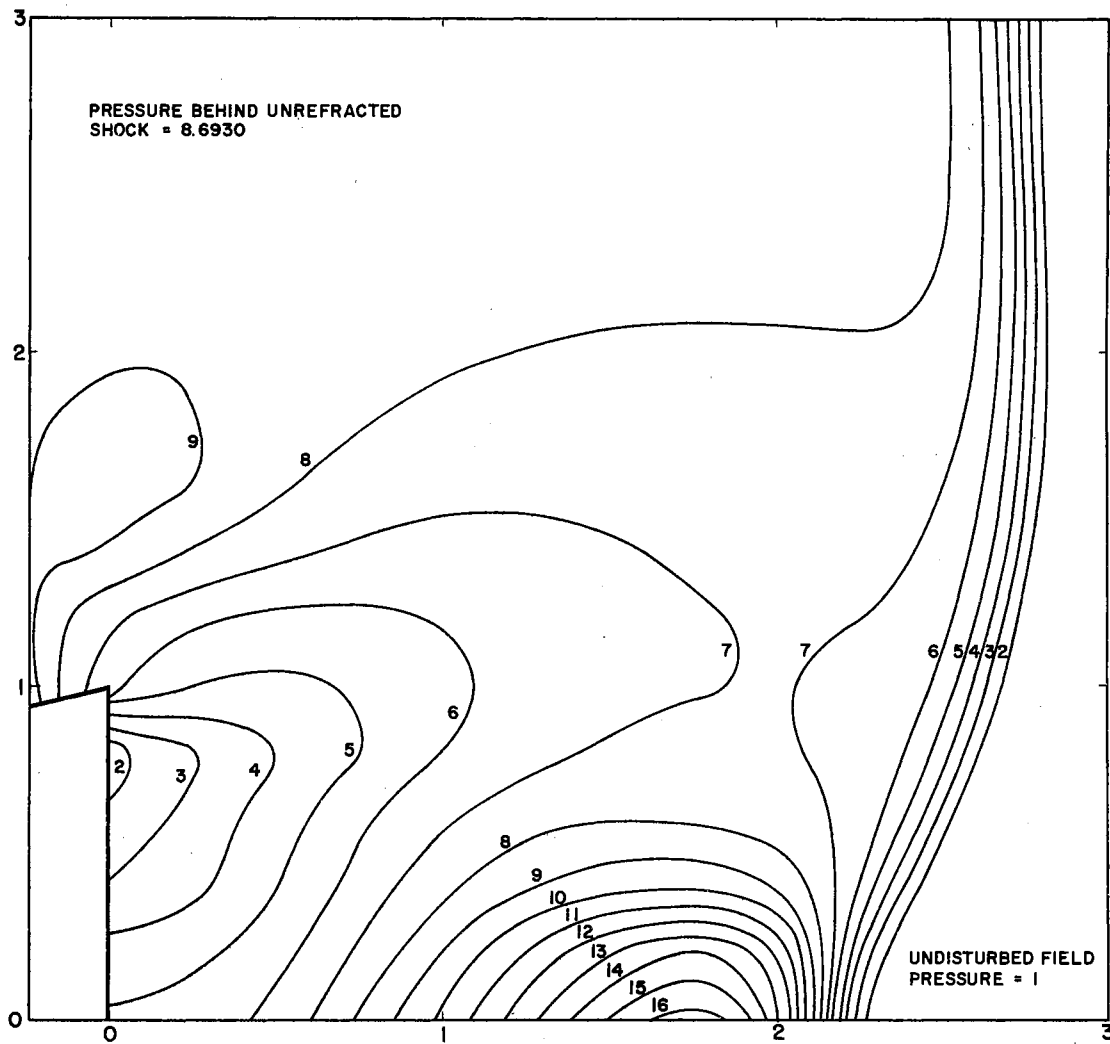


Fig. 19 Constant Pressure Lines (Isobars) for Base Region --
Time Plane 166

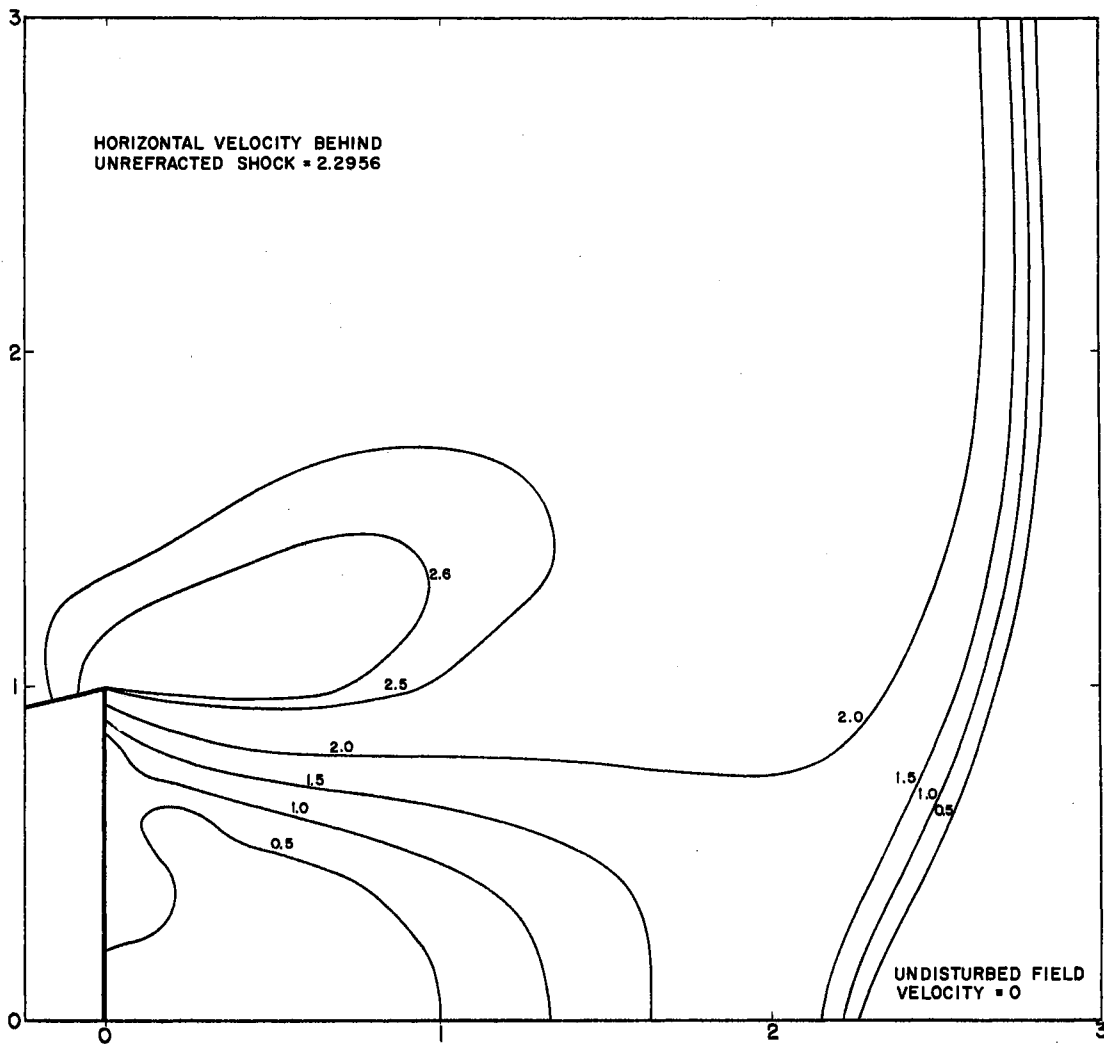


Fig. 20 Constant Velocity Lines for Base Region -- Time Plane 166

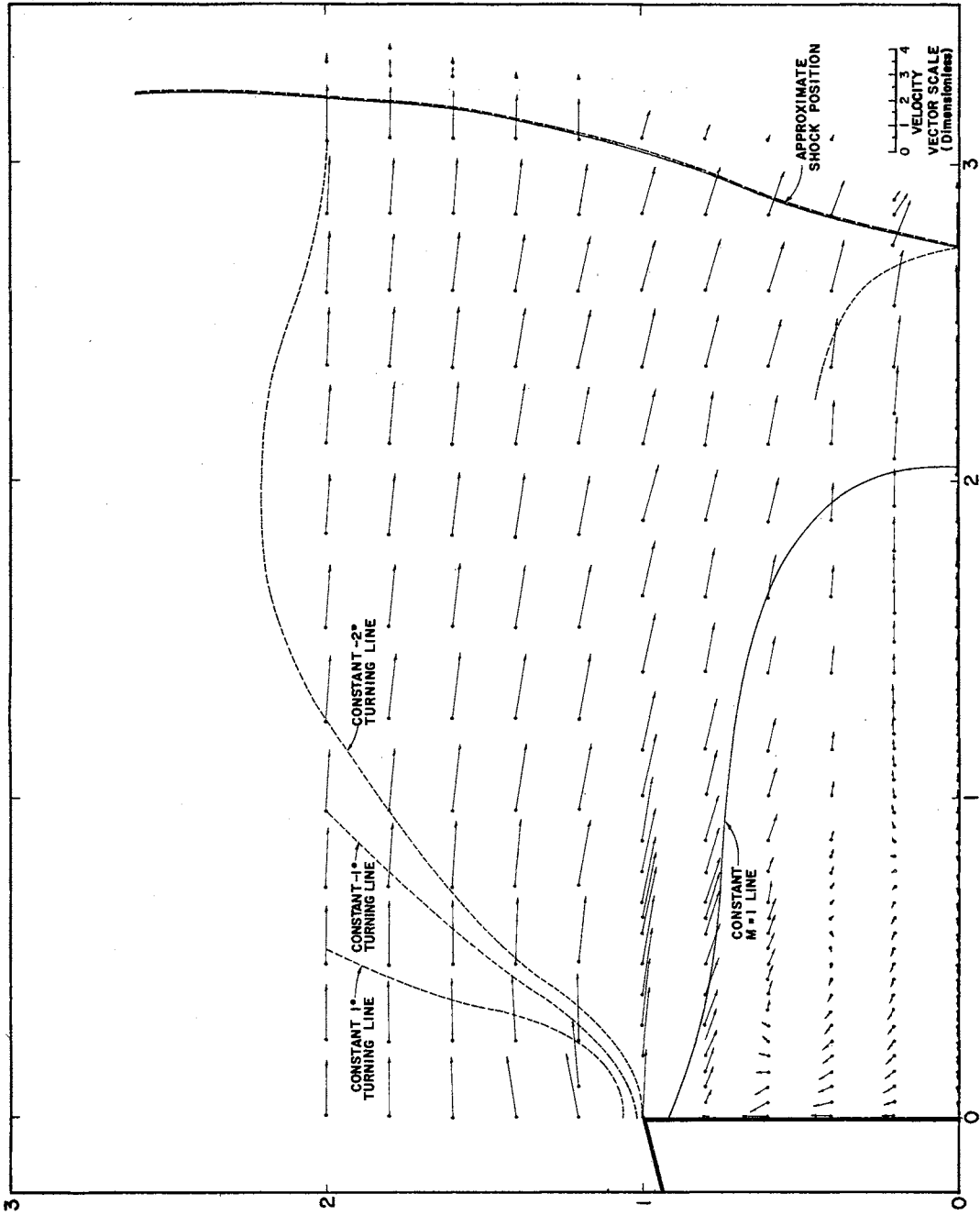


Fig. 21 Velocity Vector Plot in Base Region -- Time Plane 196

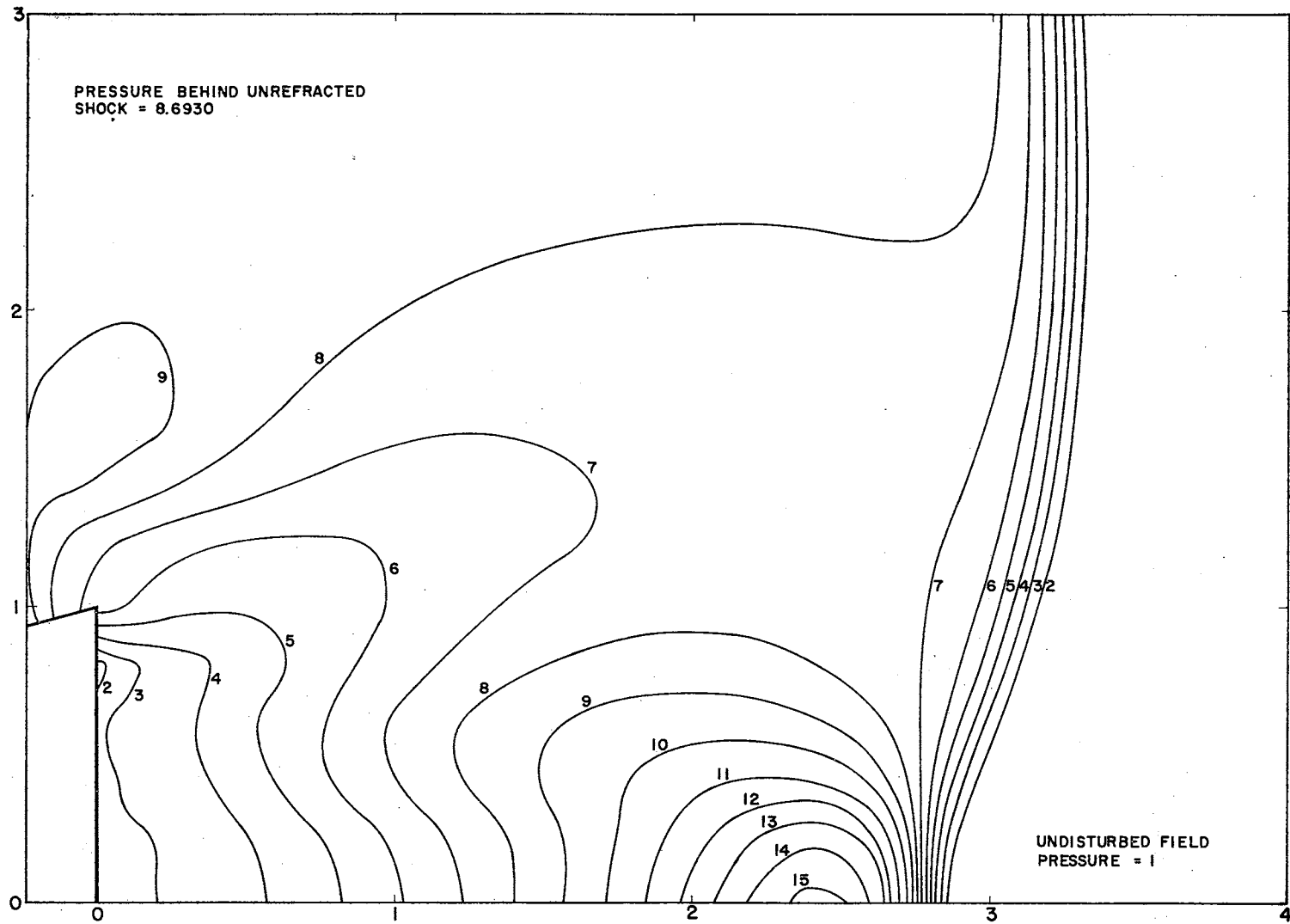


Fig. 22 Constant Pressure Lines (Isobars) for Base Region --
Time Plane 196

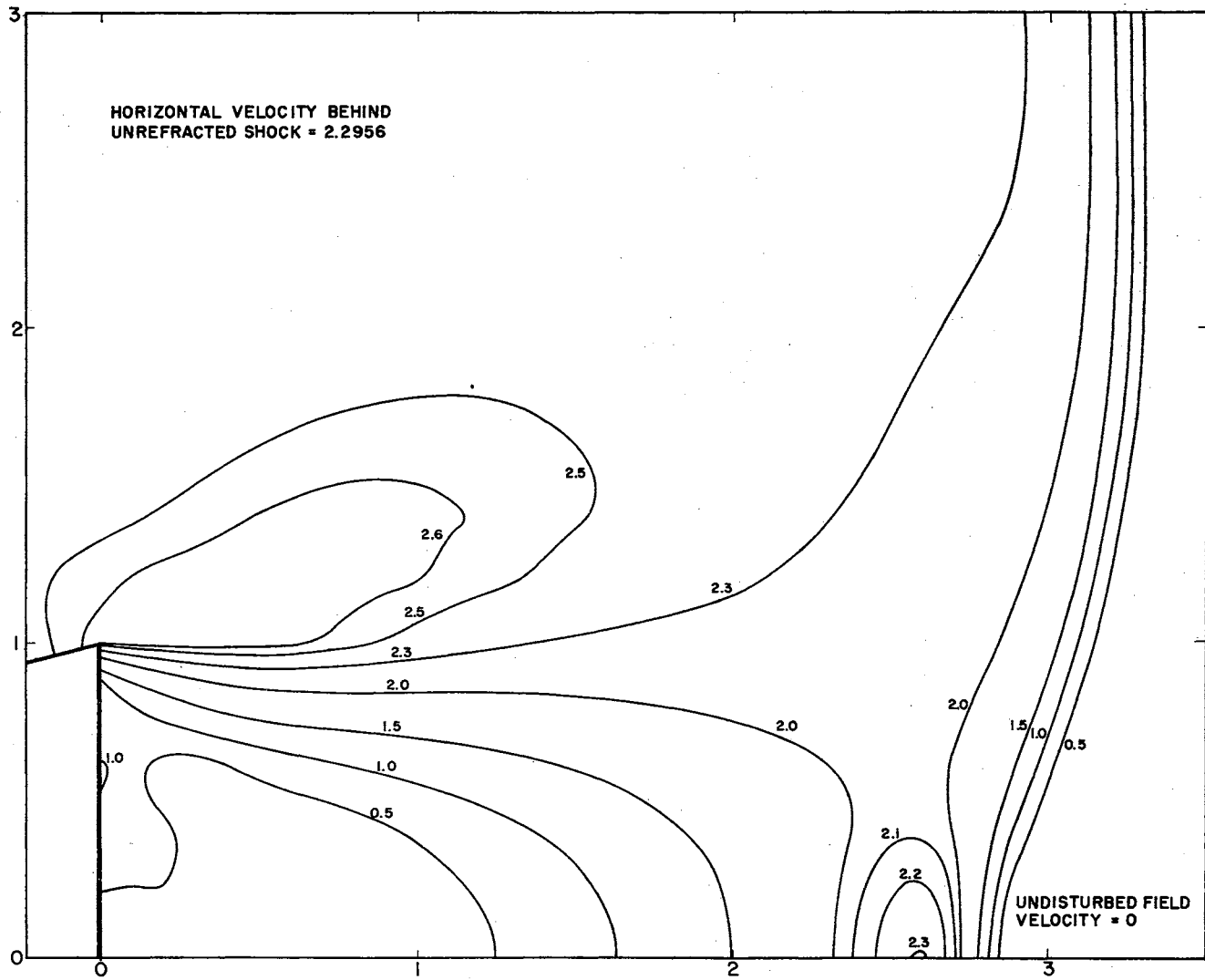


Fig. 23 Constant Velocity Lines for Base Region -- Time Plane 196

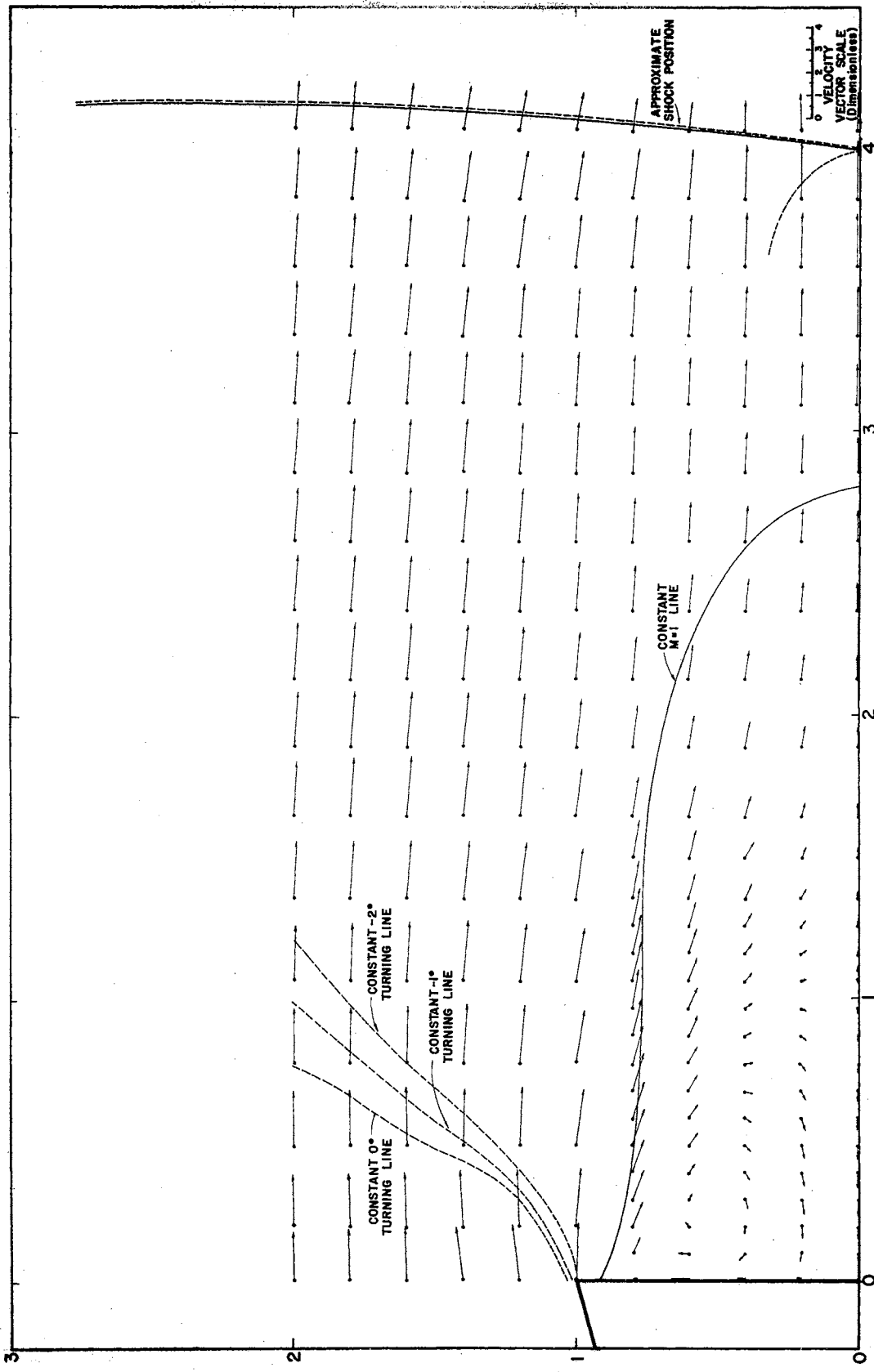


Fig. 24 Velocity Vector Plot in Base Region -- Time Plane 260

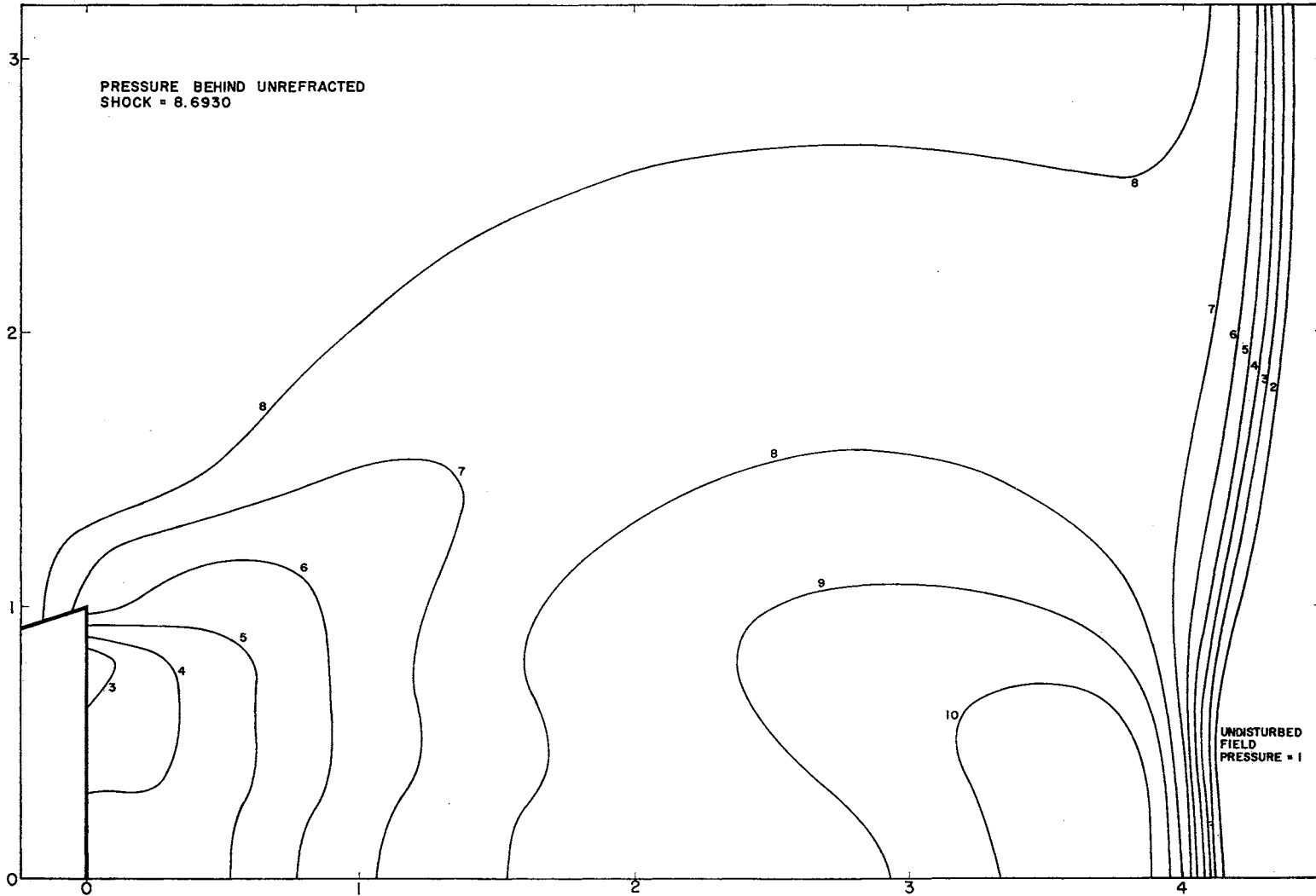


Fig. 25 Constant Pressure Lines (Isobars) for Base Region --
Time Plane 260

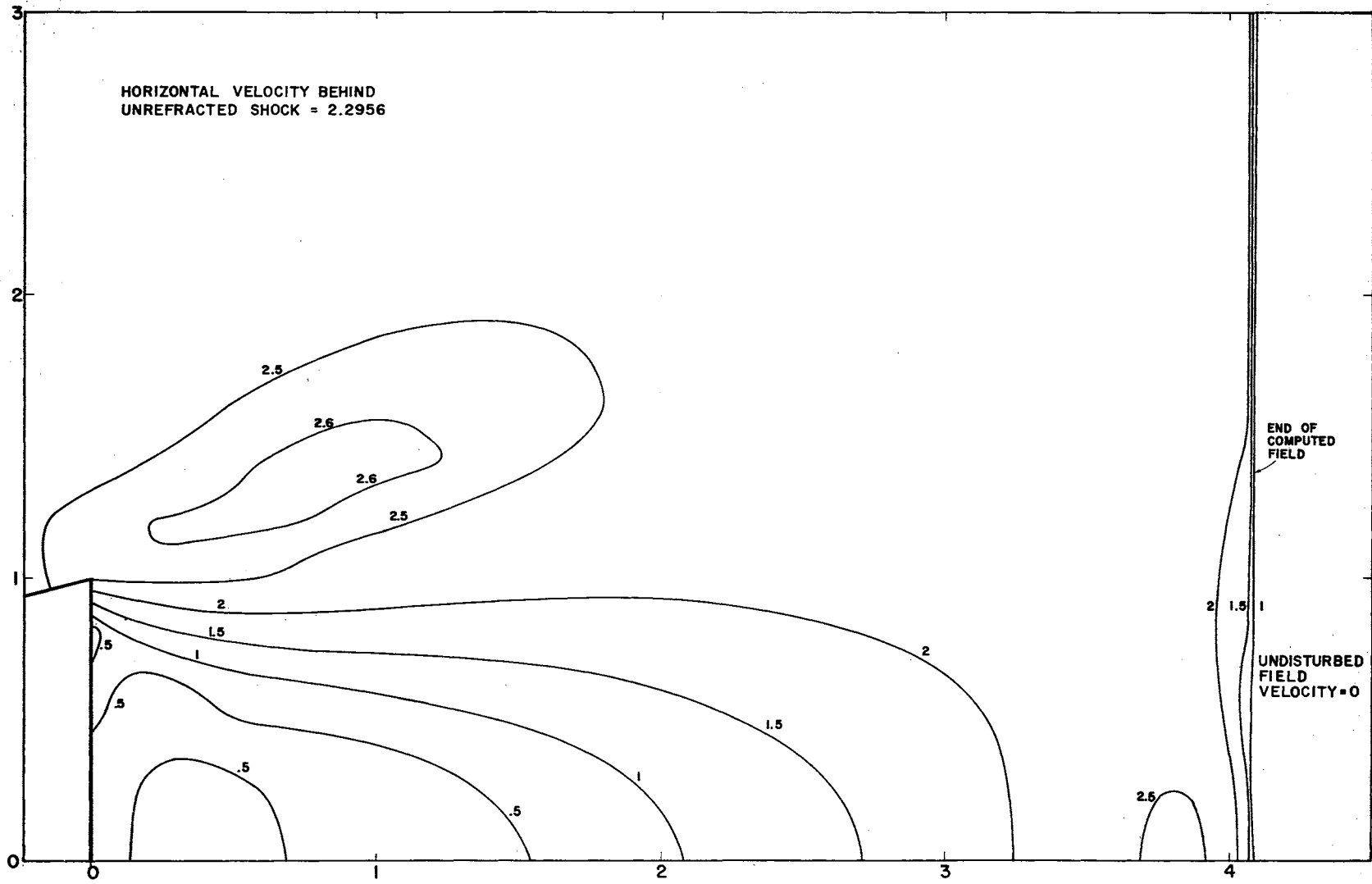


Fig. 26 Constant Velocity Lines for Base Region -- Time Plane 260

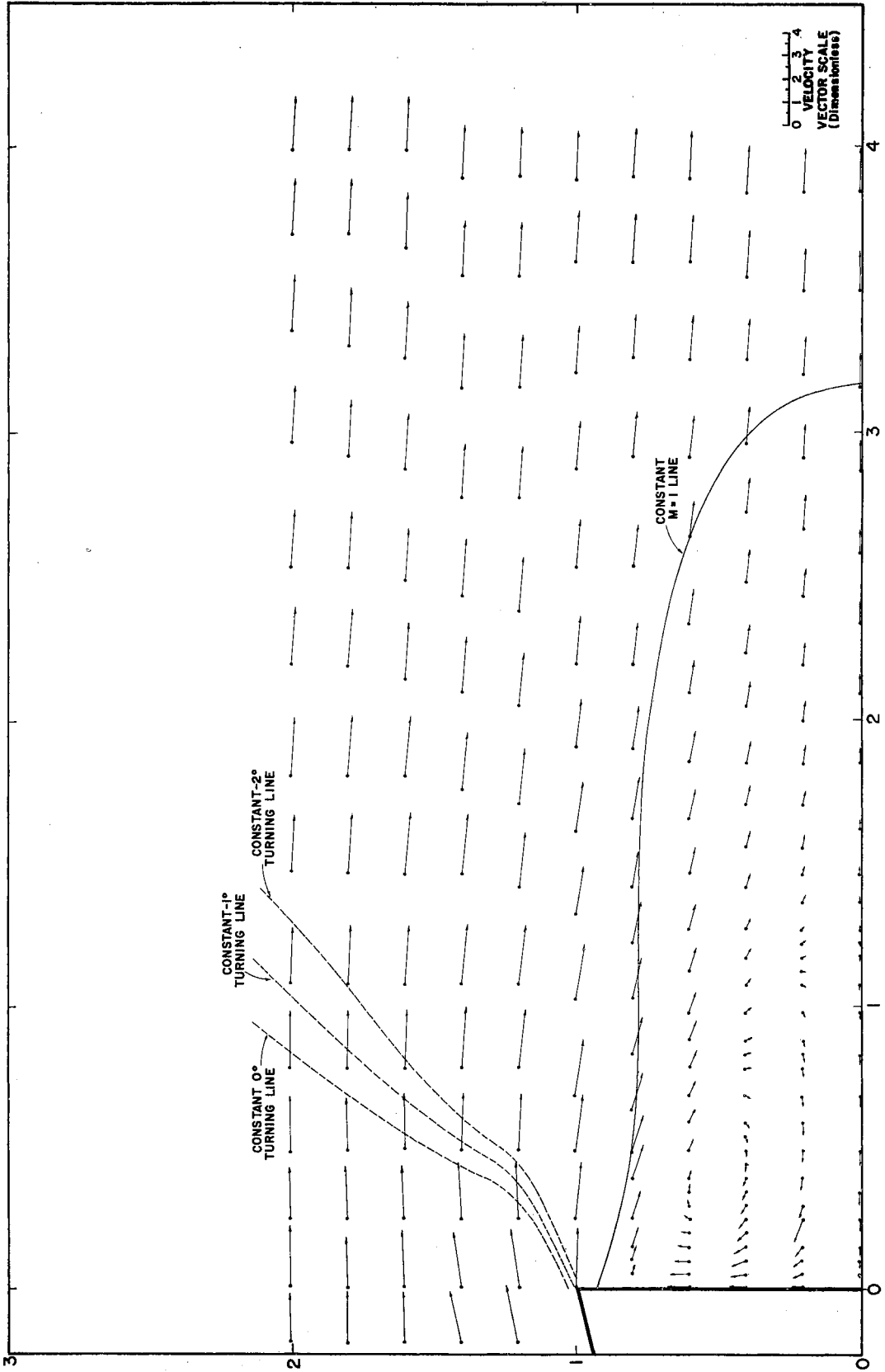


Fig. 27 Velocity Vector Plot in Base Region -- Time Plane 320

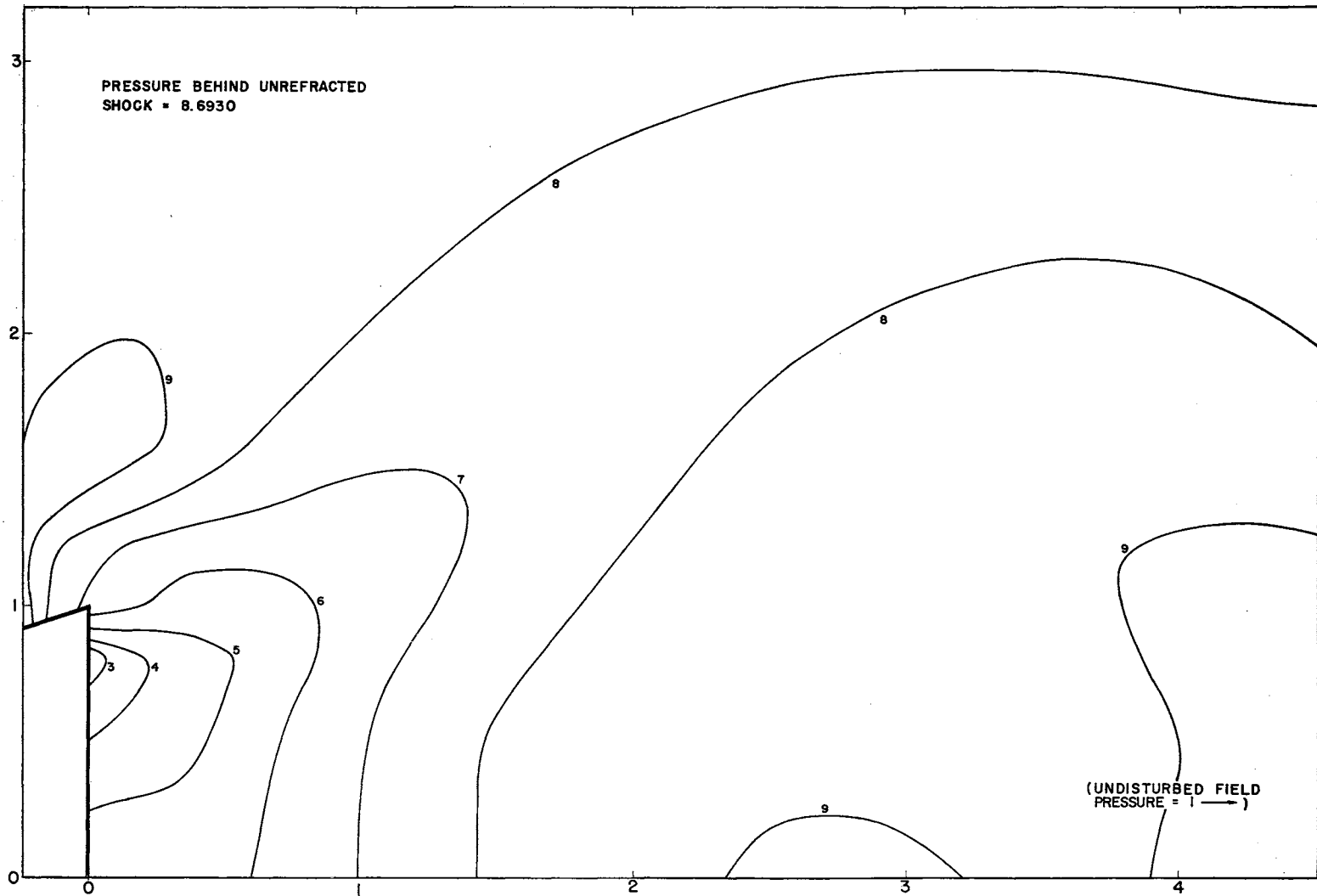


Fig. 28 Constant Pressure Lines (Isobars) for Base Region --
Time Plane 320

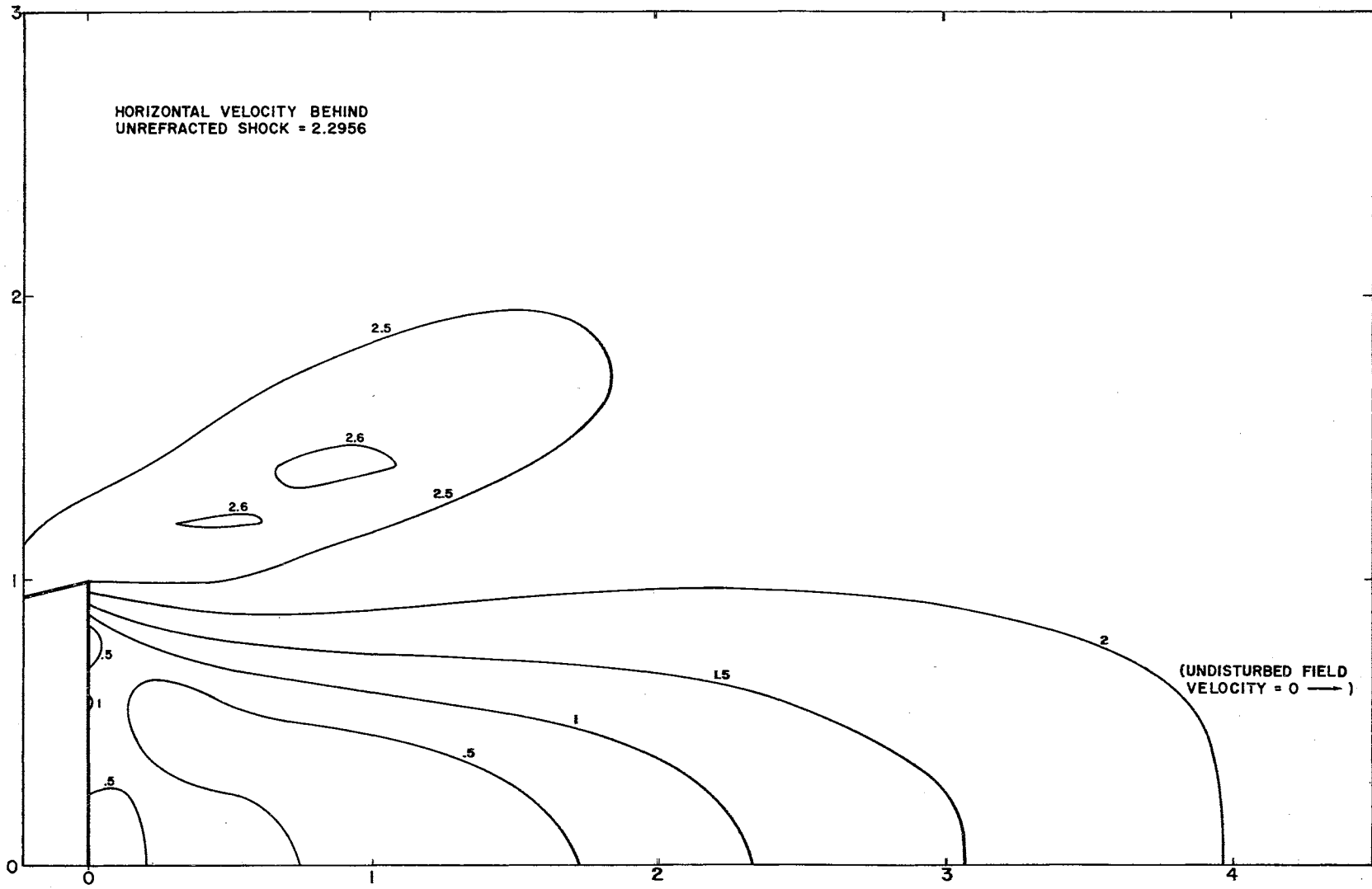


Fig. 29 Constant Velocity Lines for Base Region -- Time Plane 320

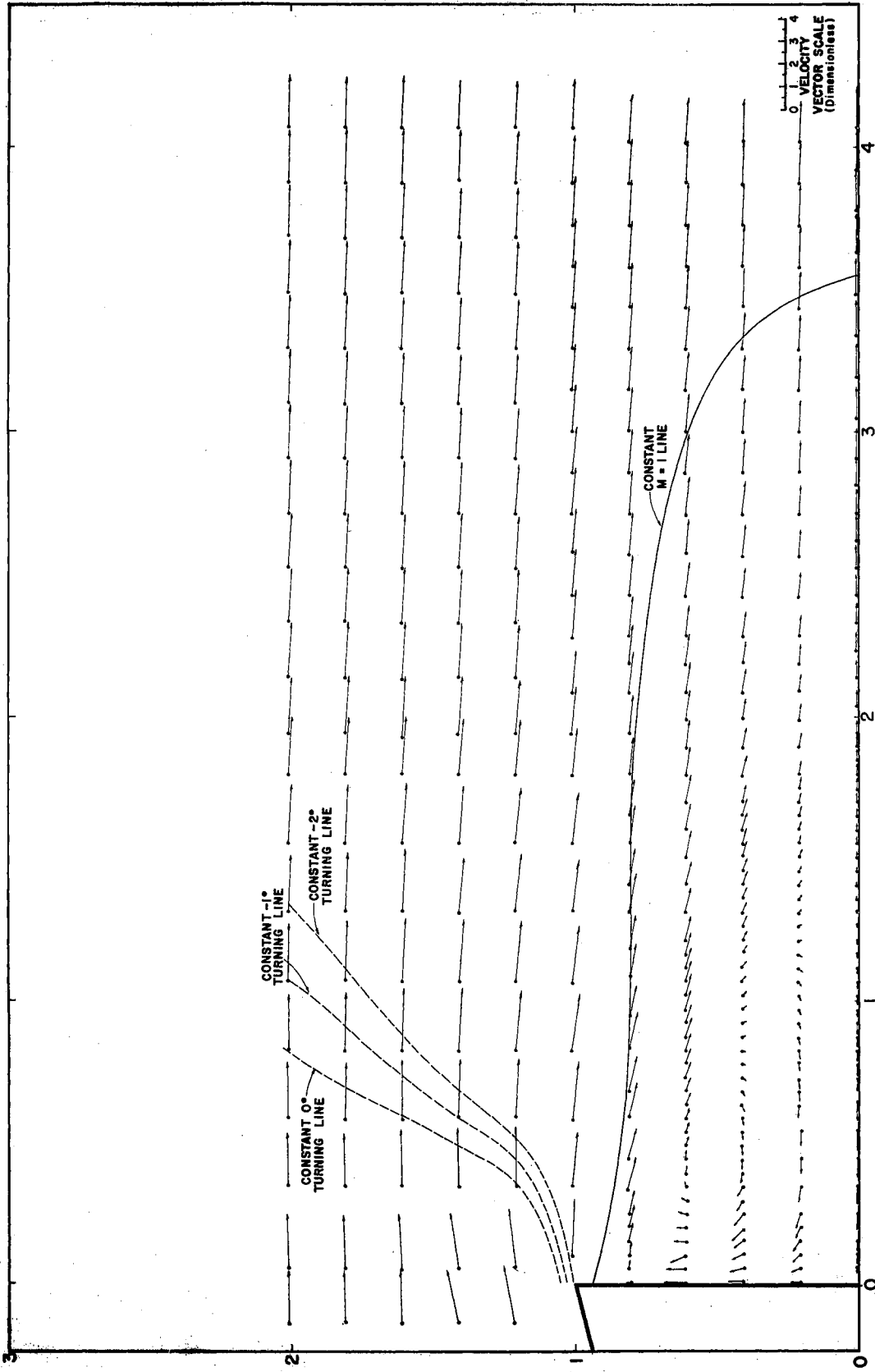


Fig. 30 Velocity Vector Plot in Base Region -- Time Plane 380

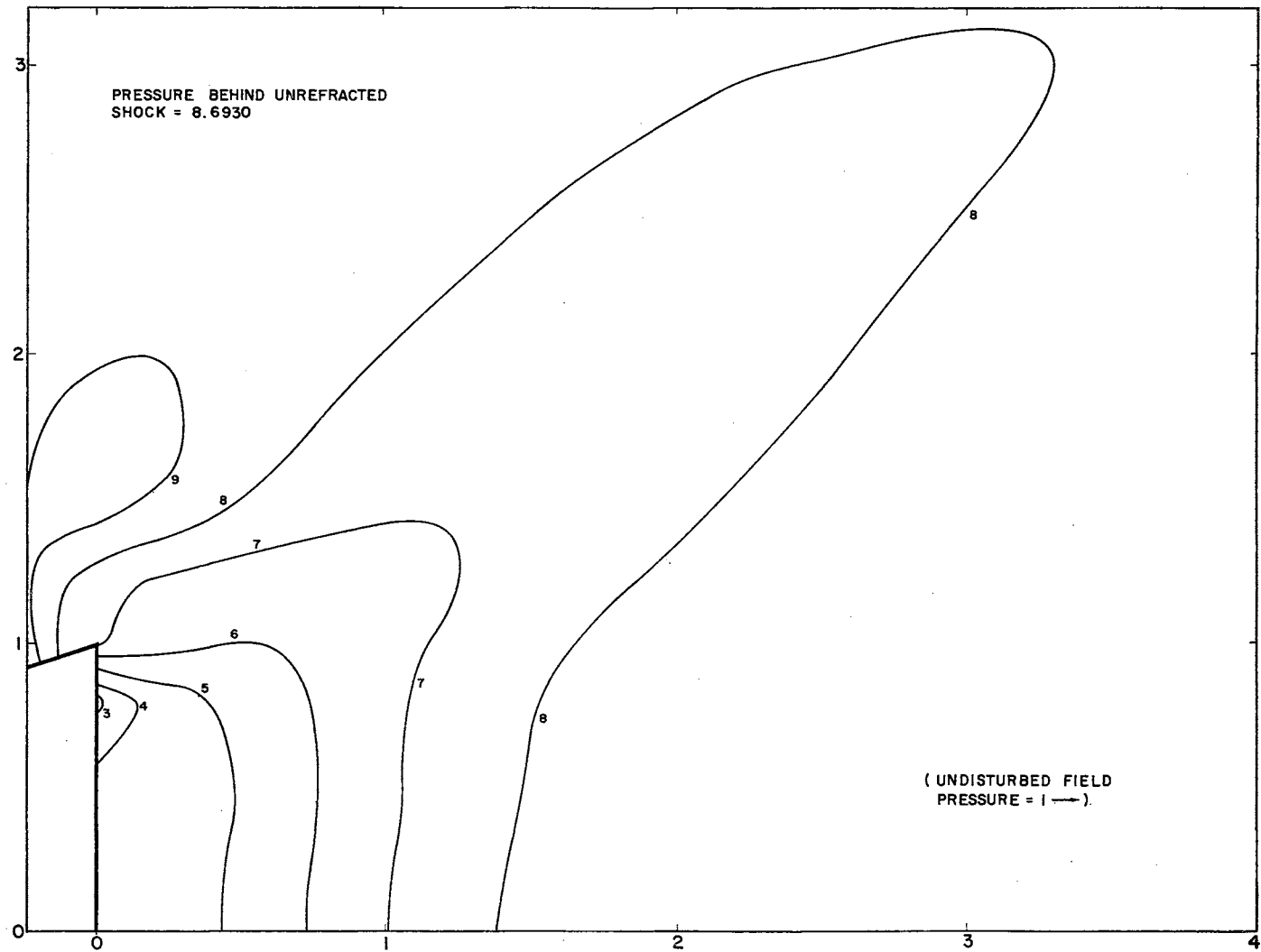


Fig. 31 Constant Pressure Lines (Isobars) for Base Region
Time Plane 380

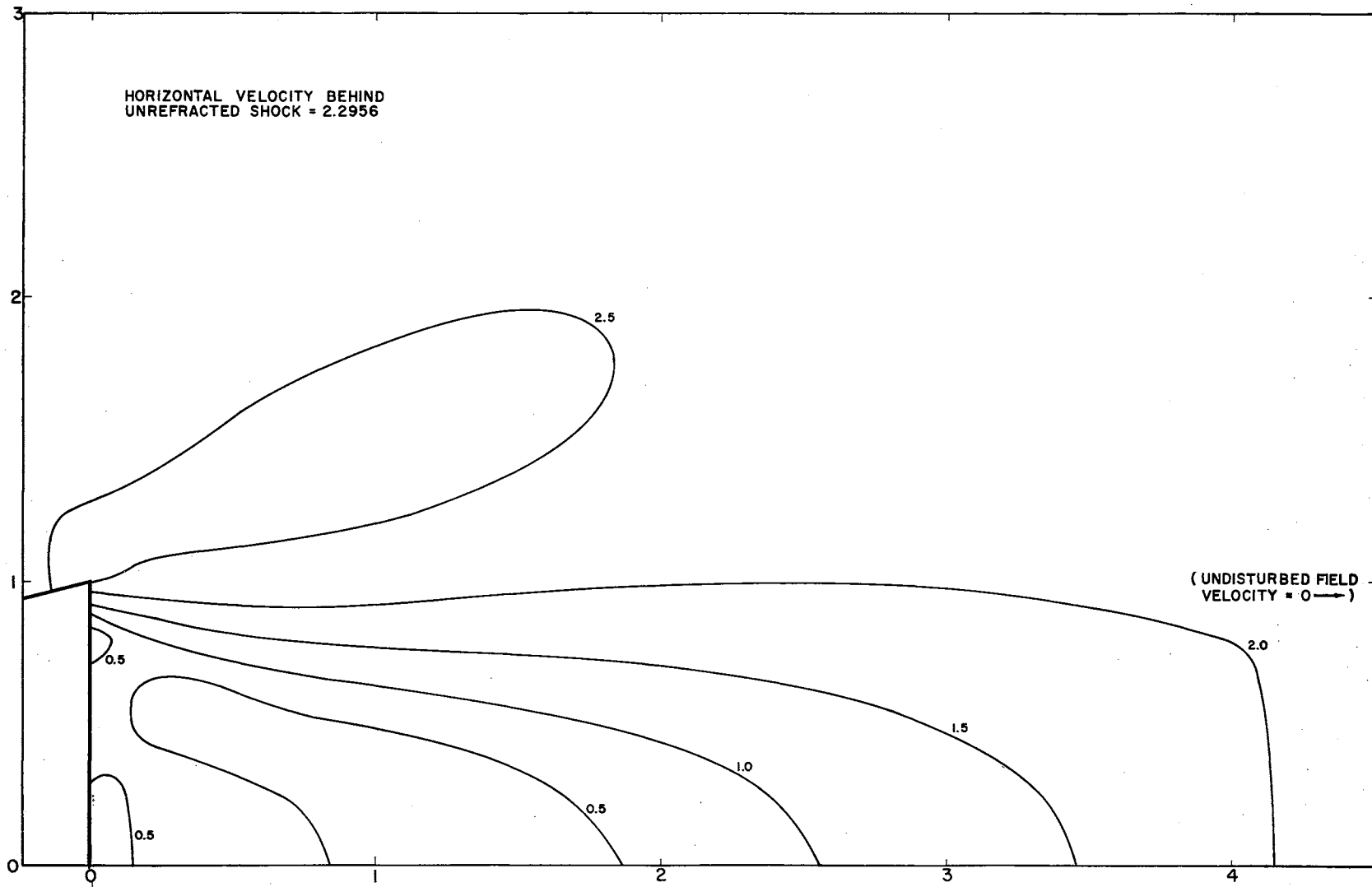


Fig. 32 Constant Velocity Line for Base Region -- Time Plane 380

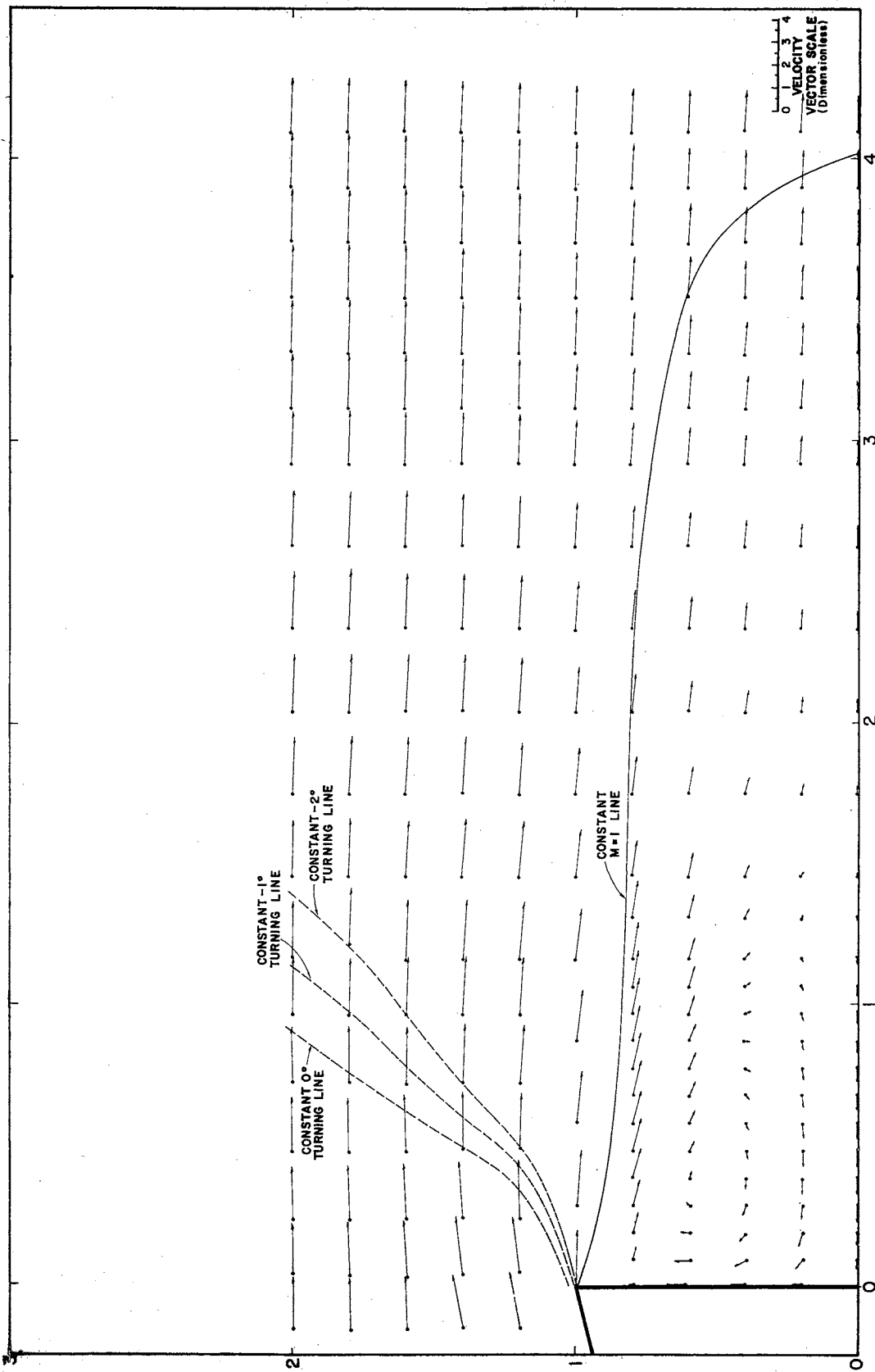


Fig. 33 Velocity Vector Plot in Base Region -- Time Plane 440

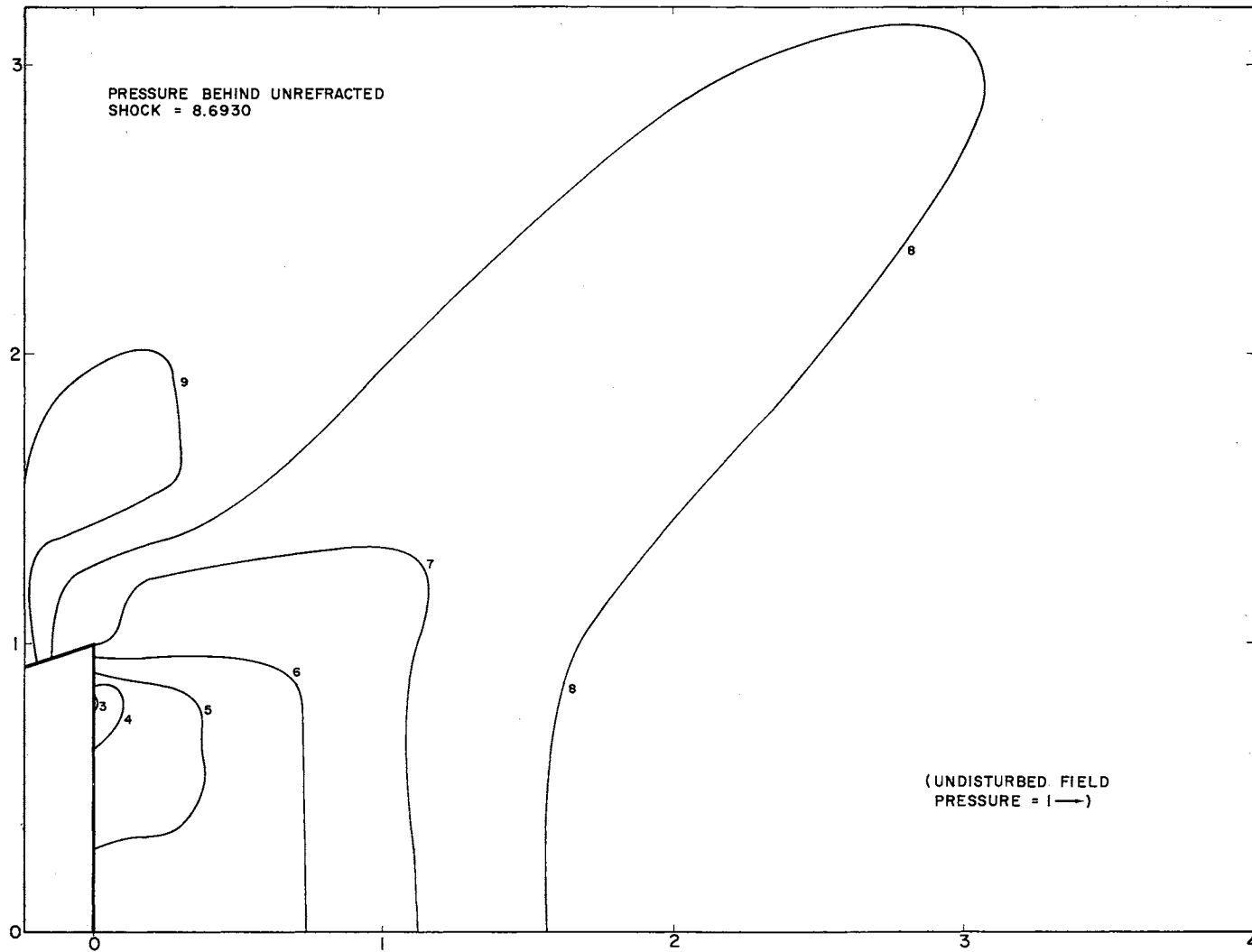


Fig. 34 Constant Pressure Lines (Isobars) for Base Region --
Time Plane 440

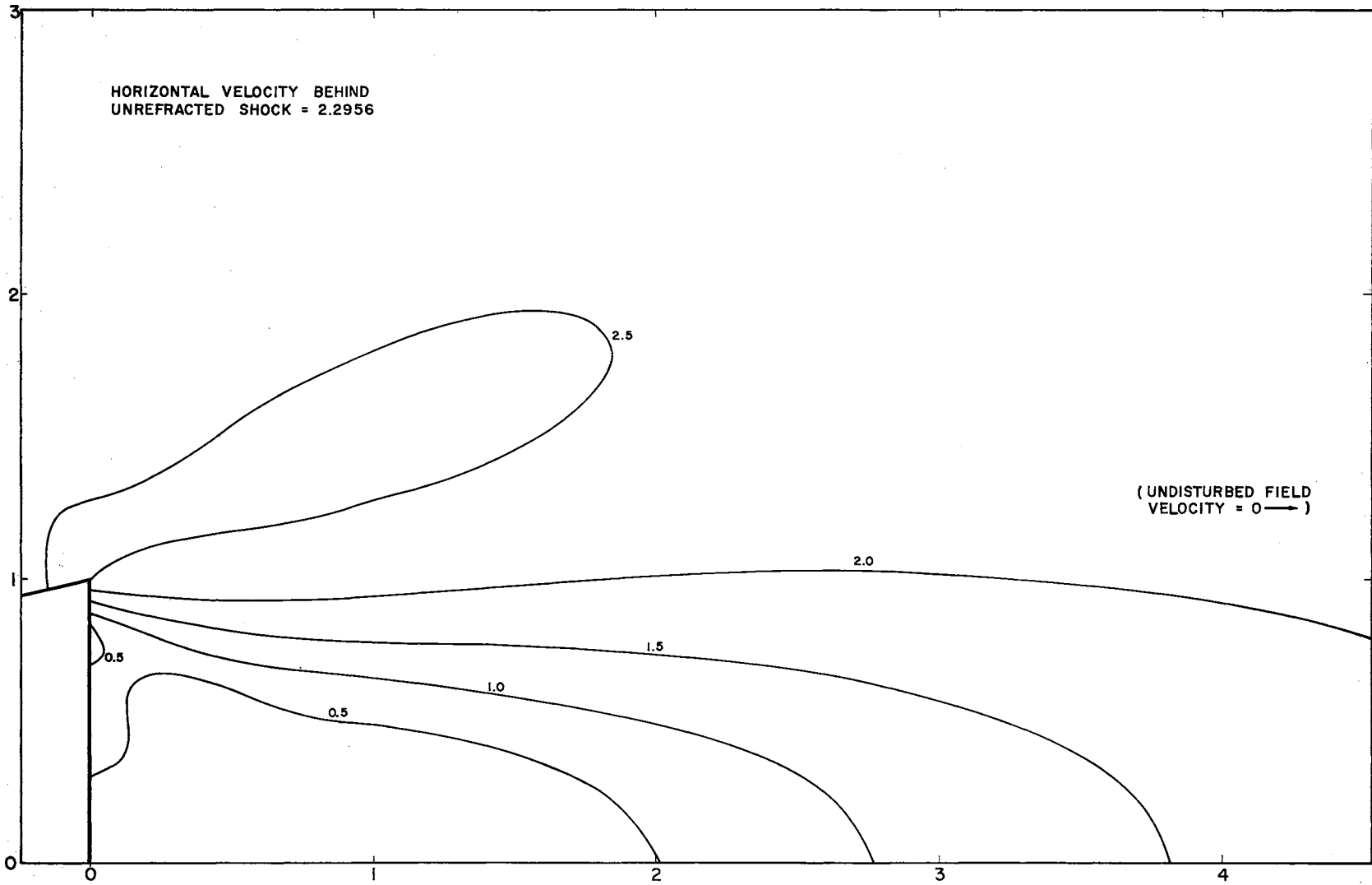


Fig. 35 Constant Velocity Line for Base Region -- Time Plane 440

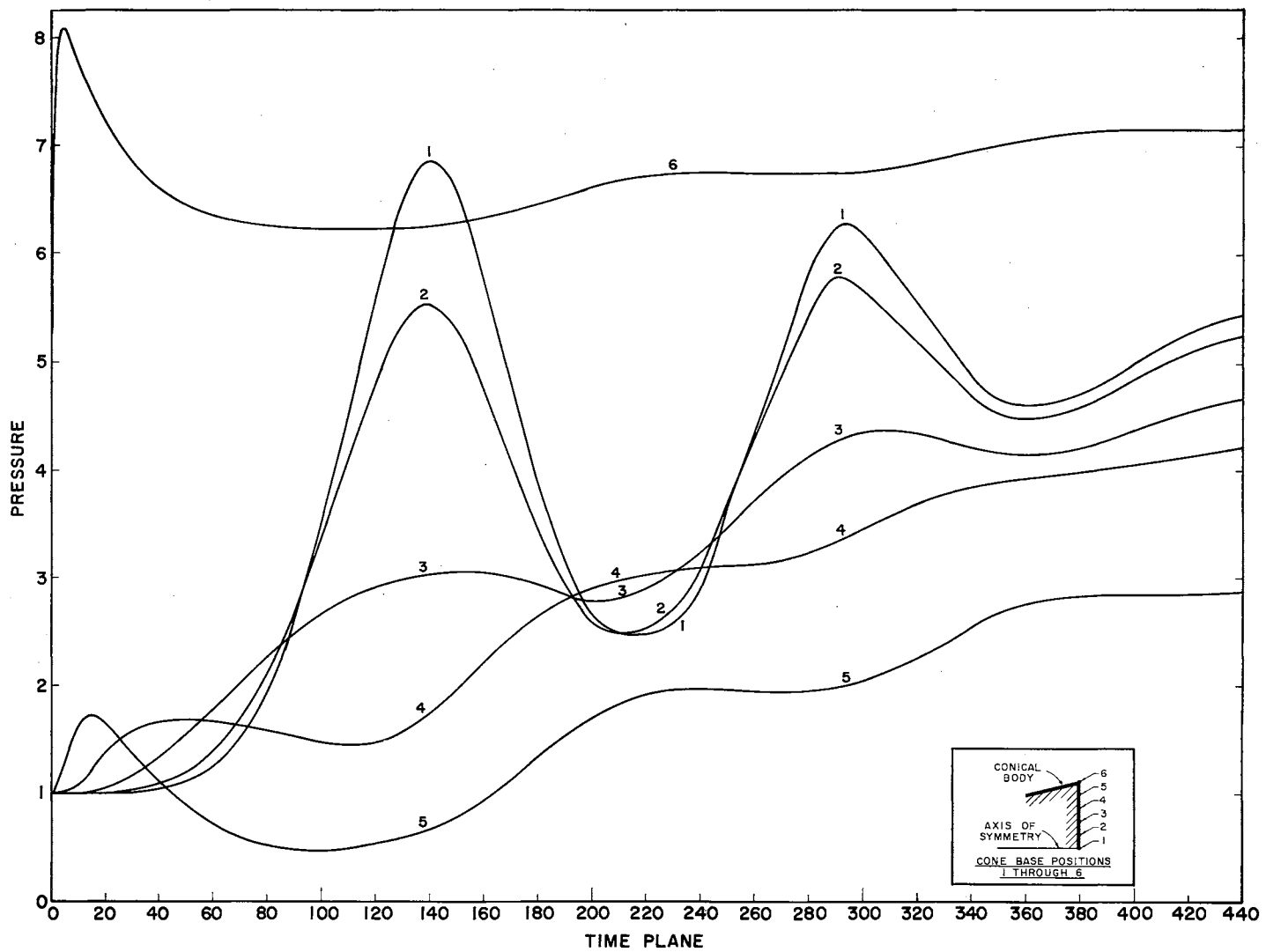


Fig. 36 Pressure Pattern Curves Past Base Positions
Over Range of Time Planes

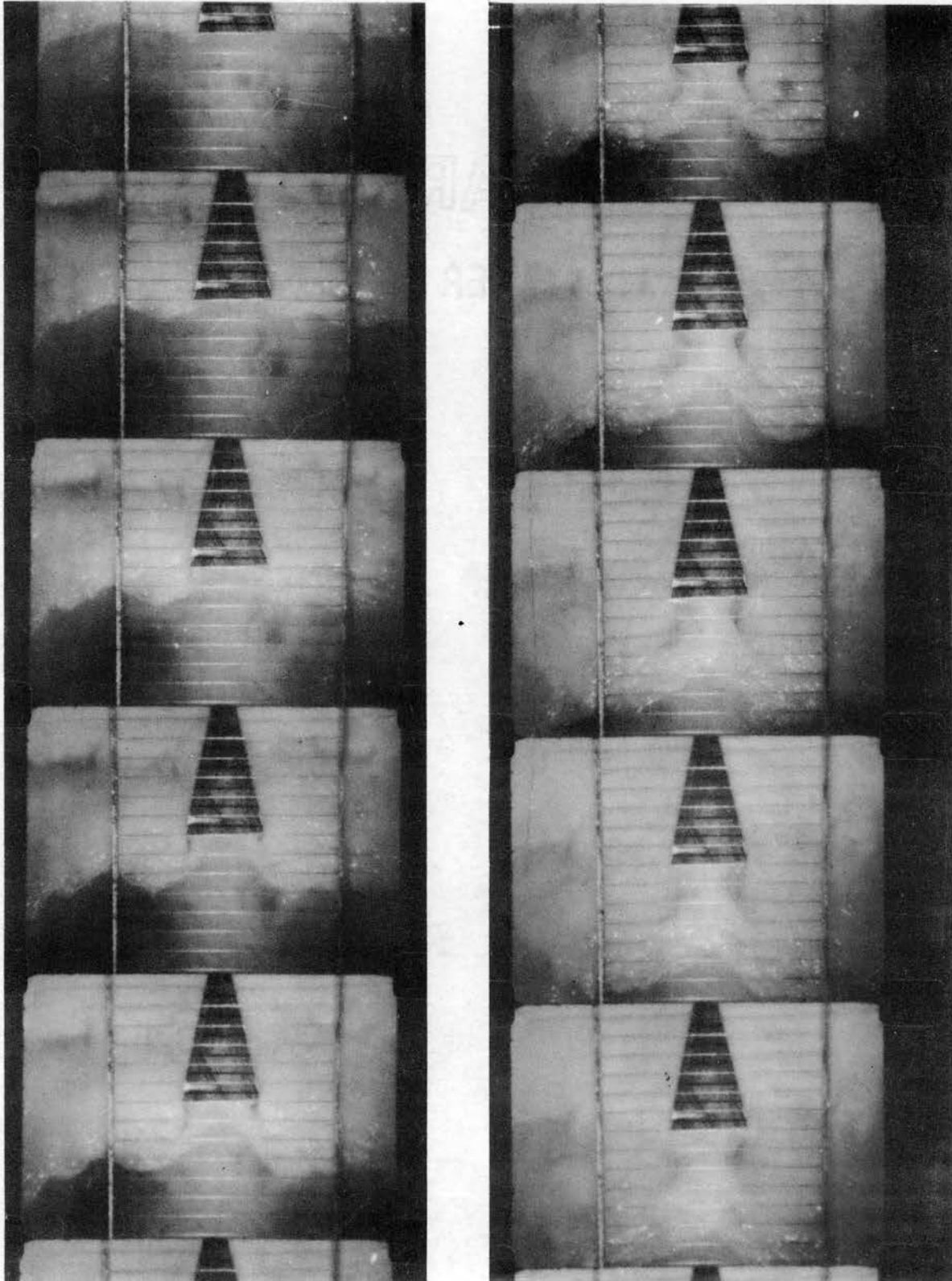


Fig. 37 Blast Wave Simulation on a Water Table

$M=1$ line separating the supersonic region of flow from the subsonic region, as well as lines of constant turning angle. Figure 14 shows the velocity modulus distribution and Figure 13 shows lines of constant pressure (isobars). Note that in these last two figures, the shock wave is represented as a rapidly varying gradient of its physical parameters.

Time Plane 126, illustrated in Figures 15, 16, and 17, depicts the flow pattern after the shock has converged and reflected at the axis of symmetry. Of special significance is the development of a circulation region near the base. This may be attributed to the non-uniform shock passing and reflecting in the base region. Associated with this circulation phenomenon is the region of reverse flow in the base. This region is clearly shown in the velocity vector plot of Figure 15. It will be noted that on the axis of symmetry, the stagnation point, which separates this region of reverse flow, may be easily located.

In Figure 16, the high pressure region behind the shock near the axis of symmetry may be seen clearly. Also, in this same figure, the reduced pressure region, representing the separated flow region, may be noted on the cone base near the separation corner.

Time Planes 166 through 440, shown as Figures 18 through 35, illustrate the transient phenomenon that occurs behind the shock as it progressively moves downstream. Particularly, it will be noted that in Time Plane 260 the shock has traveled nearly four cone radii downstream from the base. In subsequent time planes the shock wave is not visible. This is attributed to the shock passing "through" the boundary at the right

side of the flow matrix and beyond the region of interest. Further time planes depict the base region as a steady-state condition is approached. The region of subsonic flow may also be seen to increase progressively as the fluid is evacuated from the base region. The general pattern can be seen in the water analogy photographs (Figure 37) of a wave passing a wedge.

As the shock converges toward the axis of symmetry, the base pressure rapidly increases to a peak. This is illustrated in Figure 36 which shows the pressure pattern for various base positions during the time calculated. The second large pressure response for positions 1 and 2 appears to be due to a backflow surge.

The computation results can be compared with the shock tube test described in Chapter II, since both had an 8.693 to 1 pressure-ratio shock wave passing a $13,347^\circ$ cone. Points 4 and 1 of Figure 36 correspond to Points 10 and 11 of Figure 4, respectively. After adjusting time and pressure scales to coincide, the comparison is given in Figure 38. For the point on the axis, the first pressure peak and its time of occurrence are almost the same as in the experiment. At the 60 percent radius point, the first peak is somewhat low. For both points, the computed pressure fails to drop as greatly as in the test and an exaggerated second peak appears. This may be due to several factors:

- (a) The non-uniform flow behind the shock at the left boundary was kept constant throughout the calculations. This is in contrast to the transient decay of the velocity near the cone surface as the bow wave forms. This has been discussed previously (page 60).

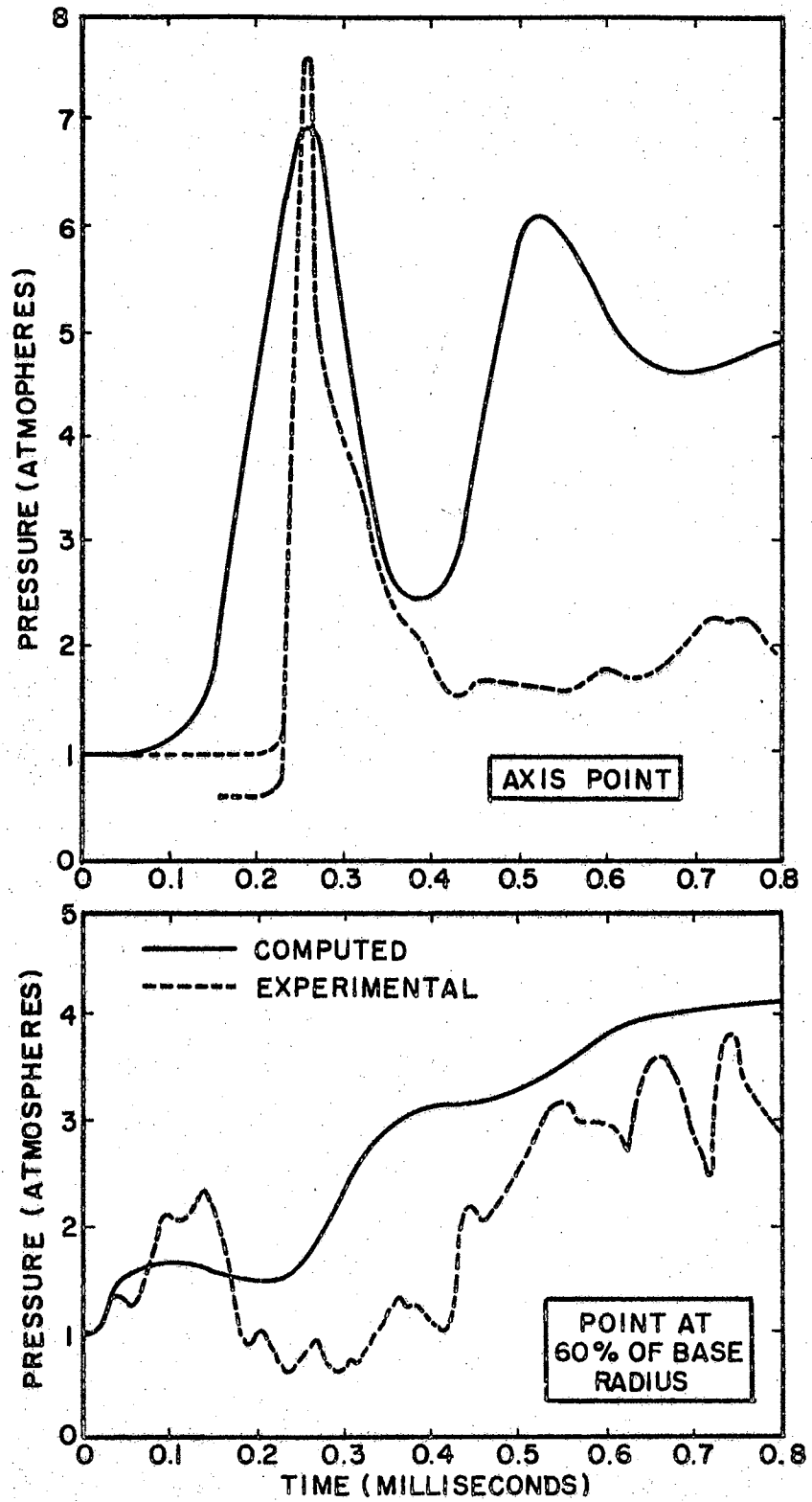


FIG. 38 COMPARISON OF PRESSURE-HISTORY ON THE BASE BY EXPERIMENT AND BY COMPUTATION.

- (b) In the experiments, expansion waves were overtaking the shock, decaying the general pressure field around the cone.
- (c) Viscous entrainment by the jet mixing region occurs and tends to prevent backflow while increasing the evacuation of mass from the base.

All of these would tend to decrease the second pressure peak, since their effects become greater with time. In addition, the tested cone had a rounded, rather than a flat, base, affecting the 60 percent radius point. In view of these differences, the agreement is considered to be very good.

Forebody Exploratory Problem

This section presents an exploratory investigation of the cone forebody problem treated by the numerical field computation method of Rusanov. The aims are two-fold: (a) develop techniques which can be used to describe the transient phenomena of the forebody flow field; (b) establish accurate initial shock and transient upstream field conditions for the blast-base interaction problem. The solution to both of these problems may be accomplished only by obtaining a continuous solution over the conical forebody. If viscous forces are neglected, the transient phenomena behind the shock may be considered entirely wave-dominated.

In an effort to determine the time history of the transient phenomena and the associated shock patterns, an extension of Rusanov's finite difference technique was attempted. This method has previously been discussed. A problem arises, however, in dealing with the cone apex. The boundary conditions of both a wall point and an axis point apply. This requires that both velocity components be zero, and thus the apex becomes a

stagnation point. The effect is that the cone is blunted for one mesh width. Appendix I shows the detailed calculations used to obtain these values for the stagnation point.

A second complexity occurs in representing the boundary conditions for a sloping wall. The mass flux perpendicular to the wall must be zero, and a local coordinate rotation transformation is required at each wall point in applying this boundary condition. Rusanov's original paper (27) explains the method for dealing with such boundaries when the rectangular mesh is so chosen that the wall lies on the diagonal of the mesh points.

Results of this analysis were somewhat disappointing. The stagnation values, being somewhat larger than the values of the original shock wave, apparently created calculation influences which distorted the field during the first several time planes. If a larger computer were available such that this solution were allowed to continue until these initial disturbances became absorbed in the field, i.e., until the stagnation values have actually reached their peak, perhaps a more satisfactory solution could be obtained. The knowledge obtained from this attempt, however, should provide the basis for a more successful solution at some future date. It must be emphasized that this forebody attempt was not the principal purpose of this study. A successful solution would have provided a method of introducing arbitrary upstream boundary field conditions instead of fixed conditions for the base region computations.

The computer program written for this exploratory solution and run on the IBM 1410 computer is shown as Appendix J. The nomenclature used is identical to that used in the Phase II computer program.

CHAPTER IV

BASE PRESSURE ANALYSIS

For a full consideration of the transient flow field and shock pattern in the base region, covering all the time from the blast approach to the quasi-steady flow condition, a base pressure analysis must be performed. The numerical computations considered no viscous effects. Essentially, the computed flow field is the result of a shock wave diffracting around the rear of a body, then reflecting from the axis and/or the body base. If sufficient time is allowed to pass, the waves move downstream and a steady flow situation is approached in the vicinity of the body. However, the steady-state base flow is known to be one determined by viscous effects, namely, the character of the jet mixing in a flow separating from the base corner. Thus, some sort of transition from a wave-dominated phenomenon to a viscosity-dominated phenomenon takes place.

For the Phase III analysis, that is, transition to the quasi-steady separated flow condition at the base, a method for mating the Phase II conditions with the steady-state base flow studies of Zumwalt and Tang (38) was developed. It will be shown that the base flow analysis of the above authors, herein offered as a suggested approach, is well adapted to this type of problem. The one feature of this approach which is of primary interest for the base region application is that it introduces a basic theoretical flow model (See Figure 39) for the jet mixing region

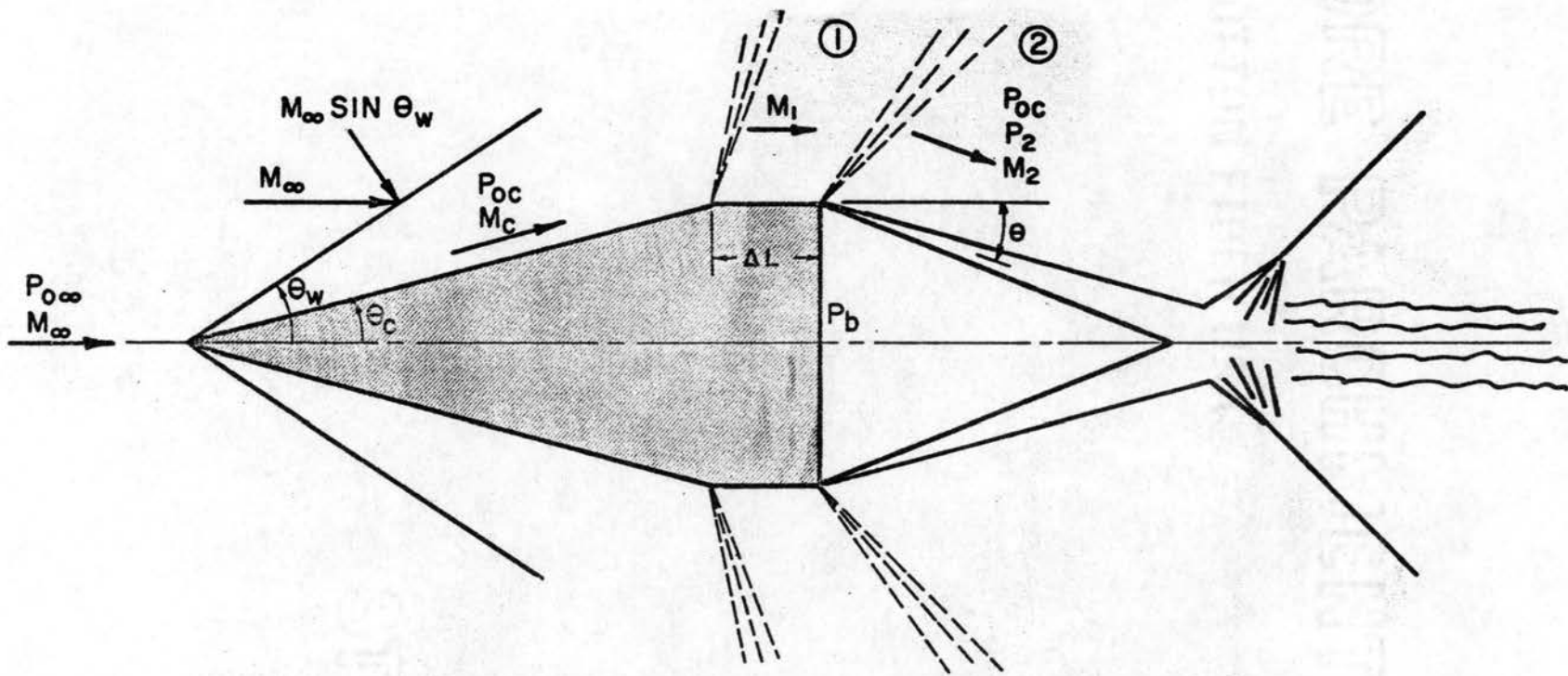


FIG. 39 FLOW MODEL FOR ZUMWALT'S STEADY-STATE CONICAL WAKE ANALYSIS.

which occurs as a result of flow separation. This conical-wake flow model, along with its associated assumptions, is used to predict the steady-state base pressure for comparison with the base pressure obtained from the Phase II computer solution. The highly complex nature of the separated flow in the base region necessitates the introduction of several simplifying assumptions. In this regard, the quasi-steady approach will be adopted in conjunction with a time iteration technique. This technique treats the highly transient flow condition as a finite number of time steps and assumes steady flow for each increment of time. Thus, successive iterations can be performed with resulting property predictions at each increment. In the method, at each iteration step, the amount of mass trapped in the separated flow region must be adjusted toward the stable steady-state condition.

However, the question arises: When do the viscous effects begin to predominate over the shock wave influence? To answer this, the growth of the boundary layer as the wave moves downstream will be considered.

Method Analysis: Phase III

The basic assumptions in this chapter are conveniently illustrated by a series of exaggerated sketches shown in Figure 40. These sketches portray, in chronological sequence, the development of the boundary layer at arbitrary blast wave positions over the entire range of blast passage.

At blast wave position A, the blast has just intercepted the cone apex. For this condition, the forebody has not yet begun to feel the effects of the blast. At blast position B, however, after the blast has

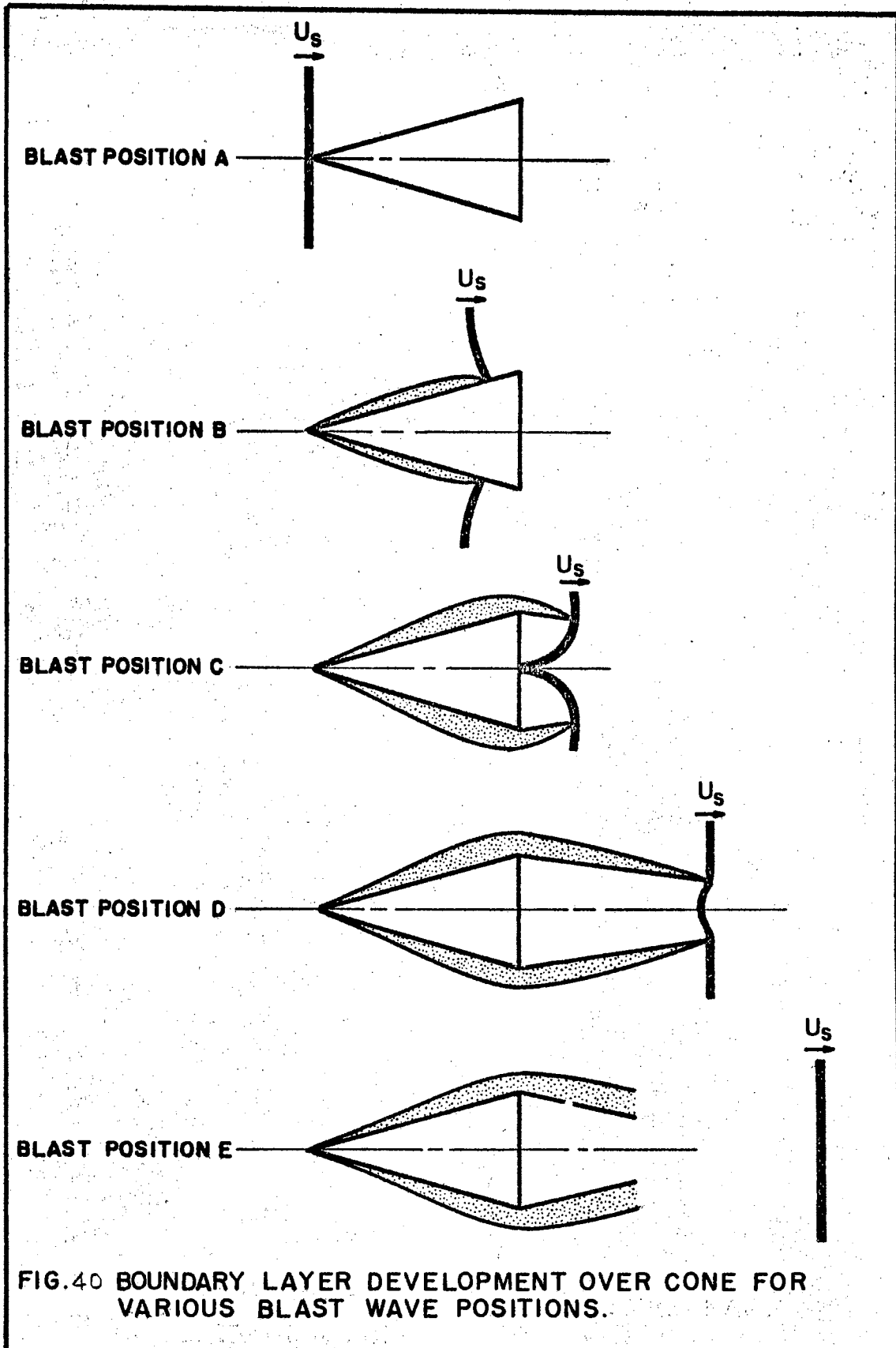


FIG.40 BOUNDARY LAYER DEVELOPMENT OVER CONE FOR VARIOUS BLAST WAVE POSITIONS.

moved to a location on the forebody, the boundary layer formation on the forebody surface can be detected. The initial disturbance caused by the blast passage during the segment of travel from position A to position B will cause a particle, initially at rest near the surface at the cone apex, to accelerate along the surface to some position behind the blast. The particle velocity will be considerably less than the blast velocity so the particle will tend to lag behind the blast wave. The boundary layer thickness depends upon the distance a particle has travelled along the frictional surface, resulting in an instantaneous boundary layer thickness distribution as shown in the figure.

After the shock passes the corner of the cone, as shown in blast position C, boundary layer separation is seen to occur. However, the same particle originally near the apex has still not yet reached the corner. Up to this point, the characteristics of wave action behind the blast predominantly influence the flow and the effects of viscosity will be ignored.

At blast position D, the figure shows the flow field resulting, after boundary layer separation, when the blast is far downstream. At this condition, the particle previously considered is assumed to have reached the corner and the blast is assumed to have progressed far enough downstream such that a quasi-steady condition can be assumed in the base region. Also, at this time, it is assumed that the turbulent boundary layer is fully formed, wave influence is negligible, and viscous forces in the separated shear layer suddenly predominate to such a degree that mass entrainment begins. From this time on, as in blast position E, only the viscous effects are considered in the turbulent mixing layer.

It should be noted that for all separated flows, due to the viscous effects of the fluid, jet mixing occurs. Although it is possible for the mixing region to exist as a laminar shear layer, the mixing region in this analysis is considered to be turbulent, since this is generally the case. A similar method could be developed for laminar mixing.

Since viscous mass entrainment is assumed to begin when a nearby particle has travelled the length of the cone surface, this time may be expressed as

$$t_v = \frac{\text{cone length}}{\text{particle speed along surface}} = \frac{R_b / \sin \theta_c}{u_y / \cos \theta_c} = \frac{R_b}{u_y \tan \theta_c} \quad (52)$$

Specifically, for the 13.347° cone with a 4-inch base radius and the computed blast, the time becomes

$$t_v = \frac{(0.333) \text{ ft} / (0.23725)}{2165 \text{ ft/sec}} = 649 \times 10^{-6} \quad (53)$$

Using the time conversion factor previously developed, and shown in Figure 10, this corresponds to a dimensionless computer solution time of

$$t_v = \frac{649 \times 10^{-6}}{1415 \times 10^{-6}} = 0.458 \quad (54)$$

From Figure 10, it can readily be seen that this corresponds to Time Plane 354. However, since this time plane was not included in the computer printout, Time Plane 360 was used as the approximation of the viscous starting time. The base pressure at this time is taken to be the sum

of the pressure forces exerted on the base surface divided by the base area.

In mathematical form, the average base pressure may be written as

$$p_{b \text{ avg}} = \frac{2\pi \int_0^R p_b r dr}{2\pi \int_0^R r dR} \quad (55)$$

Written in summation form, this equation is

$$p_{b \text{ avg}} = \frac{2 \sum_{i=1}^n p_{b_i} \left\{ \frac{r}{R} \right\}_i \left\{ \frac{\Delta r}{R} \right\}_i}{2} \quad (56)$$

where $i=1,2,3,4,5$, and $n=5$ for the computer solution presented in Chapter III. The solution of equation 56 gives p_b of 3.333 atmospheres.

Before outlining the method used to mate these Phase II results to Zumwalt's and Tang's analysis, several important features of the conical flow model should first be noted. Referring to Figure 39, which depicts the flow model which has been superimposed on the Phase II flow field, a small cylindrical surface extension is assumed to exist with an infinitesimal length, ΔL , in the limit. The flow passing the model then induces an initial conical shock followed by two Prandtl-Meyer expansions before it forms a free jet mixing layer in the base region. For small boundary layer thicknesses, where boundary layer interaction is ignored, the use of two-dimensional expansions at the turning corners is satisfactory.

To outline the calculation procedure used to obtain the steady-state base flow conditions, reference is again made to the conical model shown in Figure 39. In the analysis, the base pressure can be determined

as a function of the free stream Mach number, M_∞ ; pressure, p_∞ ; and the cone semi-angle, θ_c .

Since the free stream Mach number is known, the free stream conditions are easily determined from standard compressible flow charts or tables as in the following sequence. The symbol \longrightarrow means "yields."

$$1. \quad M_\infty \xrightarrow{\text{isentropic relations}} \frac{P_\infty}{P_{O\infty}}, \frac{T_\infty}{T_{O\infty}} .$$

$$2. \quad P_{O\infty} = \frac{P_{O\infty}}{P_\infty} \left| \frac{P_\infty}{M_\infty} \right., \quad T_{O\infty} = \frac{T_{O\infty}}{T_\infty} \left| \frac{T_\infty}{M_\infty} \right. .$$

To evaluate conditions behind the conical shock:

$$3. \quad \left. \begin{matrix} M_\infty \\ \theta_c \end{matrix} \right\} \text{conical shock} \longrightarrow \theta_c \longrightarrow M_\infty \sin \theta_w \xrightarrow{\text{normal shock}} \frac{P_{Oc}}{P_{O\infty}} \longrightarrow P_{Oc} .$$

$$4. \quad \left. \begin{matrix} M_\infty \\ \theta_c \end{matrix} \right\} \text{conical shock} \longrightarrow P_c .$$

$$5. \quad \frac{P_c}{P_{Oc}} \xrightarrow{\text{isentropic relations}} M_c \longrightarrow v_c .$$

To evaluate conditions on the cylindrical section:

$$6. \quad v_1 = v_c + \theta_c \xrightarrow{\text{isentropic relations}} M_1 \longrightarrow \frac{P_1}{P_{Oc}} \longrightarrow P_1 .$$

After the foregoing properties have been determined, Zumwalt's steady-state, non-bleed, base pressure solution, as shown in Figure 41, is used. This allows determination of the base flow conditions to include the steady-state base pressure, $p_{b_{st}}$. This may be shown in the following steps.

$$7. \quad M_1 \xrightarrow{\text{Figure 41}} \frac{P_b}{P_1} .$$

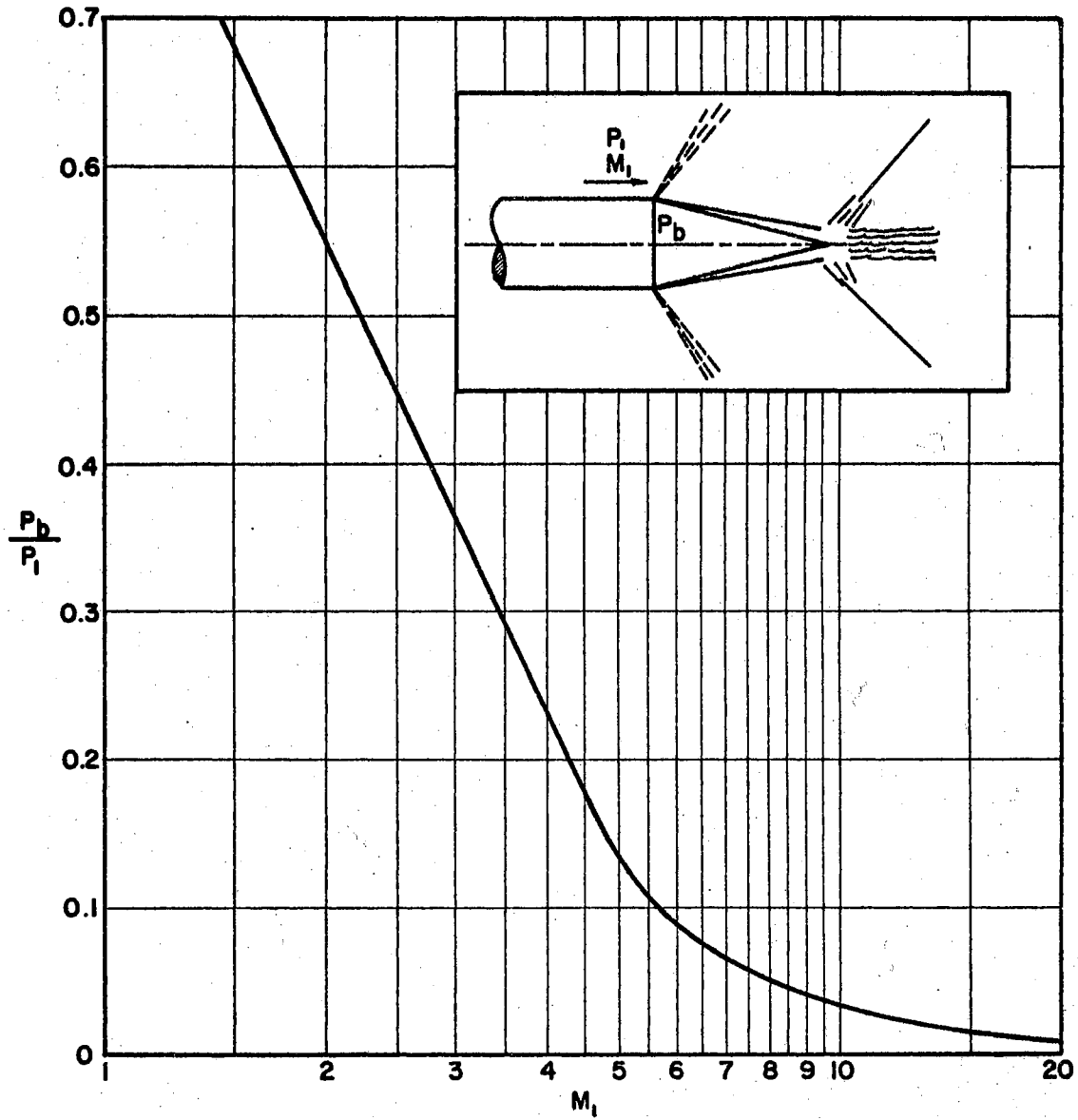


FIG. 41 STEADY, NON-BLEED, BASE PRESSURE SOLUTION USING ZUMWALT'S CONICAL WAKE ANALYSIS.

$$8. \frac{p_{bst}}{p_{\infty}} = \frac{p_{bst}}{p_1} \cdot \frac{p_1}{p_{\infty}} = \frac{p_{bst}}{p_1} \cdot \frac{p_1}{p_{o1}} \cdot \frac{p_{oc}}{p_{o\infty}} \cdot \frac{p_{o\infty}}{p_{\infty}} \longrightarrow p_{bst} .$$

$$9. \frac{p_{bst}}{p_{oc}} \xrightarrow{\left\{ \begin{array}{l} \text{P.M.} \\ \text{turn} \end{array} \right\}} M_2 \longrightarrow v_2 \longrightarrow \theta_2 = (v_2 - v_1) \longrightarrow \tan \theta_2 .$$

Following this procedure, the actual calculations for existing conditions are shown in Appendix F. The base pressure value is seen to equal 3.30 atmospheres. Thus, in spite of the relatively complicated flow existing in the base region during the wave passage, the base pressure value given by the computer solution at time t_v is almost identical to the steady-state value given by Zumwalt's (37) wake analysis. This, however, must be regarded as fortuitous, and the values cannot generally be expected to agree so closely.

Note, however, that the base pressure created by the shock wave action is slightly higher than that which will exist at steady-state. This may be interpreted as an indication of a slight mass bleed-out rate which must occur during a transient period. Some amount of mass will be pumped in or out of the base region through the mixing region until a stable steady-state condition is reached.

As given by Zumwalt and Tang for the transient period, the mass in the separated region (the "wake") at the base at any instant of time may be determined from

$$m_t = (\rho_b V_b)_t = \frac{p_{bt} \pi R^3 \cot \theta_t}{RT_{ot}} \quad (57)$$

Further, the mass in the base at time $t+\Delta t$ is given as

$$m_{(t+\Delta t)} = m_t + \dot{m} \Delta t \quad , \quad (58)$$

where \dot{m} is the rate of mass pumped into the "wake" at time t . For this latter assumption, an isoenergetic jet mixing condition is assumed. That is, the stagnation temperature of the base region and of the adjacent stream are the same. Of course, the quasi-steady concept is still maintained. The value of mass bleed rate, \dot{m} , is calculated from the \mathcal{C} curves shown as Figure 18 in Reference (38).

Knowing the $m_{(t+\Delta t)}$ value, the base pressure at time $t+\Delta t$ can be determined from equation (57). However, the value of $\theta_{(t+\Delta t)}$ must be iterated until $p_{b(t+\Delta t)}$ reached by Prandtl-Meyer expansion at the separation corner is equal to the steady-state base pressure, $p_{b_{st}}$, calculated previously. That is, the pressure across the jet-mixing surface must be constant at any particular time. Calculation details of this procedure may be found in Appendix F.

Thus, a procedure has been developed to compute the conditions at the base during the transient period from the blast wave passage to the steady flow condition.

CHAPTER V

CONCLUSIONS AND RECOMMENDATIONS

Conclusions

As part of a research program to study the principles involved in the interaction of a blast wave and the base pressure region of a missile re-entering the atmosphere, methods were sought to compute the transient phenomena which occur. The primary objective of this phase of the investigation, which has been completed, was to perform a transient flow field analysis of a plane blast wave intercepting a stationary cone at zero angle of attack. This type of analysis, though difficult, has provided considerable knowledge about methods and techniques which may be used to predict such phenomena.

Numerical solutions provide the best means of producing results for complicated flow fields, thereby permitting the influencing parameters to be calculated. The mechanisms for numerical techniques are relatively simple, although a computer capable of large storage capacity is required. With computer programs specifically designed for these large computers, larger flow fields may be considered thereby yielding more accurate results.

The approximate methods developed and investigated in this analysis are shown to be very satisfactory and may be applied, with reasonable

assurance, to other geometries. The results of this analysis have provided close representations of physical phenomena within the accuracy of the assumptions made.

To summarize, the method for the transient analysis for the stationary cone has been developed. Extensions of several methods were utilized and made compatible with existing flow conditions to provide a continuous flow solution. In Chapter II, Whitham's approximate solution was used to obtain the shock diffraction pattern past the forebody. This solution was shown to be in close agreement with experimental shock tube tests. The shock wave configuration and flow field properties were adapted to provide initial conditions for the blast-base interaction.

Chapter III discloses some of the difficulties encountered with finite difference representations of governing differential equations of motion. Even though the problem is complex, the numerical solutions show the feasibility of solving complicated axi-symmetric flow fields to determine the effects of governing variables. The method of Rusanov, as proposed in this analysis, has been demonstrated to yield excellent representations for 440 time planes, 9 of which were selected for presentation. With the introduction of satisfactory boundary conditions, this method may be applied to numerous types of flow problems. Further, a water table experiment, using several conical models, was performed to provide qualitative verification of the physical phenomena.

In Chapter IV, the results of the blast-base interaction solution were used to mate the blast passage with the formation of the separated flow region behind the body. It is shown that the steady-state base flow studies of Zumwalt and Tang provided the method used to accomplish this.

The use of Zumwalt's conical wake analysis introduced a satisfactory physical model for the jet mixing region which occurs as a result of flow separation.

Thus, a continuous flow solution, from the time the blast wave intercepts the conical body to the quasi-steady state condition has been performed.

Specific Recommendations

The theories and calculation techniques discussed herein can be applied to many shock diffraction problems utilizing a variety of physical geometries. In order to treat a wider range of such problems, the following suggestions are enumerated for further analytical and experimental work:

1. To modify this present analysis to be applicable to general cases, a solution should be attempted, using the same numerical techniques proposed in this analysis, to solve the axi-symmetric forebody problem of a blast wave intersecting a moving vehicle at arbitrary angles of attack. This problem would include several discontinuities in the flow and should consider various shock strengths.

2. Throughout this analysis, ionization and real gas effects have been completely neglected. Future analytical studies should consider these effects in addition to the force contributions from forebody pressure, forebody viscous effects, heat conduction, and base pressure for bodies which are either at rest or moving at supersonic speeds.

3. The flow field behind the shock has been assumed non-uniform but constant in this analysis. Studies of boundary conditions should be

undertaken to simulate the effect of a decaying flow field behind the shock. Thus, the boundary equations would change, but the method of solution would be the same.

4. An understanding of the mechanisms of blast wave interaction on the base region when encountering the wave front at arbitrary orientations should be pursued. This study should include blasts interacting with fully formed turbulent mixing regions.

5. This analysis has been designed to provide an understanding of the transient flow field resulting from the intercept of a blast wave and a conical body. Extensions of this analysis should be considered for application to blunt or spherical geometries.

6. When a supersonic missile flies head-on into a "fire-ball", such as might be encountered in a nuclear blast, the resulting effect on the missile is a function of the interaction of the bow shock and the incident blast wave. Studies should be performed to determine the influencing parameters which affect the missile when it exits from the blast. This should include both axial exit and exit at arbitrary orientations.

7. Numerous computing techniques are available for solving flow problems of this type. The most effective of these should be combined into a very general program which would provide as much flexibility, efficiency, and accuracy as possible.

8. Experimental programs should be initiated to verify the analytical results of all proposed studies.

If the above work is accomplished, the complex mechanisms of blast-intercept phenomena will be more completely understood and the solutions to such problems can be more accurately computed.

SELECTED BIBLIOGRAPHY

1. Bryson, A. E., and Gross, R. W. F., "Diffraction of Strong Shocks by Cones, Cylinders, and Spheres," J. Fluid Mech., Vol. 10, pp. 1 ff., 1961.
2. Chester, W., "The Propagation of Shock Waves in a Channel of Non-Uniform Width," Quart. J. Mech. and Applied Math., Vol. VI, Pt. 4, 1953.
3. Chester, W., "The Diffraction and Reflection of Shock Waves," Quart. J. Mech. and Applied Math., Vol. VII, Pt. 1, 1954.
4. Chisnell, R. F., "The Motion of a Shock Wave in a Channel, With Applications to Cylindrical and Spherical Shock Waves," J. Fluid Mech., Vol. 2, pp. 286 ff., 1957.
5. Courant, R., and Friedrichs, K., "Supersonic Flow and Shock Waves," Interscience Publishers, New York, pp. 318 ff., 1948.
6. Crocco, L., "Solving Numerically the Navier-Stokes Equations," Defense Documentation Center, U. S. Department of Commerce, AD 439220, May, 1964.
7. Filippov, I. G., "On the Theory of Diffraction of Weak Shock Waves Round Contours of Arbitrary Shape," PMM, Vol. 27, No. 1, pp. 75 ff., 1963.
8. Godunov, S. K., "A Difference Method for the Calculation of Shock Waves," American Mathematical Society Translation, Vol. 16, pp. 389 ff., 1957.
9. Godunov, S. K., "A Difference Method for the Numerical Calculation of Discontinuous Solutions of Hydrodynamic Equations," JPRS: 7225, Office of Technical Service, November, 1960.
10. Holt, R. E., and Crist, R. A., "Calibration of a Six Foot and a Two Foot Diameter Shock Tube," AFSWC-TDR-63-5, April, 1963.
11. Lax, P. D., "Discontinuous Initial Value Problems for Nonlinear Equations and Finite Difference Schemes," LAMS-1332, February, 1953.

12. Lax, P. D., "Weak Solutions of Nonlinear Hyperbolic Equations and Their Numerical Computation," *Comm. on Pure and Appl. Math.*, Vol. VII, pp. 159 ff., 1954.
13. Lax, P. D., and Richtmyer, R. D., "Survey of the Stability of Linear Finite Difference Equations," *Comm. on Pure and Appl. Math.*, Vol. IX, pp. 267 ff., 1956.
14. Lax, P. D., "Hyperbolic Systems of Conservation Laws II," *Comm. on Pure and Appl. Math.*, Vol. 10, pp. 537 ff., 1957.
15. Lax, P. D., and Wendroff, B., "Systems of Conservation Laws," *Comm. on Pure and Appl. Math.*, Vol. XIII, pp. 217 ff., 1960.
16. Lax, P. D., "Nonlinear Hyperbolic Systems of Conservation Laws," *Nonlinear Problems, Publication 8, Mathematics Research Center, United States Army, The University of Wisconsin*, pp. 3 ff., 1963.
17. Lighthill, M. J., "The Diffraction of Blast I," *Proc. Roy. Soc., Series A*, Vol. 198, pp. 454 ff., 1949.
18. Lighthill, M. J., "The Diffraction of Blast II," *Proc. Roy. Soc., Series A*, Vol. 200, pp. 554 ff., 1950.
19. Ludloff, H. F., and Friedman, M. B., "Aerodynamics of Blasts-Diffraction of Blasts Around Finite Corners," *J. Aero. Sci.*, Vol. 22, January, 1955.
20. Ludloff, H. F., and Friedman, M. B., "Difference Solution for Shock Diffraction Problem," *J. Aero. Sci.*, Vol. 22, pp. 27 ff., 1955.
21. Marquardt, R. F., and King, L. S., "Blast Wave Forces on a Conical Body," *General Dynamics, Report Prepared for Sandia Corporation, SC-4984(RR)*, 1964.
22. Miles, J. W., "Notes on the Diffraction of Blasts by Flying Vehicles," *Aerospace Corp., TDR-269(4230-30)-1*, August, 1963.
23. Pack, D. C., "The Reflection and Diffraction of Shock Waves," *J. Fluid Mech.*, pp. 549 ff., 1963.
24. Payne, R. B., "A Numerical Method for a Converging Cylindrical Shock," *J. Fluid Mech.*, Vol. II, pp. 185, 1957.
25. Randall, D. E., "Pressure Distribution Determined From the Test of a Cone Model in the AFWL Shock Tube," *Tech Memo SC-TM-64-1282, Sandia Corporation*, November, 1964.

26. Riley, N., "Interaction of a Shock Wave With a Mixing Region," J. Fluid Mech., Vol. 7, pp. 321 ff., 1959.
27. Rusanov, V. V., "The Calculation of the Interaction of Non-Stationary Shock Waves and Obstacles," National Research Council of Canada Library, Ottawa, Canada, Technical Translation 1027 by D. A. Sinclair, 1962; translated from Zhurnal Vychislitelnoi Matematiki i Matematicheskoi Fiziki, (Akademiya Nauk, SSSR), 1: No. 2, pp. 267-279, 1961.
28. Smyrl, J. L., "The Impact of a Shock-Wave on a Thin Two-Dimensional Aerofoil Moving at Supersonic Speed," J. Fluid Mech., Vol. 15, pp. 223 ff., 1963.
29. Sternberg, Joseph, "Triple-Shock-Wave Intersections," Physics of Fluids, Vol. 2, pp. 179 ff., 1959.
30. Ting, L., and Ludloff, H. F., "Aerodynamics of Blasts," J. Aero Sci., Vol. 19, pp. 317, 1952.
31. Von Neuman, J., and Richtmyer, R. D., "A Method for the Numerical Calculations of Hydrodynamical Shocks," J. Appl. Phys., Vol. 21, pp. 232, 1950.
32. Whitham, G. B., "On the Propagation of Weak Shock Waves," J. Fluid Mech., Vol. 1, pp. 290 ff., 1956.
33. Whitham, G. B., "A New Approach to Problems of Shock Dynamics, Part I, Two-Dimensional Problem," J. Fluid Mech., Vol. 2, pp. 145 ff., 1957.
34. Whitham, G. B., "On the Propagation of Shock Through Regions of Non-Uniform Area or Flow," J. Fluid Mech., Vol. 4, pp. 137 ff., 1958.
35. Whitham, G. B., "A New Approach to Problems of Shock Dynamics, Part II, Three-Dimensional Problems," J. Fluid Mech., Vol. 5, pp. 369 ff., 1959.
36. Wolf, W. S., "Transient Flow Field Analysis Around a Conical Body Exposed to a Blast Wave," Lockheed Missiles and Space Company, Report No. 4-70-64-1, 1964.
37. Zumwalt, G. W., "Analytical and Experimental Study of the Axially-Symmetric Supersonic Base Pressure Problem," Ph.D., Dissertation Department of Mechanical Engineering, Univ. of Illinois, 1959.
38. Zumwalt, G. W., and Tang, H. H., "Transient Base Pressure Study of an Axi-Symmetric Supersonic Missile Flying Head-on Through a Blast Wave," Research Report Prepared for the Aero-Thermodynamics Dept. of Sandia Corporation, Albuquerque, N. M., by the Office of Engineering Research, Okla. State Univ., Stillwater, Okla., Report No. SBW-6, February, 1964.

39. Zumwalt, G. W., and Damkevala, R. J., "Predicted Shock Wave Patterns for a Supersonic Conical Missile Passing Through a Blast Wave," Research Report Prepared for the Aero-Thermodynamics Dept. of Sandia Corporation, Albuquerque, N. M., by the Office of Engineering Research, Okla. State Univ., Stillwater, Okla., Report No. SBW-8, 1965.

APPENDIX A

WHITHAM'S RAY TUBE ANALOGY

In order to describe Whitham's analogy of the similarity of wave propagation in a ray tube to the propagation of a shock wave in a tube with solid walls, the choice of independent variables must be carefully selected. In two dimensions, the choice of these variables is based on the shock positions and the rays. However, if an attempt is made to apply such a coordinate system to an axi-symmetric problem, the solution becomes formidable. Because of this, the analogy must be formulated in a three-dimensional Cartesian coordinate system. The motion of the shock is then described as

$$c_x t = \alpha(x,y,z) \quad , \quad (A-1)$$

where t is the time at which the shock occupies that position and c_x is the speed of sound in the undisturbed gas ahead of the shock.

The problem now is to determine the function $\alpha(x,y,z)$. Since the ray is normal to the shock, the distance ds along a ray between the shock positions at t and $t+dt$ is given by

$$c_x dt = ds \left| \nabla \alpha \right| \quad . \quad (A-2)$$

To illustrate this relationship, differentiate equation (A-1). This yields

$$c_x dt = d\alpha(x,y,z) = \frac{\partial \alpha}{\partial x} dx + \frac{\partial \alpha}{\partial y} dy + \frac{\partial \alpha}{\partial z} dz \quad . \quad (A-3)$$

However, note that

$$\vec{s} = ix + jy + kz \quad ,$$

which when differentiated becomes

$$d\vec{s} = idx + jdy + kdz \quad .$$

Also, note that

$$\nabla\alpha \equiv i\frac{\partial\alpha}{\partial x} + j\frac{\partial\alpha}{\partial y} + k\frac{\partial\alpha}{\partial z} \quad ,$$

and

$$|\nabla\alpha| = \sqrt{\alpha_x^2 + \alpha_y^2 + \alpha_z^2} \quad .$$

Now, equation (A-3) may be written as

$$c_x dt = (idx + jdy + kdz) \cdot \left(i\frac{\partial\alpha}{\partial x} + j\frac{\partial\alpha}{\partial y} + k\frac{\partial\alpha}{\partial z} \right) \quad ,$$

which reduces to

$$c_x dt = d\vec{s} \cdot \nabla\alpha \quad . \quad (A-4)$$

However, $\nabla\alpha = i|\nabla\alpha|$ and $d\vec{s} = ids$, which when substituted into equation (A-4) yields

$$c_x dt = (ids) \cdot (i|\nabla\alpha|) = ds|\nabla\alpha| \quad .$$

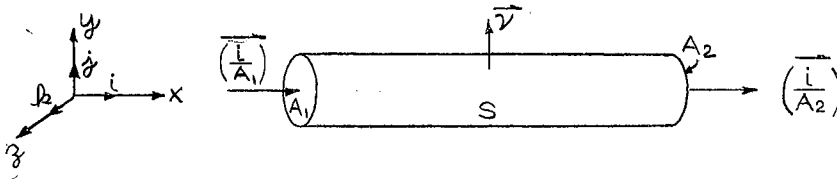
Thus, equation (A-2) is obtained. Writing this expression in terms of the Mach number, M , where $M = (ds/dt)/c_x$, then equation (A-2) may further be written as

$$M = \frac{1}{|\nabla\alpha|} \quad (A-5)$$

Next, let $i(x,y,z)$ be the unit vector in the ray direction. Since it is normal to the surfaces $\alpha(x,y,z)$, it may be expressed as

$$i = \frac{\nabla\alpha}{|\nabla\alpha|} = M\nabla\alpha \quad . \quad (A-6)$$

Now, consider a small length of narrow ray tube with end sections as parts of surfaces $\alpha = \text{constant}$ as in the following sketch.



Let A be proportional to the cross sectional area of the tube (measured by the surface $\alpha = \text{constant}$ inside the tube at that section) where the subscripts 1 and 2 represent the areas at the respective ends of the tube. In addition, the following terms are defined:

\vec{v} = outward normal to the surface s

v = volume inside the ray tube

$\left\{ \frac{\vec{i}}{A} \right\}$ = unit vector normal to surfaces A_1 and A_2 in the ray direction

Applying the Divergence Theorem to the ray tube sketch, it is shown that

$$\int_v \nabla \cdot \left\{ \frac{\vec{i}}{A} \right\} dv = \int_s \left\{ \frac{\vec{i}}{A} \right\} \cdot \vec{v} ds \quad \text{(A-7)}$$

Note that $\vec{i} \cdot \vec{v} = 0$ on the sides of the tube and $\vec{i} \cdot \vec{v} = \pm 1$ on the ends of the tube, so that the contributions from the ends cancel. Therefore, the right side of equation (A-7) vanishes; then from continuity considerations

$$\nabla \cdot \left\{ \frac{\vec{i}}{A} \right\} = 0 \quad \text{everywhere} \quad \text{(A-8)}$$

Substituting for the value of i from equation (A-6), then the above equation may be written as

$$\nabla \cdot \left\{ \frac{M}{A} \nabla \alpha \right\} = 0 \quad (\text{A-9})$$

Thus, equations (A-5) and (A-9) are obtained and are used in the development shown in Chapter II. Whitham has stated that these equations show that the flux of $M\nabla\alpha/A$ through a closed surface is zero in regions where $M\nabla\alpha/A$ is continuous. Further, these equations are always hyperbolic, corresponding to wave motions. The basic assumption is that A is a known function of M , hence equations (A-5) and (A-9) are used to determine α .

APPENDIX B

WHITHAM'S A-M RELATION

In addition to the geometrical relationships for A and M, Whitham established the functional dependence $A = A(M)$ as the only assumption in his theory. The qualitative results are independent of the precise choice of A provided only that A is a decreasing function of M. Simply, the theory assumes that as dA is increased, dM must decrease, and the converse must hold.

In an earlier paper, Chester (3) found that for a small change dA in a channel area, the corresponding change in Mach number is given by

$$\frac{dA}{A} = \frac{-2MdM}{(M^2-1)K(M)} \quad (B-1)$$

where $K(M)$ is a slowly varying function decreasing from 0.5 at $M = 1$ to 0.3941 (for $\gamma = 1.4$) as $M \rightarrow \infty$. The function $K(M)$ is given by Chester as

$$K(M) = 2 \left[\left\{ 1 + \frac{2}{\gamma+1} \frac{1-\mu^2}{\mu} \right\} (2\mu + 1 + M^{-2}) \right]^{-1} \quad (B-2)$$

where

$$\mu^2 = \frac{(\gamma-1)M^2 + 2}{2\gamma M^2 - (\gamma-1)}$$

For weak shocks, Chisnell (4) suggested that the integrated form of equation (B-1) should give a good approximation for a channel of slowly

varying cross section. His work on cylindrical shocks confirm this view. On integrating, equation (B-1) yields

$$\int_{A_s}^A \frac{dA}{A} = \int_{M_s}^M \frac{-2MdM}{(M^2-1)K(M)} ; K(M) \sim 0.5$$

Therefore,

$$\ln A \Big|_{A_s}^A = - \int_{M_s}^M \frac{4MdM}{(M^2-1)^2} ,$$

so that

$$\ln \frac{A}{A_s} = 2 \ln \frac{(M_s^2-1)}{(M^2-1)} = 2 \ln \frac{(M_s+1)(M_s-1)}{(M+1)(M-1)}$$

However, as $M \rightarrow 1$, $M+1 \rightarrow 2$, and $M_s+1 \rightarrow M+1$. Therefore,

$$\ln \frac{A}{A_s} \sim 2 \ln \frac{(M_s-1)}{(M-1)}$$

so

$$\frac{A}{A_s} \sim \left\{ \frac{M_s-1}{M-1} \right\} \quad \text{where } M-1 \ll 1 \quad . \quad (B-3)$$

Similarly, for strong shocks,

$$\ln A \Big|_{A_s}^A = \frac{-2}{K(M)} \int_{M_s}^M \frac{MdM}{M^2-1} = \frac{-2}{K(M)} \frac{1}{2} \ln(M^2-1) \Big|_{M_s}^M$$

This may be written as

$$\ln \frac{A}{A_s} = \frac{-2}{K(M)} \left\{ \frac{1}{2} \ln \frac{(M^2-1)}{(M_s^2-1)} \right\}$$

However, $K(M) \sim 0.3941$ as $M \rightarrow \infty$. Then $M^2-1 \rightarrow M^2$, $M_s^2-1 \rightarrow M_s^2$, and $n = 2/K(\infty) = 5.0734$. Therefore,

$$\ln \frac{A}{A_s} \sim n \ln \frac{M_s}{M}$$

Integrating this expression yields

$$\frac{A}{A_s} \sim \left| \frac{M_s}{M} \right|^n \quad \text{where } n = 5.0743 \quad \text{and } M \gg 1 \quad . \quad (\text{B-4})$$

This is equation (13) in the text which for strong shocks is extremely useful since it covers the most important range of shock strengths. It becomes a good approximation for $M > 3$, for example.

APPENDIX C

WHITHAM'S SHOCK-SHOCK RELATIONS

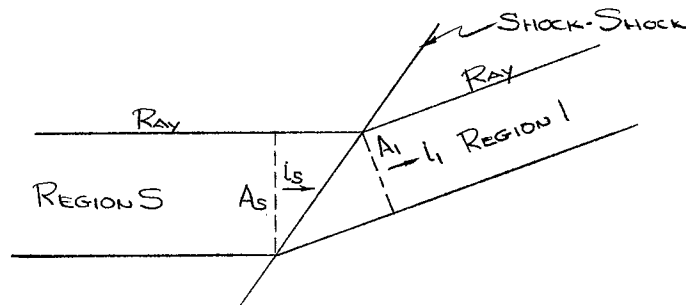
As stated in Chapter II, Whitham regards a shock-shock as a curve across which the shock Mach number, M_s , and the shock slope, θ , are discontinuous. This curve is described as the locus of the shock-shock as it moves along the shock wave. In a diffraction problem, it thus represents the motion of the shock triple-point.

To establish mathematical relationships for the propagation of shock-shocks, two specific conditions must be satisfied. First of all, since the portions of the shock wave representing the incident shock and the Mach shock must be connected, α must be continuous across the shock-shock. It follows, therefore, that the tangential derivatives of α on the two sides of the shock-shock must be equal. If the unit vector normal to the surface of the shock-shock is n , this condition may be written as

$$n \times (\nabla\alpha)_s = n \times (\nabla\alpha)_1, \quad (C-1)$$

where the subscript s and 1 denote values on the two sides of the shock-shock.

The second condition to be satisfied concerns the jump in the normal derivative of α . This may be illustrated by considering, as in the following diagram, the passage of a narrow ray tube across a shock-shock in three dimensions.



If i_s and i_1 are the directions of the ray on the two sides and A_s and A_1 are the corresponding cross sectional areas of the ray tube, it can be seen that the projections of these areas on the shock-shock are equal. This may be expressed as

$$\frac{n \cdot i_s}{A_s} = \frac{n \cdot i_1}{A_1} \quad (C-2)$$

In terms of α , this condition may further be written as

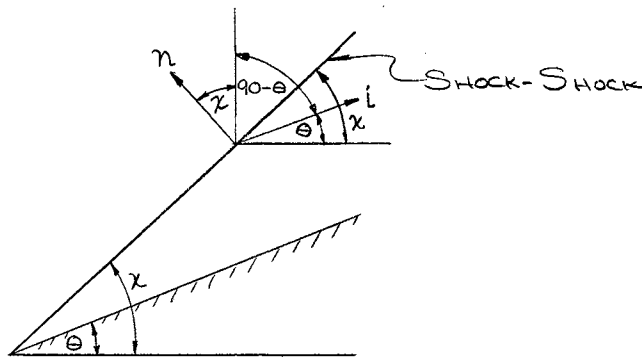
$$\frac{M_s}{A_s} n \cdot (\nabla\alpha)_s = \frac{M_1}{A_1} n \cdot (\nabla\alpha)_1 \quad (C-3)$$

Equations (C-1) and (C-3) are indicated by Whitham as the shock-shock relations for the three-dimensional problem.

As stated in the method analysis section, equation (11) must be satisfied in order to validate the analysis. To establish the relationships in this equation, recall that $\nabla\alpha = i/M$ (See Appendix A). Equation (C-1) then becomes

$$\left\{ \frac{n \times i}{M} \right\}_s = \left\{ \frac{n \times i}{M} \right\}_1 \quad (C-4)$$

However, from the following figure,



it can be seen that

$$\begin{aligned} n \cdot i &= |n| |i| \sin(n,i) = \sin(90-\theta+\chi) \\ &= \sin(90+(\chi-\theta)) = \cos(-(\chi-\theta)) \end{aligned}$$

Therefore,

$$n \cdot i = \cos(\chi-\theta)$$

Substituting this value into equation (C-3) yields

$$\frac{\cos(\chi-\theta_s)}{M_s} = \frac{\cos(\chi-\theta_1)}{M_1} \quad (C-5)$$

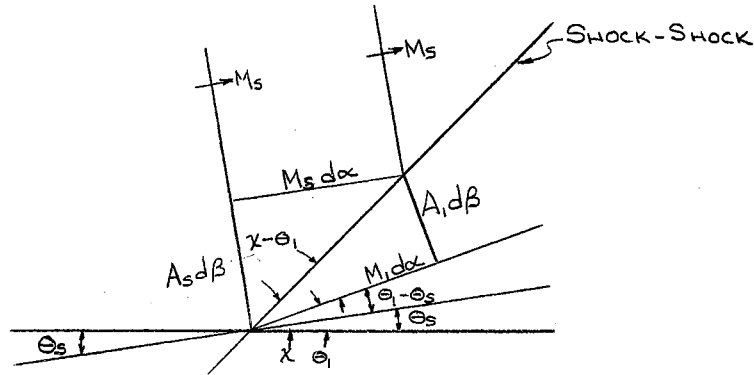
Similarly, from the figure,

$$n \cdot i = |n| |i| \cos(n,i) = \cos(90-\theta+\chi) = \sin(-(\chi-\theta))$$

and equation (C-2) then becomes

$$\frac{\sin(\chi-\theta_s)}{A_s} = \frac{\sin(\chi-\theta_1)}{A_1} \quad (C-6)$$

Equations (C-5) and (C-6) can be solved to yield θ_1 and χ in terms of M_s , θ_s , and M_1 . This may be seen by considering the following figure.



where from geometry,

$$(M_s d\alpha)^2 + (A_s d\beta)^2 = (A_1 d\beta)^2 + (M_1 d\alpha)^2 \quad .$$

Rearranging, factoring, and solving for $d\beta/d\alpha$, this equation reduces

to

$$\frac{d\beta}{d\alpha} = \left[\frac{M_1^2 - M_s^2}{A_s^2 - A_1^2} \right]^{1/2} \quad . \quad (C-7)$$

Whitham has defined this rate of change of β with respect to α as the shock-shock velocity c . Also, from the figure, note the following relationship.

$$\tan(\theta_1 - \theta_s) = \cot \{ (\chi - \theta_1) + [90 - (\chi - \theta_1)] - (\theta_1 - \theta_s) \}$$

$$= \frac{1 - \tan(\chi - \theta_1) \tan(90 - \chi + \theta_s)}{\tan(\chi - \theta_1) \tan(90 - \chi + \theta_s)}$$

$$= \frac{1 - \frac{A_1 d\beta}{M_1 d\alpha} \cdot \frac{M_s d\alpha}{A_s d\beta}}{\frac{A_1 d\beta}{M_1 d\alpha} + \frac{M_s d\alpha}{A_s d\beta}} = \frac{1 - \frac{A_1 M_s}{M_1 A_s}}{\frac{A_1}{M_1} c + \frac{M_s}{A_s} \frac{1}{c}}$$

Further reduction yields

$$\begin{aligned}
 \tan (\theta_1 - \theta_s) &= \frac{\frac{M_1 A_s - A_1 M_s}{M_1 A_s}}{\frac{A_1 (M_1^2 - M_s^2)^{\frac{1}{2}}}{M_1 (A_s^2 - A_1^2)^{\frac{1}{2}}} + \frac{M_s (A_s^2 - A_1^2)^{\frac{1}{2}}}{A_s (M_1^2 - M_s^2)^{\frac{1}{2}}}} \\
 &= \frac{(M_1 A_s - A_1 M_s) (A_s^2 - A_1^2)^{\frac{1}{2}} (M_1^2 - M_s^2)^{\frac{1}{2}}}{A_1 A_s M_1^2 - A_1 A_s M_s^2 + M_s M_1 A_s^2 - M_s M_1 A_1^2} \\
 &= \frac{(M_1 A_s - A_1 M_s) (A_s^2 - A_1^2)^{\frac{1}{2}} (M_1^2 - M_s^2)^{\frac{1}{2}}}{A_1 M_1 (A_s M_1 - M_s A_1) + A_s M_s (A_s M_1 - A_s M_s)}
 \end{aligned}$$

Therefore,

$$\tan (\theta_1 - \theta_s) = \frac{(A_s^2 - A_1^2)^{\frac{1}{2}} (M_1^2 - M_s^2)^{\frac{1}{2}}}{A_1 M_1 + A_s M_s} \quad (C-8)$$

Also, by resolving equations (C-5) and (C-6), the following relation can be obtained.

$$\begin{aligned}
 \tan (\chi - \theta_s) &= \frac{M_1 A_s \sin (\chi - \theta_1)}{A_1 M_s \cos (\chi - \theta_1)} = \frac{M_1 A_s}{A_1 M_s} \tan (\chi - \theta_1) \\
 &= \frac{M_1 A_s}{A_1 M_s} \frac{A_1 d\beta}{M_1 d\alpha} = \frac{A_s}{M_s} \frac{d\beta}{d\alpha}
 \end{aligned}$$

$$\tan (\chi - \theta_s) = \frac{A_s}{M_s} \left[\frac{M_1^2 - M_s^2}{A_s^2 - A_1^2} \right]^{\frac{1}{2}} \quad (C-9)$$

Thus, equations (C-8) and (C-9) are the shock-shock relations listed as equation (11) in Whitham's Method Analysis.

APPENDIX D

COMPUTER PROGRAM FOR AXI-SYMMETRIC CONE SOLUTION
(Symbols defined on Page 23)

```

MON$$      JOB  252740031 (BLAST WAVE DIFFRACTION)
MON$$      ASGN  MJB,A2
MON$$      ASGN  MGO,A3
MON$$      ASGN  MW1,A4
MON$$      ASGN  MW2,A5
MON$$      MODE  GO,TEST
MON$$      EXEQ  FORTRAN
1001 FORMAT (4F10.5)
2001 FORMAT (8(1X,F10.5))
2002 FORMAT (7H ERROR , F10.5, 14H IS LESS THAN , F10.5)
2003 FORMAT (5H RMAX)
2004 FORMAT (/5X,3HETD,8X,3HTHD,9X,1HR,9X,4HETXD,
17X,4HTHXD,8X,2HRX,8X,5HDIST1,6X,5HDIST2)
4 READ (1,1001) R, H, RMAX, DELR
R = R - DELR
H = -H
P=5.0743
62 WRITE (3,2004)
5 R = R + DELR
IF(R .GT. RMAX) GO TO 105
A = R*R - 1.0
B = 1.0 - R**(-2.0*P)
C = (1.0 + (R**(1.0 - P)))
TH = ATAN((SQRT(A*B))/C)
ET = ATAN(SQRT(A/B))
IF(ET .LE. TH) GO TO 61
NDX = 1
ETX = ET
THX = TH
RX = R
TANET = SIN(ETX)/COS(ETX)
GO TO 7
6 TANET = SIN(ETX)/COS(ETX)
TANTH = SIN(THX)/COS(THX)
E = (SIN(ETX))*(COS(ETX))
F = 1.0 + TANET*TANTH
TANDF = SIN(ETX-THX)/COS(ETX-THX)
G = P*TANDF*TANDF - 1.0
DTH = TANTH/(E*F*G)
DR = R*TANDF*DTH
THX = THX + (H*DTH)
RX = RX + (DR*H)
ETX = ETX + H

```

```
7 DIST1 = RX/(COS(THX)+(SIN(THX)*TANET))
  DIST2 = DIST1*TANET
  ETD = (180.0/3.14159265)*ET
  THD = (180.0/3.14159265)*TH
  ETXD = (180.0/3.14159265)*ETX
  THXD = (180.0/3.14159265)*THX
  WRITE (3,2001) ETD, THD, R, ETXD, THXD, RX, DIST1, DIST2
  IF(NDX .GT. 1000) GO TO 62
  NDX = NDX + 1
60 IF(ETX .GT. THX) GO TO 6
  GO TO 62
61 WRITE (3,2002) ET, TH
  GO TO 4
105 WRITE (3,2003)
  GO TO 4
  END
MON$$      EXEQ LINKLOAD
           PHASEENTIREPRG
           CALL MAINPGM
MON$$      EXEQ ENTIREPRG,MJB
```

APPENDIX E

MOVING BLAST WAVE TRANSFORMATION

From the information tabulated in Table IV, several flow properties relating to the shock wave are known. However, in order to determine the flow Mach number behind the shock in the physical (moving shock) plane, the transformation relationships outlined in the test analysis section of Chapter II must be used. The calculations may be illustrated from the following representation.

Physical Plane (Moving Shock)

Transform Plane (Stationary Shock)

$\begin{array}{l} \xrightarrow{\hspace{1cm}} \\ u_y = ? \\ M_y = ? \\ p_y = 8.6930 \\ \rho_y = 3.6177 \end{array}$	$u_s \xrightarrow{\hspace{1cm}}$	$\begin{array}{l} u_x = 0 \\ M_x = 0 \\ p_x = p_{ox} = 1.000 \\ \rho_x = \rho_{ox} = 1.000 \end{array}$	$u_s' = 0$	$\begin{array}{l} \xleftarrow{\hspace{1cm}} \\ u_y' = u_s - u_y \\ M_y' \\ p_y' = p_y = 8.6930 \\ \rho_y' = \rho_y = 3.617 \end{array}$	$\xleftarrow{\hspace{1cm}}$	$\begin{array}{l} u_x' = u_s \\ M_x' = 2.7557 \\ p_x' = p_x = 1.000 \\ \rho_x' = \rho_x = 1.000 \end{array}$
--	----------------------------------	---	------------	---	-----------------------------	--

It should be noted that the properties of the gas in the disturbed region behind the shock are made dimensionless with respect to the properties of the gas in the undisturbed region ahead of the shock. The velocities of the moving shock, u_s , and the flow velocity, u_y , behind the shock are made dimensionless with respect to the sonic velocity, c_x , in the undisturbed medium ahead of the shock. Therefore, by designating both the static and stagnation values of pressure and density as unity

ahead of the shock, the corresponding values of pressure and density behind the shock are equal to the values of the pressure and density ratios across a normal stationary shock wave.

From the known quantities, the speed of sound is determined as

$$c_x = c_x' = \sqrt{\frac{\alpha p_x'}{\rho_x}} = \sqrt{\frac{1.4(1.000)}{1.000}} = 1.1836 \quad .$$

From the Mach number relationship, u_x' is determined to be

$$u_x' = u_s = c_x'(M_x') = 1.1832(2.7557) = 3.2605 \quad .$$

Since the density ratio is the inverse of the velocity ratio across the shock, then

$$u_y' = \frac{u_x'}{\rho_y'/\rho_x'} = \frac{3.2605}{3.6177} = 0.9013 \quad .$$

Therefore, u_y is found from the transform plane relationships as

$$u_y = u_s - u_y' = 3.2605 - 0.913 = 2.3593 \quad .$$

If this shock is the one measured on the cone front, described in Chapter II, the free-field flow component lies in the horizontal direction; then u_y becomes

$$u_y = 2.3593 \cos 13.347^\circ = 2.2955 \quad .$$

The values of p_y and ρ_y are known quantities so it is now possible to determine the speed of sound behind the shock as

$$c_y = \sqrt{\frac{\alpha p_y}{\rho_y}} = \sqrt{\frac{1.4(8.6930)}{3.6177}} = 1.834 \quad .$$

Knowing both the flow velocity, u_y , behind the shock and the sonic velocity, c_y , behind the shock, the value of the flow Mach number behind the undiffracted shock away from the cone is

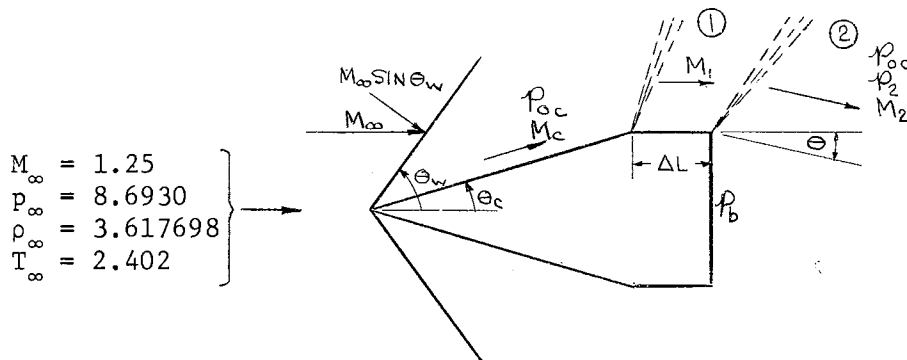
$$M_y = \frac{u_y}{c_y} = \frac{2.2956}{1.834} = 1.25 \quad .$$

Thus, it is seen that by using this transformation technique, all of the physical properties behind a moving shock wave can be determined.

APPENDIX F

CALCULATIONS USING THE ANALYSIS OF ZUMWALT AND TANG

To illustrate the calculations performed for the base pressure analysis of Chapter IV, known flow conditions were applied to Zumwalt's conical flow model. The model, and the applicable calculations, are shown by the following.



Although the calculation procedure has already been described in Chapter IV, details of the numerical values are presented here. As before, \longrightarrow means "yields."

Free Stream Conditions:

$$1. \quad M_\infty = 1.25 \left\{ \begin{array}{l} \text{isentropic} \\ \text{relations} \end{array} \right\} \longrightarrow \frac{p_\infty}{p_{0\infty}} = 0.386, \quad \frac{T_\infty}{T_{0\infty}} = 0.7619$$

$$2. \quad p_{0\infty} = \frac{p_{0\infty}}{p_\infty} \Big|_{M_\infty} p_\infty = \frac{8.6930}{.3861} = 22.5$$

$$T_{0\infty} = \frac{T_\infty}{T_\infty} \Big|_{M_\infty} T_\infty = \frac{2.402}{.7619} = 3.16$$

Conditions Behind Nose Shock:

$$3. \left. \begin{array}{l} M_{\infty} = 1.25 \\ \theta_c = 13.347^\circ \end{array} \right\} \begin{array}{l} \text{conical} \\ \text{shock} \end{array} \rightarrow \theta_w = 55.75^\circ$$

$$M_{\infty} \sin \theta_w = 1.032 \xrightarrow{\text{normal shock}} \frac{p_{oc}}{p_{\infty o}} = 1.00 \rightarrow p_{oc} = 22.5$$

$$4. \left. \begin{array}{l} M_{\infty} = 1.25 \\ \theta_c = 13.347^\circ \end{array} \right\} \begin{array}{l} \text{conical} \\ \text{shock} \end{array} \rightarrow p_c = 10.95$$

$$5. \frac{p_c}{p_{oc}} \xrightarrow{\text{isentropic relations}} M_c = 1.070 \rightarrow v_c = .7973^\circ$$

Conditions on the Imaginary Cylindrical Section:

$$6. v_1 = v_c + \theta_c = 14.144^\circ \xrightarrow{\text{isentropic relations}} M_1 = 1.574 \rightarrow \frac{p_1}{p_{oc}} = 0.2444 \rightarrow p_1 = 5.5$$

Conditions on the Base:

$$7. M_1 = 1.574 \text{ --- (Figure 41) ---} \rightarrow \frac{p_b}{p_1} \approx 0.60$$

$$8. \frac{p_b}{p_{\infty}} = \frac{p_b}{p_1} \cdot \frac{p_1}{p_{\infty}} = \frac{p_b}{p_1} \cdot \frac{p_1}{p_{o1}} \cdot \frac{p_{oc}}{p_{o\infty}} \cdot \frac{p_{o\infty}}{p_{\infty}} = p_{b_{st}} = 3.3 \text{ atmospheres}$$

The above calculations all apply to the steady state solution.

From Time Plane 360, p_b was determined to be 3.3328 atmospheres.

To determine the mass in the base region at the time of viscous mass entrainment, the following calculations apply.

$$9. \frac{p_b}{p_{oc}} = 0.148 \xrightarrow{\text{P.M. turn}} M_2 = 1.90546 \rightarrow v_2 = 23.74 \rightarrow \theta_2 = v_2 - v_1$$

$$= 9.596 \rightarrow \tan \theta_2 = .169$$

$$10. m_{t_v} = (\rho_b V_b)_{t_v} = \frac{p_{b_{t_v}} \pi R^3 \cot \theta_{t_v}}{R T_{o_{t_v}}} = 0.0554 \text{ lb}_m$$

To determine the mass bleed rate, \dot{m} , for the base region;

$$11. \left. \begin{array}{l} \frac{p_b}{p_1} = .606 \\ M_1 = 1.574 \end{array} \right\} \begin{array}{l} \text{Fig. 18} \\ \text{Ref. 38} \end{array} \longrightarrow \mathcal{K} \approx 1.0005$$

$$12. \dot{m}_{t_v} = -\mathcal{K} \frac{p_o A_b}{\sqrt{T_o}} \sqrt{\frac{\mathcal{E}Y}{R}} = -88.9 \times 10^{-6} \text{ lb}_m/\text{sec}.$$

The negative \dot{m}_{t_v} value implies that mass is being extracted from the base region by mixing action.

At time $t + \Delta t$, the mass in the base is

$$13. m_{(t_v+\Delta t)} = m_t + m_{t_v} \Delta t \approx 0.552 \text{ lb}_m/\text{sec}, \text{ where } \Delta t = 2 \text{ seconds.}$$

The base pressure at this same time becomes

$$14. p_b(t_v+\Delta t) = \frac{M_{(t_v+\Delta t)}(R T_o)}{\pi R^3 \cot \theta_{(t_v+\Delta t)}} = 19.65 \tan \theta_{(t_v+\Delta t)}$$

Iterating, it can be seen that when $\theta_{(t_v+\Delta t)} = 9.54^\circ$, then $p_b(t_v+\Delta t) = 3.3$ atmospheres. Note that this is the same value as the steady-state base pressure. The mass in the base at this time is found from the following.

$$15. \frac{p_b(t_v+\Delta t)}{p_{oc}} = .147 \xrightarrow{\text{P.M. turn}} M_2 = 1.91 \rightarrow v_2 = 23.869^\circ \rightarrow \theta_2 = v_2 - v_1$$

$$= 9.725 \rightarrow \tan \theta_2 = .1708$$

$$16. M_{(t_v+\Delta t)} = \frac{p_b(t_v+\Delta t) \pi R^3 \cot \theta_2}{(R T_o)} = 0.544 \text{ lb}_m$$

Repeating the procedure for finding \dot{m} , using the new values,
the solution continues as

$$\begin{array}{l}
 17. \quad \left. \begin{array}{l} \frac{P_b(t_v + \Delta t)}{P_1} \approx .60 \\ M_1 = 1.574 \end{array} \right\} \begin{array}{l} \text{[Fig. 18]} \\ \text{[Ref. 38]} \end{array} \rightarrow \mathcal{K} \approx 0 .
 \end{array}$$

$$18. \quad \dot{m}(t_v + \Delta t) = 0 .$$

These values indicate that no mass is feeding in or out of the mixing region. Hence, the solution has reached the stable condition.

APPENDIX G

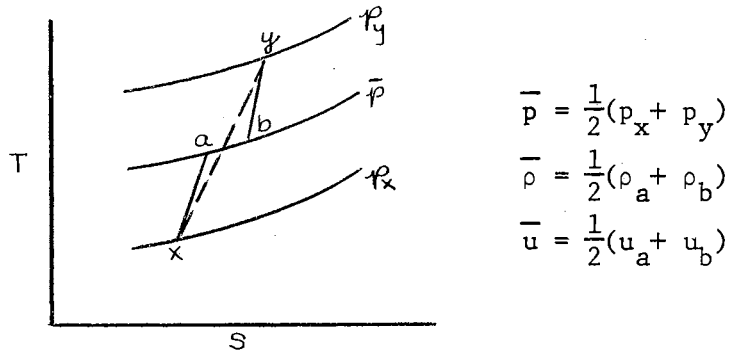
CALCULATIONS FOR SHOCK WAVE INITIAL CONDITIONS-PHASE II

This appendix serves to illustrate the calculation techniques used to determine the initial shock conditions for the Phase II solution. In this analysis, the properties in front of and behind the shock are assumed to be known. These were obtained from the transformation technique illustrated in Appendix E.

The shock initial conditions have been universally represented as a simple discontinuity between two mesh points. That is, the adjacent points are given property values corresponding to conditions before and after the shock. However, this pure discontinuity fails locally to satisfy the conservation laws. It has been found (See Reference 15) that this causes a "ripple" in the various flow properties to be propagated upstream, where conditions should be constant for plane waves. A similar calculation ripple may propagate downstream (ahead of the shock) but this is not apparent since the field itself is changing.

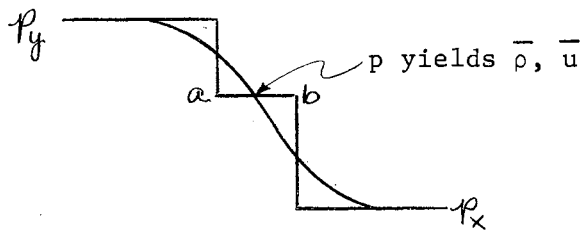
To eliminate this erroneous initial shock condition, a method was devised which has essentially eliminated the ripple phenomenon. For the finite difference calculations, the initial shock wave is assumed to be defined over two mesh widths. The pressure is taken to be the arithmetic mean of the pressures in front of and behind the wave. The other physical parameters, that is, density and velocity, at the shock center are made

compatible with the average pressure value. This may best be illustrated by considering the following T-S diagram.



In this diagram, the barred symbols represent values at the center of the shock. The symbols x and y represent conditions in front of and behind a normal shock corresponding to p_x and p_y , respectively.

To determine the value of \bar{u} and $\bar{\rho}$ which correspond to the known value of \bar{p} at the center of the shock, it is suggested that the problem be solved in two segments. The first segment considers a normal shock relationship with known pressure ratio, p_y/\bar{p} , and conditions u_y and ρ_y . The second segment considers a normal shock relationship with known pressure ratio, \bar{p}/p_x and conditions u_x and ρ_x . Solving both of these segments in the transform plane, then re-transforming back to the physical plane, the value of u and ρ at points a and b are determined. These values are then averaged to yield a good approximation of the values of \bar{u} and $\bar{\rho}$ to satisfy the conservation equations locally. The shock wave representation for this technique may be illustrated by the following diagram.



The calculations performed for the first segment of the problem are as follows.

Physical Plane (Moving Shock)

Transform Plane (Stationary Shock)

$\begin{array}{l} \xrightarrow{\hspace{1cm}} \\ M_y = 1.25 \\ p_y = 8.6930 \\ \rho_y = 3.6177 \end{array} \quad \left \quad \begin{array}{l} \xrightarrow{u_s} \\ p_b = 4.8465 \\ \rho_b = ? \end{array} \right.$	$\begin{array}{l} u_s' = 0 \\ \xleftarrow{\hspace{1cm}} \quad \xleftarrow{\hspace{1cm}} \\ u_y' = u_s - u_y \\ p_y' = p_y = 8.6930 \\ \rho_y' = \rho_y = 3.6177 \end{array} \quad \left \quad \begin{array}{l} u_b' = u_s - u_x \\ p_b' = 4.8465 \\ \rho_b' = \rho_b = ? \end{array} \right.$
--	--

1. $p_y' / p_b' = 1.7937 \xrightarrow{\text{normal shock}} M_b' = 1.2962, \rho_y' / \rho_b' = u_b' / u_y' = 1.5092$
2. $\rho_b = \rho_b' = \rho_y' / (u_b' / u_y') = 2.3971$
3. $c_b' = \sqrt{\frac{\gamma p_b'}{\rho_b'}} = 1.6824$
4. $u_b' = c_b' (M_b') = 2.1808$
5. $u_y' = u_b' / (\rho_y' / \rho_b') = 1.4450$
6. $u_s = u_y' + u_y = 3.7406$
7. $u_b = u_s - u_b' = 1.5598$

Thus, u_b and ρ_b are determined. Similarly, the u_a and ρ_a calculations for the second segment are as follows.

Physical Plane (Moving Shock)

$$\begin{array}{c}
 \xrightarrow{\quad} \\
 p_a = 4.8465 \\
 \rho_a = ? \\
 u_a = ?
 \end{array}
 \left|
 \begin{array}{c}
 \xrightarrow{u_s} \\
 p_x = 1.000 \\
 \rho_x = 1.000 \\
 u_x = 0
 \end{array}
 \right.$$

Transform Plane (Stationary Shock)

$$\begin{array}{c}
 \xleftarrow{\quad} \\
 u_a' = u_s - u_a \\
 p_a' = p_a = 4.8465 \\
 \rho_a' = \rho_a = ?
 \end{array}
 \left|
 \begin{array}{c}
 u_s' = 0 \\
 \xleftarrow{\quad} \\
 u_x' = u_s \\
 p_x' = p_x = 1.000 \\
 \rho_x' = \rho_x = 1.000
 \end{array}
 \right.$$

1. $p_a'/p_x' = 4.8465 \xrightarrow{\text{normal shock}} M_x' = 2.0730, \rho_a'/\rho_x' = u_x'/u_a' = 2.7731$
2. $\rho_a = \rho_a' = \rho_x'(u_x'/u_a') = 2.7731$
3. $c_x' \sqrt{\frac{\gamma p_x'}{\rho_x'}} = 1.1832$
4. $u_x' = u_s = c_x'(M_x') = 2.4528$
5. $u_a' = u_x' / (\rho_a' / \rho_x') = 0.8845$
6. $u_a = u_s - u_a' = u_x - u_a' = 1.5683$

Therefore, from the first and second segments, the average values of $\bar{\rho}$ and \bar{u} , corresponding to \bar{p} are

$$\bar{\rho} = \frac{1}{2}(\rho_a + \rho_b) = 2.5851, \quad \bar{u} = \frac{1}{2}(u_a + u_b) = 1.5640.$$

Thus, a sample calculation for the initial conditions at the shock center, as used for the computer solution, has been shown. Note that these calculations were determined for Point A of Figure 9. For the other shock points in Figure 9, the conditions across the shock locally were used to determine the \bar{p} , $\bar{\rho}$, and \bar{u} at these shock points, namely,

points A, 3, 6, 10, 15, and B. For example, Point 14 is the "y" point and an undisturbed field condition is the "x" point for "s" Point 15.

APPENDIX H

COMPUTER SOLUTION FOR BLAST-BASE INTERACTION - PHASE II

* * *

```

COMMON RHO(105,27),P(105,27),U(105,27),V(105,27),R(105,27),
1S(105,27),E(105,27),H1M,H2M,SINX,COSX,SIN2X,COS2X,NU,GAMMA,OMEGA,
2 SIGMAO,H1,H2,K,K1,K2,T,CNT,T1
COMMON XXQ(105,27)
INTEGER H1M, H2M, CNT
REAL NU,MAX,K,K1,K2
REWIND 4
1001 FORMAT (10X, 7F10.4)
1002 FORMAT (10X, 2I5,3F10.4,I5)
READ 1002,H1M,H2M,H1,H2,X,CNT
T1=0.0
X = X*(3.141592653/180.0)
SINX = SIN(X)
SIN2X = SINX*SINX
COSX = COS(X)
COS2X = COSX*COSX
NU = 1.0
GAMMA = 1.4
OMEGA = 1.345
SIGMAO = 0.5
READ 1001,((RHO(M,L),M=1,H1M),L=1,H2M)
READ 1001,((P(M,L),M=1,H1M),L=1,H2M)
READ 1001,((U(M,L),M=1,H1M),L=1,H2M)
READ 1001,((V(M,L),M=1,H1M),L=1,H2M)
MAX = 0.0
DO 100L = 1,H2M
DO 100M = 1,H1M
IF(RHO(M,L)-.9E6)400,100,400
400 CONTINUE
TEST=SQRT(U(M,L)*U(M,L)+V(M,L)*V(M,L))+SQRT(GAMMA*P(M,L)/RHO(M,L))
IF(TEST-MAX)100,100,401
401 MAX=TEST
100 CONTINUE
K = SIGMAO/MAX
K1 = SINX*K
K2 = COSX*K
T = K*H1*H2/(SQRT(H1*H1+H2*H2))
DO 10 L=1,H2M
DO 10 M=1,H1M
IF(RHO(M,L)-.9E6)402,9,402
402 CONTINUE
R(M,L) = RHO(M,L)*U(M,L)
GO TO 10
9 R(M,L) = 0.9E+6
10 CONTINUE
DO 20 L = 1,H2M
DO 20 M = 1,H1M
IF(RHO(M,L)-.9E6)403,19,403
403 CONTINUE
S(M,L) = RHO(M,L)*V(M,L)

```

```
      GO TO 20
19  S(M,L) = 0.9E+6
20  CONTINUE
      DO 30 L = 1,H2M
      DO 30 M = 1,H1M
      IF(RHO(M,L)-.9E6)404,29,404
404  CONTINUE
      W = SQRT(U(M,L)*U(M,L) + V(M,L)*V(M,L))
      E(M,L) = (RHO(M,L)*W*W*0.5) + (P(M,L)/(GAMMA-1.0))
      GO TO 30
29  E(M,L) = 0.9E+6
30  CONTINUE
510  CONTINUE
      IF(SENSE SWITCH 1)880,881
880  REWIND 5
      CALL DOT(5)
      REWIND 5
      END FILE 4
      REWIND 4
      PAUSE 1
881  CONTINUE
      CALL BLAST2
      GO TO 510
      END
```

```

SUBROUTINE BLAST2
COMMON RHO(105,27),P(105,27),U(105,27),V(105,27),R(105,27),
1S(105,27),E(105,27),H1M,H2M,SINX,COSX,SIN2X,COS2X,NU,GAMMA,OMEGA,
2 SIGMA0,H1,H2,K,K1,K2,T,CNT,T1
COMMON RHO1(105,27)
INTEGER H1M, H2M, CNT
REAL NU,MAX,K,K1,K2
DO 300 J=1,2160
800 RHO1(J)=0.
2001 FORMAT (10(1X,E12.6))
DO 120 L=1,H2M
DO 120 M=1,H1M
IF(RHO(M,L)-.9E6)405,210,405
405 CONTINUE
PSI = 0.0
FX = 0.0
FY = 0.0
PHIX = 0.0
PHIY = 0.0
IF(L-1)406,114,406
406 CONTINUE
YL = L-1
PSI = -T*NU*V(M,L)*RHO(M,L)/(YL*H2)
GO TO 115
114 V(M,L) = 0.0
115 ALPHA = OMEGA*K*(SQRT(U(M,L)*U(M,L)+V(M,L)*V(M,L))
1 +SQRT(GAMMA*P(M,L)/RHO(M,L)))
BETA = ALPHA*COS2X
ALPHA = ALPHA*SIN2X
IF(L-1)407,300,407
407 CONTINUE
IF(RHO(M,L-1)-.9E6)408,116,408
408 CONTINUE
IF(L-H2M)500,132,500
500 CONTINUE
IF(RHO(M,L+1)-.9E6)410,117,410
410 CONTINUE
FY = -0.5*K2*(S(M,L+1)-S(M,L-1))
300 BETA1 = OMEGA*K*(SQRT(U(M,L+1)*U(M,L+1)+V(M,L+1)*V(M,L+1))
1 +SQRT(GAMMA*P(M,L+1)/RHO(M,L+1))) *COS2X
IF(L-1)411,301,411
411 CONTINUE
BETA2 = OMEGA*K*(SQRT(U(M,L-1)*U(M,L-1)+V(M,L-1)*V(M,L-1))
1 +SQRT(GAMMA*P(M,L-1)/RHO(M,L-1))) *COS2X
PHIY = 0.25*((BETA1+BETA)*(RHO(M,L+1)-RHO(M,L))
1 -(BETA+BETA2)*(RHO(M,L)-RHO(M,L-1)))
GO TO 200
301 PHIY = 0.5*((BETA1+BETA)*(RHO(M,L+1)-RHO(M,L)))
PSI = -T*NU*V(M,L+1)*RHO(M,L)/H2
116 FY = -K2*S(M,L+1)

```

SUBROUTINE BLAST2

```

      GO TO 200
117  FY = K2*S(M,L-1)
200  IF(M-1)412,209,412
412  CONTINUE
      IF(RHO(M-1,L)-.9E6)413,118,413
413  CONTINUE
      IF(M-H1M)414,130,414
414  CONTINUE
      IF(RHO(M+1,L)-.9E6)415,119,415
415  CONTINUE
      FX = -0.5*K1*(R(M+1,L)-R(M-1,L))
      ALPHA1 = OMEGA*K*(SQRT(U(M+1,L)*U(M+1,L)+V(M+1,L)*V(M+1,L))
1    +SQRT(GAMMA*P(M+1,L)/RHO(M+1,L)))*SIN2X
      ALPHA2 = OMEGA*K*(SQRT(U(M-1,L)*U(M-1,L)+V(M-1,L)*V(M-1,L))
1    +SQRT(GAMMA*P(M-1,L)/RHO(M-1,L)))*SIN2X
      PHIX = 0.25*((ALPHA1+ALPHA)*(RHO(M+1,L)-RHO(M,L))
1    -(ALPHA+ALPHA2)*(RHO(M,L)-RHO(M-1,L)))
      GO TO 110
118  FX = -K1*R(M+1,L)
      GO TO 110
119  FX = K1*R(M-1,L)
110  RH01(M,L) = RHO(M,L)+PSI+FX+FY+PHIX+PHLY
      GO TO 120
130  RH01(M,L) = RHO(M-1,L)
      GO TO 120
132  RH01(M,L) = RHO(M,L-1)
      GO TO 120
209  RH01(M,L) = RHO(M,L)
      GO TO 120
210  RH01(M,L) = 0.9E+6
120  CONTINUE
      WRITE(5) RH01
      CALL BLAST3
      RETURN
      END

```

```

SUBROUTINE BLAST3
COMMON RHO(105,27),P(105,27),U(105,27),V(105,27),R(105,27),
1S(105,27),E(105,27),H1M,H2M,SINX,COSX,SIN2X,COS2X,NU,GAMMA,OMEGA,
2 SIGMA0,H1,H2,K,K1,K2,T,CNT,T1
COMMON R1(105,27)
INTEGER H1M, H2M, CNT
REAL NU,MAX,K,K1,K2
DO 800 J=1,2160
800 R1(J)=0.
2001 FORMAT (10(1X,E12.6))
DO 120 L=1,H2M
DO 120 M=1,H1M
IF(RHO(M,L)-.9E6)416,210,416
416 CONTINUE
PSI = 0.0
FX = 0.0
FY = 0.0
PHIX = 0.0
PHIY = 0.0
IF(L-1)417,114,417
417 CONTINUE
YL = L-1
PSI = -T*NU*V(M,L)*R(M,L)/(YL*H2)
GO TO 115
114 V(M,L) = 0.0
115 ALPHA = OMEGA*K*(SQRT(U(M,L)*U(M,L)+V(M,L)*V(M,L))
1 +SQRT(GAMMA*P(M,L)/RHO(M,L)))
BETA = ALPHA*COS2X
ALPHA = ALPHA*SIN2X
IF(L-1)418,300,418
418 CONTINUE
IF(RHO(M,L-1)-.9E6)501,116,501
501 CONTINUE
IF(L-H2M)502,132,502
502 CONTINUE
IF(RHO(M,L+1)-.9E6)503,117,503
503 CONTINUE
FY = -0.5*K2*(S(M,L+1)*U(M,L+1)-S(M,L-1)*U(M,L-1))
300 BETA1 = OMEGA*K*(SQRT(U(M,L+1)*U(M,L+1)+V(M,L+1)*V(M,L+1))
1 +SQRT(GAMMA*P(M,L+1)/RHO(M,L+1)))*COS2X
IF(L-1)422,301,422
422 CONTINUE
BETA2 = OMEGA*K*(SQRT(U(M,L-1)*U(M,L-1)+V(M,L-1)*V(M,L-1))
1 +SQRT(GAMMA*P(M,L-1)/RHO(M,L-1)))*COS2X
PHIY = 0.25*((BETA1+BETA)*(R(M,L+1)-R(M,L))
1 -(BETA+BETA2)*(R(M,L)-R(M,L-1)))
GO TO 200
301 PHIY = 0.5*((BETA1+BETA)*(R(M,L+1)-R(M,L)))
PSI = -T*NU*V(M,L+1)*R(M,L)/H2
116 FY = -K2*S(M,L+1)*U(M,L+1)

```


SUBROUTINE BLAST3

```

      GO TO 200
117  FY = K2*S(M,L-1)*U(M,L-1)
200  IF(M-1)504,209,504
504  CONTINUE
      IF(RHO(M-1,L)-.9E6)424,118,424
424  CONTINUE
      IF(M-H1M)425,130,425
425  CONTINUE
      IF(RHO(M+1,L)-.9E6)426,119,426
426  CONTINUE
      FX = -0.5*K1*((P(M+1,L)+R(M+1,L)*U(M+1,L))
1  -(P(M-1,L)+R(M-1,L)*U(M-1,L)))
      ALPHA1 = OMEGA*K*(SQRT(U(M+1,L)*U(M+1,L)+V(M+1,L)*V(M+1,L))
1  +SQRT(GAMMA*P(M+1,L)/RHO(M+1,L)))*SIN2X
      ALPHA2 = OMEGA*K*(SQRT(U(M-1,L)*U(M-1,L)+V(M-1,L)*V(M-1,L))
1  +SQRT(GAMMA*P(M-1,L)/RHO(M-1,L)))*SIN2X
      PHIX = 0.25*((ALPHA1+ALPHA2)*(R(M+1,L)-R(M,L))
1  -(ALPHA1+ALPHA2)*(R(M,L)-R(M-1,L)))
      GO TO 110
118  R1(M,L) = 0.0
      GO TO 120
119  FX = K1*(P(M-1,L)+R(M-1,L)*U(M-1,L))
110  R1(M,L) = R(M,L)+PSI+FX+FY+PHIX+PHIY
      GO TO 120
130  R1(M,L) = R(M-1,L)
      GO TO 120
132  R1(M,L) = R(M,L-1)
      GO TO 120
209  R1(M,L) = R(M,L)
      GO TO 120
210  R1(M,L) = 0.9E+6
120  CONTINUE
      WRITE(5) R1
      CALL BLAST4
      RETURN
      END

```

```

SUBROUTINE BLAST4
COMMON RHO(105,27),P(105,27),U(105,27),V(105,27),R(105,27),
1S(105,27),E(105,27),H1M,H2M,SINX,COSX,SIN2X,COS2X,NU,GAMMA,OMEGA,
2 SIGMA0,H1,H2,K,K1,K2,T,CNT,T1
COMMON S1(105,27)
INTEGER H1M, H2M, CNT
REAL NU,MAX,K,K1,K2
DO 800 J=1,2160
800 S1(J)=0.
2001 FORMAT (10(1X,E12.6))
DO 120 L=1,H2M
DO 120 M=1,H1M
IF(RHO(M,L)-.9E6)427,210,427
427 CONTINUE
PSI = 0.0
FX = 0.0
FY = 0.0
PHIX = 0.0
PHIY = 0.0
IF(L-1)428,114,428
428 CONTINUE
YL = L-1
PSI = -T*NU*V(M,L)*S(M,L)/(YL*H2)
GO TO 115
114 V(M,L) = 0.0
115 ALPHA = OMEGA*K*(SQRT(U(M,L)*U(M,L)+V(M,L)*V(M,L))
1 +SQRT(GAMMA*P(M,L)/RHO(M,L)))
BETA = ALPHA*COS2X
ALPHA = ALPHA*SIN2X
IF(L-1)429,300,429
429 CONTINUE
IF(RHO(M,L-1)-.9E6)430,116,430
430 CONTINUE
IF(L-H2M)431,132,431
431 CONTINUE
IF(RHO(M,L+1)-.9E6)432,117,432
432 CONTINUE
FY = -0.5*K2*((P(M,L+1)+S(M,L+1)*V(M,L+1))
1 -(P(M,L-1)+S(M,L-1)*V(M,L-1)))
300 BETA1 = OMEGA*K*(SQRT(U(M,L+1)*U(M,L+1)+V(M,L+1)*V(M,L+1))
1 +SQRT(GAMMA*P(M,L+1)/RHO(M,L+1)))*COS2X
IF(L-1)433,301,433
433 CONTINUE
BETA2 = OMEGA*K*(SQRT(U(M,L-1)*U(M,L-1)+V(M,L-1)*V(M,L-1))
1 +SQRT(GAMMA*P(M,L-1)/RHO(M,L-1)))*COS2X
PHIY = 0.25*((BETA1+BETA2)*(S(M,L+1)-S(M,L))
1 -(BETA+BETA2)*(S(M,L)-S(M,L-1)))
GO TO 200
301 PHIY = 0.5*((BETA1+BETA)*(S(M,L+1)-S(M,L)))
PSI = -T*NU*V(M,L+1)*S(M,L)/H2

```

SUBROUTINE BLAST4

```

      FY = -K2*(P(M,L+1)+S(M,L+1)*V(M,L+1))
116  S1(M,L) = 0.0
      GO TO 120
117  FY = K2*(P(M,L-1)+S(M,L-1)*V(M,L-1))
200  IF(M-1)434,209,434
434  CONTINUE
      IF(RHO(M-1,L)-.9E6)435,118,435
435  CONTINUE
      IF(M-H1M)436,130,436
436  CONTINUE
      IF(RHO(M+1,L)-.9E6)437,119,437
437  CONTINUE
      FX = -0.5*K1*(R(M+1,L)*V(M+1,L)-R(M-1,L)*V(M-1,L))
      ALPHA1 = OMEGA*K*(SQRT(U(M+1,L)*U(M+1,L)+V(M+1,L)*V(M+1,L))
1      +SQRT(GAMMA*P(M+1,L)/RHO(M+1,L)))*SIN2X
      ALPHA2 = OMEGA*K*(SQRT(U(M-1,L)*U(M-1,L)+V(M-1,L)*V(M-1,L))
1      +SQRT(GAMMA*P(M-1,L)/RHO(M-1,L)))*SIN2X
      PHIX = 0.25*((ALPHA1+ALPHA2)*(S(M+1,L)-S(M,L))
1      -(ALPHA1+ALPHA2)*(S(M,L)-S(M-1,L)))
      GO TO 110
118  FX = -K1*(R(M+1,L)*V(M+1,L))
      GO TO 110
119  FX = K1*(R(M-1,L)*V(M-1,L))
110  S1(M,L) = S(M,L)+PSI+FX+FY+PHIX+PHIY
      GO TO 120
130  S1(M,L) = S(M-1,L)
      GO TO 120
132  S1(M,L) = S(M,L-1)
      GO TO 120
209  S1(M,L) = S(M,L)
      GO TO 120
210  S1(M,L) = 0.9E+6
120  CONTINUE
      WRITE(5) S1
      CALL BLAST 5
      RETURN
      END

```

```

SUBROUTINE BLAST5
COMMON RHO(105,27),P(105,27),U(105,27),V(105,27),R(105,27),
1S(105,27),E(105,27),H1M,H2M,SINX,COSX,SIN2X,COS2X,NU,GAMMA,OMEGA,
2 SIGMAO,H1,H2,K,K1,K2,T,CNT,T1
COMMON E1(105,27)
INTEGER H1M, H2M, CNT
REAL NU,MAX,K,K1,K2
DO 800 J=1,2160
800 E1(J)=0.
2001 FORMAT (10(1X,F12.6))
DO 120 L=1,H2M
DO 120 M=1,H1M
IF(RHO(M,L)-.9E6)438,210,438
438 CONTINUE
PSI = 0.0
FX = 0.0
FY = 0.0
PHIX = 0.0
PHIY = 0.0
IF(L-1)439,114,439
439 CONTINUE
YL = L-1
PSI = -T*NU*V(M,L)*(E(M,L)+P(M,L))/(YL*H2)
GO TO 115
114 V(M,L) = 0.0
115 ALPHA = OMEGA*K*(SQRT(U(M,L)*U(M,L)+V(M,L)*V(M,L))
1 +SQRT(GAMMA*P(M,L)/RHO(M,L)))
BETA = ALPHA*COS2X
ALPHA = ALPHA*SIN2X
IF(L-1)440,300,440
440 CONTINUE
IF(RHO(M,L-1)-.9E6)441,116,441
441 CONTINUE
IF(L-H2M)442,132,442
442 CONTINUE
IF(RHO(M,L+1)-.9E6)443,117,443
443 CONTINUE
FY = -0.5*K2*(((E(M,L+1)+P(M,L+1))*V(M,L+1))
1 -((E(M,L-1)+P(M,L-1))*V(M,L-1)))
300 BETA1 = OMEGA*K*(SQRT(U(M,L+1)*U(M,L+1)+V(M,L+1)*V(M,L+1))
1 +SQRT(GAMMA*P(M,L+1)/RHO(M,L+1)))*COS2X
IF(L-1)444,301,444
444 CONTINUE
BETA2 = OMEGA*K*(SQRT(U(M,L-1)*U(M,L-1)+V(M,L-1)*V(M,L-1))
1 +SQRT(GAMMA*P(M,L-1)/RHO(M,L-1)))*COS2X
PHIY = 0.25*((BETA1+BETA)*(E(M,L+1)-E(M,L))
1 -(BETA+BETA2)*(E(M,L)-E(M,L-1)))
GO TO 200
301 PHIY = 0.5*((BETA1+BETA)*(E(M,L+1)-E(M,L))
PSI = -T*NU*V(M,L+1)*(E(M,L)+P(M,L))/H2

```

SUBROUTINE BLAST5

```

116 FY = -K2*((E(M,L+1)+P(M,L+1))*V(M,L+1))
    GO TO 200
117 FY = K2*((E(M,L-1)+P(M,L-1))*V(M,L-1))
200 IF(M-1)445,209,445
445 CONTINUE
    IF(RHO(M-1,L)-.9E6)446,118,446
446 CONTINUE
    IF(M-H1M)447,130,447
447 CONTINUE
    IF(RHO(M+1,L)-.9E6)448,119,448
448 CONTINUE
    FX = -0.5*K1*(((E(M+1,L)+P(M+1,L))*U(M+1,L))
1  -((E(M-1,L)+P(M-1,L))*U(M-1,L)))
    ALPHA1 = OMEGA*K*(SQRT(U(M+1,L)*U(M+1,L)+V(M+1,L)*V(M+1,L))
1  +SQRT(GAMMA*P(M+1,L)/RHO(M+1,L)))*SIN2X
    ALPHA2 = OMEGA*K*(SQRT(U(M-1,L)*U(M-1,L)+V(M-1,L)*V(M-1,L))
1  +SQRT(GAMMA*P(M-1,L)/RHO(M-1,L)))*SIN2X
    PHIX = 0.25*((ALPHA1+ALPHA)*(E(M+1,L)-E(M,L))
1  -(ALPHA+ALPHA2)*(E(M,L)-E(M-1,L)))
    GO TO 110
118 FX = -K1*((E(M+1,L)+P(M+1,L))*U(M+1,L))
    GO TO 110
119 FX = K1*((E(M-1,L)+P(M-1,L))*U(M-1,L))
110 E1(M,L) = E(M,L)+PSI+FX+FY+PHIX+PHIY
    GO TO 120
130 E1(M,L) = E(M-1,L)
    GO TO 120
132 E1(M,L) = E(M,L-1)
    GO TO 120
209 E1(M,L) = E(M,L)
    GO TO 120
210 E1(M,L) = 0.9E+6
120 CONTINUE
    WRITE(5) E1
    CALL BLAST6
    RETURN
    END

```

```

SUBROUTINE BLAST6
COMMON RHO(105,27),P(105,27),U(105,27),V(105,27),R(105,27),
1S(105,27),E(105,27),H1M,H2M,SINX,COSX,SIN2X,COS2X,NU,GAMMA,OMEGA,
2 SIGMA0,H1,H2,K,K1,K2,T,CNT,T1
INTEGER H1M, H2M, CNT, CNT1, CNT2
REAL NU, MAX, K, K1, K2
2001 FORMAT (12H RHO = 0 AT I2,1H,I2)
2002 FORMAT (10(1X,F12.5))
2003 FORMAT (//9H DENSITY//)
2004 FORMAT (//10H PRESSURE//)
2005 FORMAT (//21H HORIZONTAL VELOCITY//)
2006 FORMAT (//19H VERTICAL VELOCITY//)
2007 FORMAT (//22H HORIZONTAL MASS FLUX//)
2008 FORMAT (//20H VERTICAL MASS FLUX//)
2009 FORMAT (//8H ENERGY//)
2010 FORMAT(1H160X,11HTIME PLANE I3,2X,4HPAGE,I2/57X,7HTIME = E14.8)
REWIND 5
READ(5) RHO
READ(5) R
RFAD(5) S
READ(5) E
DO 900 M=1,H1M
MMM=H2M-1
RHO(M,H2M)=RHO(M,MMM)
R(M,H2M)=R(M,MMM)
S(M,H2M)=S(M,MMM)
900 E(M,H2M)=E(M,MMM)
DO 10 L=1,H2M
DO 10 M=1,H1M
IF(RHO(M,L)-.9E6)449,100,449
449 CONTINUE
IF(RHO(M,L))450,200,450
450 CONTINUE
U(M,L) = R(M,L)/RHO(M,L)
V(M,L) = S(M,L)/RHO(M,L)
P(M,L) = (GAMMA-1.0)*(E(M,L)-RHO(M,L)
1 *(U(M,L)*U(M,L)+V(M,L)*V(M,L)))*0.5)
10 CONTINUE
MAX=0.0
DO 20 L=1,H2M
DO 20 M=1,H1M
IF(RHO(M,L)-.9E6)451,20,451
451 CONTINUE
TEST=SQRT(U(M,L)*U(M,L)+V(M,L)*V(M,L))+SQRT(GAMMA*P(M,L)/RHO(M,L))
IF(TEST-MAX)20,20,452
452 MAX=TEST
20 CONTINUE
K=SIGMA0/MAX
K1=SINX*K
K2=COSX*K

```

SUBROUTINE BLAST6

```

T1=T1+T
T=K*H1*H2/SQRT(H1*H1+H2*H2)
CNT=CNT-1
REWIND 5
CNT2 = CNT1-CNT
IPL=IPL+1
IP1=1
IP2=10
IZ1=0
H1MSV=H1M
WRITE(4) IPL,T1,RHO
WRITE (4) P
WRITE (4) U
WRITE (4) V
WRITE (4) R
WRITE (4) S
WRITE (4) E
IF(MOD(IPL-1,1))507,602,507
IF(MOD(IPL-1,3))507,602,507
IF(MOD(IPL-1,5))507,602,507
IF(SENSE SWITCH 1)602,507
602 DO 601 KK=1,H1M
DO 600 JJ=1,H2M
IF(U(KK,JJ))601,600,601
600 CONTINUE
H1MSV=H1M
H1M=KK
GO TO 603
601 CONTINUE
603 CONTINUE
520 CONTINUE
IZ1=IZ1+1
PRINT 2010,IPL,IZ1,T1
PRINT 2003
DO 50 L=1,H2M
L1=H2M-L+1
50 PRINT 2002,(RHO(M,L1),M=IP1,IP2)
PRINT 2004
DO 51 L=1,H2M
L1=H2M-L+1
51 PRINT 2002,(P(M,L1),M=IP1,IP2)
PRINT 2005
DO 52 L=1,H2M
L1=H2M-L+1
52 PRINT 2002,(U(M,L1),M=IP1,IP2)
PRINT 2006
DO 53 L=1,H2M
L1=H2M-L+1
53 PRINT 2002,(V(M,L1),M=IP1,IP2)
PRINT 2007

```

SUBROUTINE BLAST6

```
DO 54 L=1,H2M
L1=H2M-L+1
54 PRINT 2002,(R(M,L1),M=IP1,IP2)
PRINT 2008
DO 55 L=1,H2M
L1=H2M-L+1
55 PRINT 2002,(S(M,L1),M=IP1,IP2)
PRINT 2009
DO 56 L=1,H2M
L1=H2M-L+1
56 PRINT 2002,(E(M,L1),M=IP1,IP2)
IF(IP2-H1M)521,522,522
521 IP1=IP2+1
IP2=IP2+10
IF(IP2-H1M)520,520,523
523 IP2=H1M
GO TO 520
522 CONTINUE
IF(CNT)506,506,507
506 STOP
100 U(M,L)=0.9E+6
V(M,L)=0.9E+6
P(M,L)=0.9E+6
GO TO 10
200 PRINT 2001,M,L
U(M,L)=0.0
V(M,L)=0.0
P(M,L)=0.0
GO TO 10
507 CONTINUE
H1M=H1MSV
RETURN
END
```


APPENDIX I

STAGNATION POINT CALCULATIONS

The purpose of this appendix is to illustrate the calculation procedure used to obtain the stagnation values of pressure and density at the cone apex for the exploratory solution. The subscript "o" denotes stagnation values, and primes here indicate the transform plane.

Physical Plane (Moving Shock)

Transform Plane (Stationary Shock)

$M_s = 2.657$ <div style="text-align: center;"> \longrightarrow \longrightarrow </div> <table style="width: 100%; border-collapse: collapse;"> <tr> <td style="width: 50%; border-right: 1px solid black; padding: 5px;"> $M_y = 1.254$ $p_y = 8.0673$ $\rho_y = 3.5123$ </td> <td style="width: 50%; padding: 5px;"> $M_x = 0$ $p_x = p_{ox} = 1.000$ $\rho_x = \rho_{ox} = 1.000$ </td> </tr> </table> <p style="text-align: center;">$T_{oy} \neq T_{ox}$</p>	$M_y = 1.254$ $p_y = 8.0673$ $\rho_y = 3.5123$	$M_x = 0$ $p_x = p_{ox} = 1.000$ $\rho_x = \rho_{ox} = 1.000$	$M_s' = 0$ <div style="text-align: center;"> \longleftarrow \longleftarrow </div> <table style="width: 100%; border-collapse: collapse;"> <tr> <td style="width: 50%; border-right: 1px solid black; padding: 5px;"> $u_y' = u_s - u_y$ $M_y' = 0.4991$ $p_y' = p_y = 8.0673$ $\rho_y' = \rho_y = 3.5123$ </td> <td style="width: 50%; padding: 5px;"> $u_x' = u_s$ $M_x' = 2.657$ $p_x' = p_x = 1.000$ $\rho_x' = \rho_x = 1.000$ </td> </tr> </table> <p style="text-align: center;">$T_{oy}' = T_{ox}'$</p>	$u_y' = u_s - u_y$ $M_y' = 0.4991$ $p_y' = p_y = 8.0673$ $\rho_y' = \rho_y = 3.5123$	$u_x' = u_s$ $M_x' = 2.657$ $p_x' = p_x = 1.000$ $\rho_x' = \rho_x = 1.000$
$M_y = 1.254$ $p_y = 8.0673$ $\rho_y = 3.5123$	$M_x = 0$ $p_x = p_{ox} = 1.000$ $\rho_x = \rho_{ox} = 1.000$				
$u_y' = u_s - u_y$ $M_y' = 0.4991$ $p_y' = p_y = 8.0673$ $\rho_y' = \rho_y = 3.5123$	$u_x' = u_s$ $M_x' = 2.657$ $p_x' = p_x = 1.000$ $\rho_x' = \rho_x = 1.000$				

1. $M_x' = M_s = 2.657 \xrightarrow{\text{normal shock}} p_y'/p_x' = 8.0673, u_x'/u_y' = \rho_y'/\rho_x' = 3.5123,$

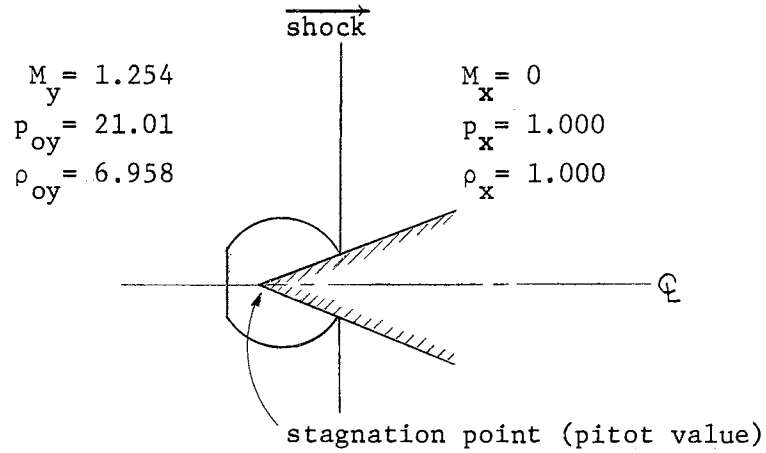
$M_y' = 0.4991, T_y'/T_x' = 2.2974$

2. $M_y = \frac{u_y}{c_y} = \frac{u_s}{c_y} - \frac{u_y'}{c_y} = \frac{u_x'}{c_x} \frac{c_x}{c_y} - M_y' = M_x' \sqrt{\frac{T_x'}{T_y'}} - M_y' = 1.254$

3. $M_y = 1.254 \xrightarrow{\text{isentropic relations}} \frac{p_y}{p_{oy}} = 0.384, \frac{\rho_y}{\rho_{oy}} = 0.5048$

4. $p_{oy} = \frac{p_y}{p_y/p_{oy}} = 21.0085, \rho_{oy} = \frac{\rho_y}{\rho_y/\rho_{oy}} = 6.9578$

The following configuration now exists:



$$5. \quad M_y = 1.254 \xrightarrow{\text{normal shock}} \frac{P_{oy}(\text{pitot})}{P_{oy}} = 0.9865, \quad \frac{\rho_{oy}(\text{pitot})}{\rho_{oy}} = \frac{P_{oy}(\text{pitot})}{P_{oy}} = 0.8965$$

$$6. \quad P_{oy}(\text{pitot}) = P_{oy} \left\{ \frac{P_{oy}(\text{pitot})}{P_{oy}} \right\} = 20.7249$$

$$7. \quad \rho_{oy}(\text{pitot}) = \rho_{oy} \left\{ \frac{\rho_{oy}(\text{pitot})}{\rho_{oy}} \right\} = 6.8639$$

Thus, the values indicated in steps 5 and 6 are the stagnation values of pressure and density used for the computer solution. These values are the stagnation values that exist at the cone apex for a steady-state solution.

APPENDIX J

COMPUTER PROGRAM FOR FOREBODY EXPLORATORY PROBLEM

```

MON$$ JOB 252740031 (BLAST WAVE DIFFRACTION)
MON$$ ASGN MGO,A2
MON$$ ASGN MJB,A3
MON$$ ASGN MW1,A4
MON$$ ASGN MW2,A5
MON$$ MODE GO,TEST
MON$$ EXEQ FORTRAN,,,,,,,,,BLSTWV1
      INTEGER H1M, H2M, CNT
      REAL NU,MAX,K,K1,K2
      DIMENSION RHO(9,13),P(9,13),U(9,13),V(9,13)
      1 ,R(9,13),S(9,13),E(9,13)
1001 FORMAT (10X, 7F10.4)
1002 FORMAT (10X, 2I5,3F10.4,I5)
      READ (1,1002) H1M, H2M, H1, H2, X, CNT
      REWIND 4
      T1=C.0
      X = X*(3.141592653/180.0)
      SINX = SIN(X)
      SIN2X = SINX*SINX
      COSX = COS(X)
      COS2X = COSX*COSX
      NU = 1.0
      GAMMA = 1.4
      OMEGA = 1.345
      SIGMA0 = 0.5
      READ (1,1001) RHO
      READ (1,1001) P
      READ (1,1001) U
      READ (1,1001) V
      MAX = 0.0
      DO 100L = 1,H2M
      DO 100M = 1,H1M
      IF(RHO(M,L).EQ.0.9E+6) GO TO 100
      TEST=SQRT(U(M,L)*U(M,L)+V(M,L)*V(M,L))+SQRT(GAMMA*P(M,L)/RHO(M,L))
      IF(TEST.GT.MAX) MAX = TEST
100 CONTINUE
      K = SIGMA0/MAX
      K1 = SINX*K
      K2 = COSX*K
      T = K*H1*H2/(SQRT(H1*H1+H2*H2))
      WRITE(4) H1M,H2M,SINX,COSX,SIN2X,COS2X,NU,GAMMA,OMEGA,SIGMA0,H1,H2
      1 ,K,K1,K2,T,CNT,CNT,T1
      WRITE(4) RHO
      WRITE(4) P
      WRITE(4) U
      WRITE(4) V
      DO 10 L=1,H2M
      DO 10 M=1,H1M
      IF(RHO(M,L).EQ.0.9E+6) GO TO 9
      R(M,L) = RHO(M,L)*U(M,L)
      GO TO 10
      9 R(M,L) = 0.9E+6
10 CONTINUE

```

```
WRITE(4) R
DO 20 L = 1,H2M
DO 20 M = 1,H1M
IF(RHO(M,L).EQ.0.9E+6) GO TO 19
S(M,L) = RHO(M,L)*V(M,L)
GO TO 20
19 S(M,L) = 0.9E+6
20 CONTINUE
WRITE(4) S
DO 30 L = 1,H2M
DO 30 M = 1,H1M
IF(RHO(M,L).EQ.0.9E+6) GO TO 29
W = SQRT(U(M,L)*U(M,L) + V(M,L)*V(M,L))
E(M,L) = (RHO(M,L)*W*W*0.5) + (P(M,L)/(GAMMA-1.0))
GO TO 30
29 E(M,L) = 0.9E+6
30 CONTINUE
WRITE(4) E
CALL NEXTPH
END
```

```

MON$$      EXEQ FORTRAN,,,,,,BLSTWV2
INTEGER H1M, H2M, CNT
REAL NU,MAX,K,K1,K2
DIMENSION RHO(9,13),P(9,13),U(9,13),V(9,13)
1 ,R(9,13),S(9,13),E(9,13),RHO1(9,13)
2001 FORMAT (10(1X,E12.6))
REWIND 4
READ(4) H1M,H2M,SINX,COSX,SIN2X,COS2X,NU,GAMMA,OMEGA,SIGMA0,H1,H2
1 ,K,K1,K2,T,CNT,CNT,T1
READ(4) RHO
READ(4) P
READ(4) U
READ(4) V
READ(4) R
READ(4) S
READ(4) E
DO 120 L=1,H2M
DO 120 M=1,H1M
IF(RHO(M,L).EQ.0.9E+6) GO TO 210
PSI = 0.0
FX = 0.0
FY = 0.0
PHIX = 0.0
PHIY = 0.0
IF(L.EQ.1) GO TO 209
YL = L-1
PSI = -T*NU*V(M,L)*RHO(M,L)/(YL*H2)
115 ALPHA = OMEGA*K*(SQRT(U(M,L)*U(M,L)+V(M,L)*V(M,L))
1 +SQRT(GAMMA*P(M,L)/RHO(M,L)))
BETA = ALPHA*COS2X
ALPHA = ALPHA*SIN2X
IF(RHO(M,L-1).EQ.0.9E+6) GO TO 116
IF(L.EQ.H2M) GO TO 117
FY = -0.5*K2*(S(M,L+1)-S(M,L-1))
300 BETA1 = OMEGA*K*(SQRT(U(M,L+1)*U(M,L+1)+V(M,L+1)*V(M,L+1))
1 +SQRT(GAMMA*P(M,L+1)/RHO(M,L+1)))*COS2X
BETA2 = OMEGA*K*(SQRT(U(M,L-1)*U(M,L-1)+V(M,L-1)*V(M,L-1))
1 +SQRT(GAMMA*P(M,L-1)/RHO(M,L-1)))*COS2X
PHIY = 0.25*((BETA1+BETA2)*(RHO(M,L+1)-RHO(M,L))
1 -(BETA+BETA2)*(RHO(M,L)-RHO(M,L-1)))
GO TO 200
116 U(M,L)=U(M,L)*COSX+V(M,L)*SINX
V(M,L)=-R(M,L)*SINX/RHO(M,L)+V(M,L)*COSX
PSI=-T*NU*V(M,L)*RHO(M,L)/(YL*H2)
FY=-K*(S(M,L+1)*COS2X+S(M-1,L)*SIN2X)
GO TO 200
117 FY = K2*S(M,L-1)
200 IF(M.EQ.1) GO TO 209
IF(RHO(M-1,L).EQ.0.9E+6) GO TO 118
IF(M.EQ.H1M) GO TO 130
IF(RHO(M+1,L).EQ.0.9E+6) GO TO 119
FX = -0.5*K1*(R(M+1,L)-R(M-1,L))
ALPHA1 = OMEGA*K*(SQRT(U(M+1,L)*U(M+1,L)+V(M+1,L)*V(M+1,L))
1 +SQRT(GAMMA*P(M+1,L)/RHO(M+1,L)))*SIN2X
ALPHA2 = OMEGA*K*(SQRT(U(M-1,L)*U(M-1,L)+V(M-1,L)*V(M-1,L))
1 +SQRT(GAMMA*P(M-1,L)/RHO(M-1,L)))*SIN2X
PHIX = 0.25*((ALPHA1+ALPHA)*(RHO(M+1,L)-RHO(M,L))
1 -(ALPHA+ALPHA2)*(RHO(M,L)-RHO(M-1,L)))

```

```

      GO TO 110
118 FX = -K1*R(M+1,L)
      GO TO 110
119 FX=-0.5*K1*COSX*(R(M+1,L+1)-R(M-1,L-1))
      ALPHA=OMEGA*K*(SQRT(U(M,L)*U(M,L)+V(M,L)*V(M,L))
1  +SQRT(GAMMA*P(M,L)/RHO(M,L)))
      ALPHA=ALPHA*SIN2X
      ALPHA1=OMEGA*K*(SQRT(U(M+1,L+1)*U(M+1,L+1)+V(M+1,L+1)*V(M+1,L+1))
1  +SQRT(GAMMA*P(M+1,L+1)/RHO(M+1,L+1)))*SIN2X
      ALPHA2=OMEGA*K*(SQRT(U(M-1,L-1)*U(M-1,L-1)+V(M-1,L-1)*V(M-1,L-1))
1  +SQRT(GAMMA*P(M-1,L-1)/RHO(M-1,L-1)))*SIN2X
      PHIX=0.25*COS2X*((ALPHA1+ALPHA)*(RHO(M+1,L+1)-RHO(M,L))
1  -(ALPHA2+ALPHA)*(RHO(M,L)-RHO(M-1,L-1)))
110 RHO1(M,L) = RHO(M,L)+PSI+FX+FY+PHIX+PHIY
      GO TO 120
130 RHO1(M,L) = RHO(M-1,L)
      GO TO 120
209 RHO1(M,L) = RHO(M,L)
      GO TO 120
210 RHO1(M,L) = 0.9E+6
120 CONTINUE
      REWIND 5
      WRITE(5) RHO1
      CALL NEXTPH
      END

```

```

MON$$      EXEQ FORTRAN,,,,,,,,,BLSTWV3
INTEGER H1M, H2M, CNT
REAL NU,MAX,K,K1,K2
DIMENSION RHO(9,13),P(9,13),U(9,13),V(9,13)
1 ,R(9,13),S(9,13),F(9,13),R1(9,13)
2001 FORMAT (10(1X,E12.6))
REWIND 4
READ(4) H1M,H2M,SINX,COSX,SIN2X,COS2X,NU,GAMMA,OMEGA,SIGMA0,H1,H2
1 ,K,K1,K2,T,CNT,CNT,T1
READ(4) RHO
READ(4) P
READ(4) U
READ(4) V
READ(4) R
RFAD(4) S
READ(4) E
DO 120 L=1,H2M
DO 120 M=1,H1M
IF(RHO(M,L).EQ.0.9E+6) GO TO 210
PSI = 0.0
FX = 0.0
FY = 0.0
PHIX = 0.0
PHIY = 0.0
IF(L.EQ.1) GO TO 209
YL = L-1
PSI = -T*NU*V(M,L)*R(M,L)/(YL*H2)
115 ALPHA = OMEGA*K*(SQRT(U(M,L)*U(M,L)+V(M,L)*V(M,L))
1 +SQRT(GAMMA*P(M,L)/RHO(M,L)))
BETA = ALPHA*COS2X
ALPHA = ALPHA*SIN2X
IF(RHO(M,L-1).EQ.0.9E+6) GO TO 116
IF(L.EQ.H2M) GO TO 117
FY = -0.5*K2*(S(M,L+1)*U(M,L+1)-S(M,L-1)*U(M,L-1))
300 BETA1 = OMEGA*K*(SQRT(U(M,L+1)*U(M,L+1)+V(M,L+1)*V(M,L+1))
1 +SQRT(GAMMA*P(M,L+1)/RHO(M,L+1)))*COS2X
BETA2 = OMEGA*K*(SQRT(U(M,L-1)*U(M,L-1)+V(M,L-1)*V(M,L-1))
1 +SQRT(GAMMA*P(M,L-1)/RHO(M,L-1)))*COS2X
PHIY = 0.25*((BETA1+BETA)*(R(M,L+1)-R(M,L))
1 -(BETA+BETA2)*(R(M,L)-R(M,L-1)))
GO TO 200
116 U(M,L)=U(M,L)*COSX+V(M,L)*SINX
V(M,L)=-R(M,L)*SINX/RHO(M,L)+V(M,L)*COSX
PSI=-T*NU*V(M,L)*R(M,L)/(YL*H2)
FY=-K*(S(M,L+1)*U(M,L+1)*COS2X+S(M-1,L)*U(M-1,L)*SIN2X)
GO TO 200
117 FY = K2*S(M,L-1)*U(M,L-1)
200 IF(M.EQ.1) GO TO 209
IF(RHO(M-1,L).EQ.0.9E+6) GO TO 118
IF(M.EQ.H1M) GO TO 130
IF(RHO(M+1,L).EQ.0.9E+6) GO TO 119
FX = -0.5*K1*((P(M+1,L)+R(M+1,L))*U(M+1,L))
1 -(P(M-1,L)+R(M-1,L))*U(M-1,L))
ALPHA1 = OMEGA*K*(SQRT(U(M+1,L)*U(M+1,L)+V(M+1,L)*V(M+1,L))
1 +SQRT(GAMMA*P(M+1,L)/RHO(M+1,L)))*SIN2X
ALPHA2 = OMEGA*K*(SQRT(U(M-1,L)*U(M-1,L)+V(M-1,L)*V(M-1,L))
1 +SQRT(GAMMA*P(M-1,L)/RHO(M-1,L)))*SIN2X
PHIX = 0.25*((ALPHA1+ALPHA)*(R(M+1,L)-R(M,L))

```

```

1 -(ALPHA+ALPHA2)*(R(M,L)-R(M-1,L)))
GO TO 110
118 R1(M,L) = 0.0
GO TO 120
119 FX=-0.5*K1*COSX*((P(M+1,L+1)+R(M+1,L+1))*U(M+1,L+1))
1 -(P(M-1,L-1)+R(M-1,L-1))*U(M-1,L-1)))
ALPHA=OMEGA*K*(SQRT(U(M,L)*U(M,L)+V(M,L)*V(M,L)))
1 +SQRT(GAMMA*P(M,L)/RHO(M,L)))
ALPHA=ALPHA*SIN2X
ALPHA1=OMEGA*K*(SQRT(U(M+1,L+1)*U(M+1,L+1)+V(M+1,L+1)*V(M+1,L+1)))
1 +SQRT(GAMMA*P(M+1,L+1)/RHO(M+1,L+1)))*SIN2X
ALPHA2=OMEGA*K*(SQRT(U(M-1,L-1)*U(M-1,L-1)+V(M-1,L-1)*V(M-1,L-1)))
1 +SQRT(GAMMA*P(M-1,L-1)/RHO(M-1,L-1)))*SIN2X
PHIX=0.25*COS2X*((ALPHA1+ALPHA)*(R(M+1,L+1)-R(M,L))
1 -(ALPHA2+ALPHA)*(R(M,L)-R(M-1,L-1)))
110 R1(M,L) = R(M,L)+PSI+FX+FY+PHIX+PHIY
IF(ABS(R1(M,L)).LT.0.000001) R1(M,L)=0.0
GO TO 120
130 R1(M,L) = R(M-1,L)
GO TO 120
209 R1(M,L) = R(M,L)
GO TO 120
210 R1(M,L) = 0.9E+6
120 CONTINUE
WRITE(5) R1
CALL NEXTPH
END

```



```

MON$$      EXEC FORTRAN,,,,,BLSTWV4
  INTEGER H1M, H2M, CNT
  REAL NU,MAX,K,K1,K2
  DIMENSION RHO(9,13),P(9,13),U(9,13),V(9,13)
  1 ,R(9,13),S(9,13),E(9,13),S1(9,13)
2001 FORMAT (10(1X,F12.6))
  REWIND 4
  READ(4) H1M,H2M,SINX,COSX,SIN2X,COS2X,NU,GAMMA,OMEGA,SIGMAO,H1,H2
  1 ,K,K1,K2,T,CNT,CNT,T1
  READ(4) RHO
  READ(4) P
  READ(4) U
  READ(4) V
  READ(4) R
  READ(4) S
  READ(4) E
  DO 120 L=1,H2M
  DO 120 M=1,H1M
  IF(RHO(M,L).EQ.0.9E+6) GO TO 210
  PSI = 0.0
  FX = 0.0
  FY = 0.0
  PHIX = 0.0
  PHIY = 0.0
  IF(L.EQ.1) GO TO 209
  YL = L-1
  PSI = -T*NU*V(M,L)*S(M,L)/(YL*H2)
115 ALPHA = OMEGA*K*(SQRT(U(M,L)*U(M,L)+V(M,L)*V(M,L)))
  1 +SQRT(GAMMA*P(M,L)/RHO(M,L)))
  BFTA = ALPHA*COS2X
  ALPHA = ALPHA*SIN2X
  IF(RHO(M,L-1).EQ.0.9E+6) GO TO 116
  IF(L.EQ.H2M) GO TO 117
  FY = -0.5*K2*((P(M,L+1)+S(M,L+1)*V(M,L+1))
  1 -(P(M,L-1)+S(M,L-1)*V(M,L-1)))
300 BETA1 = OMEGA*K*(SQRT(U(M,L+1)*U(M,L+1)+V(M,L+1)*V(M,L+1)))
  1 +SQRT(GAMMA*P(M,L+1)/RHO(M,L+1)))*COS2X
  BETA2 = OMEGA*K*(SQRT(U(M,L-1)*U(M,L-1)+V(M,L-1)*V(M,L-1)))
  1 +SQRT(GAMMA*P(M,L-1)/RHO(M,L-1)))*COS2X
  PHIY = 0.25*((BETA1+BETA2)*(S(M,L+1)-S(M,L))
  1 -(BFTA+BETA2)*(S(M,L)-S(M,L-1)))
  GO TO 200
116 U(M,L)=U(M,L)*COSX+V(M,L)*SINX
  V(M,L)=-R(M,L)*SINX/RHO(M,L)+V(M,L)*COSX
  GO TO 200
117 S1(M,L)=0.0
  GO TO 120
200 IF(M.EQ.1) GO TO 209
  IF(RHO(M-1,L).EQ.0.9E+6) GO TO 118
  IF(M.EQ.H1M) GO TO 130
  IF(RHO(M+1,L).EQ.0.9E+6) GO TO 119
  FX = -0.5*K1*(R(M+1,L)*V(M+1,L)-R(M-1,L)*V(M-1,L))
  ALPHA1 = OMEGA*K*(SQRT(U(M+1,L)*U(M+1,L)+V(M+1,L)*V(M+1,L)))
  1 +SQRT(GAMMA*P(M+1,L)/RHO(M+1,L)))*SIN2X
  ALPHA2 = OMEGA*K*(SQRT(U(M-1,L)*U(M-1,L)+V(M-1,L)*V(M-1,L)))
  1 +SQRT(GAMMA*P(M-1,L)/RHO(M-1,L)))*SIN2X
  PHIX = 0.25*((ALPHA1+ALPHA2)*(S(M+1,L)-S(M,L))
  1 -(ALPHA+ALPHA2)*(S(M,L)-S(M-1,L)))

```

```
      GO TO 110
118 FX = -K1*(R(M+1,L)*V(M+1,L))
      GO TO 110
119 S1(M,L)=0.0
      GO TO 120
110 S1(M,L) = S(M,L)+PSI+FX+FY+PHIX+PHIY
      IF(ABS(S1(M,L)).LT.0.000001) S1(M,L)=0.0
      GO TO 120
130 S1(M,L) = S(M-1,L)
      GO TO 120
209 S1(M,L) = S(M,L)
      GO TO 120
210 S1(M,L) = 0.9E+6
120 CONTINUE
      WRITE(5) S1
      CALL NEXTPH
      END
```

```

MON$$      EXEQ FORTRAN,,,,,,BLSTWV5
INTEGER H1M, H2M, CNT
REAL NU,MAX,K,K1,K2
DIMENSION RHO(9,13),P(9,13),U(9,13),V(9,13)
1 ,R(9,13),S(9,13),E(9,13),E1(9,13)
2001 FORMAT (10(1X,E12.6))
REWIND 4
READ(4) H1M,H2M,SINX,COSX,SIN2X,COS2X,NU,GAMMA,OMEGA,SIGMA0,H1,H2
1 ,K,K1,K2,T,CNT,CNT,T1
READ(4) RHO
READ(4) P
READ(4) U
READ(4) V
READ(4) R
READ(4) S
READ(4) E
DO 120 L=1,H2M
DO 120 M=1,H1M
IF(RHO(M,L).EQ.0.9E+6) GO TO 210
PSI = 0.0
FX = 0.0
FY = 0.0
PHIX = 0.0
PHIY = 0.0
IF(L.EQ.1) GO TO 209
YL = L-1
PSI = -T*NU*V(M,L)*(E(M,L)+F(M,L))/(YL*H2)
115 ALPHA = OMEGA*K*(SQRT(U(M,L)*U(M,L)+V(M,L)*V(M,L))
1 +SQRT(GAMMA*P(M,L)/RHO(M,L)))
BETA = ALPHA*COS2X
ALPHA = ALPHA*SIN2X
IF(RHO(M,L-1).EQ.0.9E+6) GO TO 116
IF(L.EQ.H2M) GO TO 117
FY = -0.5*K2*(((E(M,L+1)+P(M,L+1))*V(M,L+1))
1 -((E(M,L-1)+P(M,L-1))*V(M,L-1)))
300 BETA1 = OMEGA*K*(SQRT(U(M,L+1)*U(M,L+1)+V(M,L+1)*V(M,L+1))
1 +SQRT(GAMMA*P(M,L+1)/RHO(M,L+1)))*COS2X
BETA2 = OMEGA*K*(SQRT(U(M,L-1)*U(M,L-1)+V(M,L-1)*V(M,L-1))
1 +SQRT(GAMMA*P(M,L-1)/RHO(M,L-1)))*COS2X
PHIY = 0.25*((BETA1+BETA)*E(M,L+1)-E(M,L))
1 -(BETA+BETA2)*E(M,L)-E(M,L-1))
GO TO 200
116 U(M,L)=U(M,L)*COSX+V(M,L)*SINX
V(M,L)=-R(M,L)*SINX/RHO(M,L)+V(M,L)*COSX
PSI=-T*NU*V(M,L)*(E(M,L)+P(M,L))/(YL*H2)
FY=-K*(((E(M,L+1)+P(M,L+1))*V(M,L+1))*COS2X)
1 +(((E(M-1,L)+P(M-1,L))*V(M-1,L))*SIN2X))
GO TO 200
117 FY = K2*(((E(M,L-1)+P(M,L-1))*V(M,L-1))
200 IF(M.EQ.1) GO TO 209
IF(RHO(M-1,L).EQ.0.9E+6) GO TO 118
IF(M.EQ.H1M) GO TO 130
IF(RHO(M+1,L).EQ.0.9E+6) GO TO 119
FX = -0.5*K1*(((E(M+1,L)+P(M+1,L))*U(M+1,L))
1 -((E(M-1,L)+P(M-1,L))*U(M-1,L)))
ALPHA1 = OMEGA*K*(SQRT(U(M+1,L)*U(M+1,L)+V(M+1,L)*V(M+1,L))
1 +SQRT(GAMMA*P(M+1,L)/RHO(M+1,L)))*SIN2X
ALPHA2 = OMEGA*K*(SQRT(U(M-1,L)*U(M-1,L)+V(M-1,L)*V(M-1,L))

```

```

1   +SQRT(GAMMA*P(M-1,L)/RHO(M-1,L))*SIN2X
   PHIX = 0.25*((ALPHA1+ALPHA)*(E(M+1,L)-E(M,L))
1   -(ALPHA+ALPHA2)*(E(M,L)-E(M-1,L)))
   GO TO 110
118 FX = -K1*((E(M+1,L)+P(M+1,L))*U(M+1,L))
   GO TO 110
119 FX=-0.5*K1*COSX*((E(M+1,L+1)+P(M+1,L+1))*U(M+1,L+1))
1   -((E(M-1,L-1)+P(M-1,L-1))*U(M-1,L-1))
   ALPHA=OMEGA*K*(SQRT(U(M,L)*U(M,L)+V(M,L)*V(M,L))
1   +SQRT(GAMMA*P(M,L)/RHO(M,L)))
   ALPHA=ALPHA*SIN2X
   ALPHA1=OMEGA*K*(SQRT(U(M+1,L+1)*U(M+1,L+1)+V(M+1,L+1)*V(M+1,L+1))
1   +SQRT(GAMMA*P(M+1,L+1)/RHO(M+1,L+1))) *SIN2X
   ALPHA2=OMEGA*K*(SQRT(U(M-1,L-1)*U(M-1,L-1)+V(M-1,L-1)*V(M-1,L-1))
1   +SQRT(GAMMA*P(M-1,L-1)/RHO(M-1,L-1))) *SIN2X
   PHIX=0.25*COS2X*((ALPHA1+ALPHA)*(E(M+1,L+1)-E(M,L))
1   -(ALPHA2+ALPHA)*(E(M,L)-E(M-1,L-1)))
110 E1(M,L) = E(M,L)+PSI+FX+FY+PHIX+PHIY
   GO TO 120
130 E1(M,L) = E(M-1,L)
   GO TO 120
209 E1(M,L) = E(M,L)
   GO TO 120
210 E1(M,L) = 0.9E+6
120 CONTINUE
   WRITE(5) E1
   CALL NEXTPH
   END

```

```

MON$$      EXEQ FORTRAN,,,,,,BLSTWV6
      INTEGER H1M, H2M, CNT, CNT1, CNT2
      REAL NU, MAX, K, K1, K2
      DIMENSION RHO(9,13),P(9,13),U(9,13),V(9,13)
      1 ,R(9,13),S(9,13),E(9,13),W(9,13)
2001 FORMAT (12H RHO = 0 AT I2,I1H,I2)
2002 FORMAT (10(1X,E12.6))
2003 FORMAT (//9H DENSITY/)
2004 FORMAT (//10H PRESSURE/)
2005 FORMAT (//21H HORIZONTAL VELOCITY/)
2006 FORMAT (//19H VERTICAL VELOCITY/)
2007 FORMAT (//22H HORIZONTAL MASS FLUX/)
2008 FORMAT (//20H VERTICAL MASS FLUX/)
2009 FORMAT (//8H ENERGY/)
2011 FORMAT (//18H VELOCITY MODULUS/)
2010 FORMAT (//1H160X,11HTIME PLANE I2/57X,7HTIME = E14.8)
      REWIND 4
      READ(4) H1M,H2M,SINX,COSX,SIN2X,COS2X,NU,GAMMA,OMEGA,SIGMA0,H1,H2
      1 ,K,K1,K2,T,CNT,CNT1,T1
      REWIND 5
      READ(5) RHO
      READ(5) R
      READ(5) S
      READ(5) E
      DO 10 L=1,H2M
      DO 10 M=1,H1M
      IF(RHO(M,L).EQ.0.9E+6) GO TO 100
      IF(RHO(M,L).EQ.0.0) GO TO 200
      IF(RHO(M,L-1).EQ.0.9E+6) GO TO 30
      GO TO 15
30 RHO(M,L)=RHO(M,L)
      E(M,L)=E(M,L)
      U(M,L)=R(M,L)/RHO(M,L)
      V(M,L)=S(M,L)/RHO(M,L)
      P(M,L) = (GAMMA-1.0)*(E(M,L)-RHO(M,L)
      1 *(U(M,L)*U(M,L)+V(M,L)*V(M,L)))*0.5)
      R(M,L)=R(M,L)*COSX
      IF(ABS(R(M,L)).LT.0.000001) R(M,L)=0.0
      S(M,L)=R(M,L)*SINX/COSX
      IF(ABS(S(M,L)).LT.0.000001) S(M,L)=0.0
      U(M,L)=R(M,L)/RHO(M,L)
      V(M,L)=S(M,L)/RHO(M,L)
      W(M,L)=SQRT(U(M,L)*U(M,L)+V(M,L)*V(M,L))
      GO TO 10
15 U(M,L)=R(M,L)/RHO(M,L)
      V(M,L)=S(M,L)/RHO(M,L)
      P(M,L)=(GAMMA-1.0)*(E(M,L)-RHO(M,L)
      1 *(U(M,L)*U(M,L)+V(M,L)*V(M,L)))*0.5)
      W(M,L)=SQRT(U(M,L)*U(M,L)+V(M,L)*V(M,L))
10 CONTINUE
40 MAX=0.0
      DO 20 L=1,H2M
      DO 20 M=1,H1M
      IF(RHO(M,L).EQ.0.9E+6) GO TO 20
      TEST=SQRT(U(M,L)*U(M,L)+V(M,L)*V(M,L))+SQRT(GAMMA*P(M,L)/RHO(M,L))
      IF(TEST.GT.MAX) MAX = TEST
20 CONTINUE
      K=SIGMA0/MAX

```

```

K1=SINX*K
K2=COSX*K
T1=T1+T
T=K*H1*H2/SQRT(H1*H1+H2*H2)
REWIND 4
CNT=CNT-1
WRITE(4) H1M,H2M,SINX,COSX,SIN2X,COS2X,NU,GAMMA,OMEGA,SIGMA0,H1,H2
1 ,K,K1,K2,T,CNT,CNT1,T1
WRITE(4) RHO
WRITE(4) P
WRITE(4) U
WRITE(4) V
WRITE(4) R
WRITE(4) S
WRITE(4) E
WRITE(4) W
REWIND 5
CNT2 = CNT1-CNT
WRITE (3,2010) CNT2,T1
WRITE(3,2003)
DO 50 L=1,H2M
L1=H2M-L+1
50 WRITE(3,2002) (RHO(M,L1), M=1,H1M)
WRITE(3,2004)
DO 51 L=1,H2M
L1=H2M-L+1
51 WRITE(3,2002) (P(M,L1), M=1,H1M)
WRITE(3,2005)
DO 52 L=1,H2M
L1=H2M-L+1
52 WRITE(3,2002) (U(M,L1), M=1,H1M)
WRITE(3,2006)
DO 53 L=1,H2M
L1=H2M-L+1
53 WRITE(3,2002) (V(M,L1), M=1,H1M)
WRITE(3,2007)
DO 54 L=1,H2M
L1=H2M-L+1
54 WRITE(3,2002) (R(M,L1), M=1,H1M)
WRITE(3,2008)
DO 55 L=1,H2M
L1=H2M-L+1
55 WRITE(3,2002) (S(M,L1), M=1,H1M)
WRITE(3,2009)
DO 56 L=1,H2M
L1=H2M-L+1
56 WRITE(3,2002) (E(M,L1), M=1,H1M)
WRITE(3,2011)
DO 57 L=1,H2M
L1=H2M-L+1
57 WRITE(3,2002) (W(M,L1),M=1,H1M)
IF(CNT.EQ.0) CALL EXIT
CALL PHASE (2)
100 U(M,L)=0.9E+6
V(M,L)=0.9E+6
P(M,L)=0.9E+6
W(M,L)=0.9E+6
GO TO 10
200 WRITE(3,2001)M,L
U(M,L)=0.0
V(M,L)=0.0
P(M,L)=0.0

```

```
W(M,L)=0.0
GO TO 10
END
MON$$      EXEQ LINKLOAD
           PHASEOPBLSTWV
           CALL BLSTWV1
           PHASE
           BASE1BLSTWV1
           CALL BLSTWV2
           PHASE
           BASE1BLSTWV2
           CALL BLSTWV3
           PHASE
           BASE1BLSTWV3
           CALL BLSTWV4
           PHASE
           BASE1BLSTWV4
           CALL BLSTWV5
           PHASE
           BASE1BLSTWV5
           CALL BLSTWV6
MON$$      EXEQ OPBLSTWV,MJB
```

VITA

William N. Jackomis

Candidate for the Degree of

Doctor of Philosophy

Thesis: TRANSIENT FLOW FIELD ANALYSIS OF A PLANE BLAST WAVE INTERCEPTING A STATIONARY CONE AT ZERO ANGLE OF ATTACK.

Major Field: Mechanical Engineering (Aerospace)

Biographical:

Personal Data: Born in Gary, Indiana, January 17, 1930, the son of Nicholas and Helen Jackomis.

Education: Graduated from Tolleston High School, Gary, Indiana, June, 1947. Attended Indiana University - Gary College from 1947 to 1949; attended U. S. Military Academy, West Point, New York, from 1949 to 1951; entered the University of Notre Dame, Notre Dame, Indiana, in September, 1951, and received the Bachelor of Science Degree in Mechanical Engineering in January, 1954. Entered Oklahoma State University in January, 1961, received the Master of Science Degree in Mechanical Engineering (Aerospace) in June, 1962; completed requirements for the Doctor of Philosophy Degree in May, 1965.

Professional Experience: Employed as Petroleum Sales Engineer at E. I. DuPont de Nemours and Company, Wilmington, Delaware, in 1954. Employed at Inland Steel Company, East Chicago, Indiana, as a Junior Field Engineer for two summers, 1952-53. Entered the U. S. Air Force in June, 1954, and currently serving on active duty in grade of Regular Captain. Served overseas at Harmon AFB, Newfoundland, as a Jet Fighter Pilot and Administrative Officer from 1955 to 1958. Served as Helicopter Flight Test Pilot and Standardization Instructor Pilot (26th Air Division, ADC) while stationed at Suffolk County AFB, Long Island, New York, from 1958 to 1961.

Professional Organizations: American Institute of Aeronautics and Astronautics.